UNIVERSIDADE FEDERAL DO CEARÁ
CENTRO DE TECNOLOGIA
DEPARTAMENTO DE ENGENHARIA QUÍMICA
PROGRAMA DE PÓS-GRADUAÇÃO EM ENGENHARIA QUÍMICA

RAFAEL MAGALHÃES SIQUEIRA

CARBON DIOXIDE CAPTURE BY PRESSURE SWING ADSORPTION

FORTALEZA

2020

RAFAEL MAGALHÃES SIQUEIRA

CARBON DIOXIDE CAPTURE BY PRESSURE SWING ADSORPTION

Thesis presented to the Programa de Pós-Graduação em Engenharia Química da Universidade Federal do Ceará, as a dissertation partial fulfillment of the requirements for the degree of Doctor of Philosophy in Chemical Engineering. Research area: Desenvolvimento de Processos Químicos e Bioquímicos.

Supervisors:
Prof. Dr. Moisés Bastos Neto
Prof. Dr. Alírio Egídio Rodrigues

Co-supervisors:
Prof. Dr. Diana Cristina Silva de Azevedo
Prof. MSc. Antônio Eurico Belo Torres

FORTALEZA

2020

Dados Internacionais de Catalogação na Publicação
Universidade Federal do Ceará
Biblioteca Universitária
Gerada automaticamente pelo módulo Catalog, mediante os dados fornecidos pelo(a) autor(a)

S632c Siqueira, Rafael Magalhães.
Carbon Dioxide Capture by Pressure Swing Adsorption / Rafael Magalhães Siqueira. – 2020.
116 f. : il. color.

Tese (doutorado) – Universidade Federal do Ceará, Centro de Tecnologia, Programa de Pós-Graduação em Engenharia Química, Fortaleza, 2020.
Orientação: Prof. Dr. Moisés Bastos Neto; Prof. Dr. Alírio Egídio Rodrigues.
Coorientação: Profa. Dra. Diana Cristina Silva de Azevedo.

1. CO2 capture. 2. Adsorption Equilibrium. 3. Activated Carbon. 4. PSA simulation. I. Título.
CDD 660

RAFAEL MAGALHÃES SIQUEIRA

CARBON DIOXIDE CAPTURE BY PRESSURE SWING ADSORPTION

Thesis presented to the Programa de Pós-Graduação em Engenharia Química da Universidade Federal do Ceará, as a dissertation partial fulfillment of the requirements for the degree of Doctor of Philosophy in Chemical Engineering. Research area: Desenvolvimento de Processos Químicos e Bioquímicos.

Date: ___/___/______.

COMMITEE MEMBERS

____

Dr. Samuel Jorge Marques Cartaxo
Universidade Federal do Ceará (UFC)

____

Dr. Sebastião Mardônio Pereira de Lucena
Universidade Federal do Ceará (UFC)

____

Dr. Rafael Barbosa Rios
Universidade Federal Rural do Semi-Árido (UFERSA)

____

Dr. Regina de Fátima Peralta Muniz Moreira
Universidade Federal de Santa Catarina (UFSC)

A Deus.

Aos meus pais, João Siqueira e Wanderlea.

ACKNOWLEDGMENTS

A CAPES e PETROBRÁS, pelo apoio financeiro com a manutenção da bolsa de auxílio.

Aos professores participantes da banca examinadora.

Ao professor William M. Barcellos por todo ensinamento didático e conselhos de vida dados até hoje.

Aos professores A. Eurico Belo Torres e Diana Azevedo por esta oportunidade ímpar que me foi dada.

Ao professor Moisés Bastos Neto pela orientação, todos os ensinamentos, puxões de orelha e a paciência que teve comigo durante esse tempo.

Ao Alexandre Ferreira, pela imensa e importante ajuda que me deu desde que o conheci.

À Wladiana por estar sempre ao meu lado durante esse tempo e apoiar muito sempre com muita força e amor.

Às pessoas do LPA que ainda estão ou que tiveram uma rápida passagem, mas que marcaram muito durante esse período; Débora, Karine, Enrique, Bianca, Jorge, Thalles, Morales, Randreanne, Juliana e Rafaelle.

“We are the first generation to feel
the effect of climate change and the last
generation who can do something about it.”
Barack Obama

ABSTRACT

The high concentration of carbon dioxide (CO_2) in the atmosphere originated from combustion processes has been frequently pointed as the main responsible for global warming and climatic changes. To mitigate the adverse effects of global warming and to reduce CO_2 concentration, many technologies have been developed in the last decades to capture CO_2 in different scenarios. Among the available technologies for post-combustion Carbon Capture and Storage (CCS), one of the most studied processes is the adsorption in porous media, such as activated carbon. Pressure Swing Adsorption (PSA) is a cyclic adsorption process, which allows continuous separation of gas streams. The performance of a PSA process is usually evaluated by the purity, recovery, and productivity when the process reaches the cyclic steady state. This study presents experimental and simulated data obtained from a bench-scale PSA. It aims to improve the simulation of PSA process using more adequate parameter values and detailed models thermodynamically consistent to describe accurate results according to experimental data. Also, it aims to evaluate the model validation using three different activated carbons: Norit RB4, Filtron N and Charbon 500. The first one, for instance, presents pellet shape and relative high microporosity in comparison to the other ones. The unit was tested with a mixture simulating dry flue gases containing 85% of N_2 and 15% of CO_2 (on a molar basis). A mathematical-phenomenological model combining momentum, mass and heat balances, using the Linear Driving Force approach (LDF) for mass transport were applied. This parameter is commonly determined by experimental data of breakthrough curves, conversely in this work it has been estimated by experimental results of the respective gas uptake. Sips model was used to describe the adsorption equilibrium of single component, and for binary mixture Ideal Adsorption Solution Theory (IAST) was applied in this study to simulate the dynamic behavior of the process. In this work, the IAST equations were directly applied in the simulation which is not very common in literature for simulation of gas separation on PSA. The model predicted reasonably well the breakthrough curves and temperature history. PSA process simulation was validated according to experimental data and has shown to be in agreement with them. Estimation procedure of Linear Driving Force (LDF) parameter has shown to be reliable. Model parameters were adequately determined and IAST was more appropriate to simulate separation process of a binary mixture.

Keywords: CO_2 capture. Adsorption Equilibrium. Activated Carbon. PSA simulation.

LIST OF FIGURES

LIST OF TABLES

ABBREVIATION

ADS	Adsorption
BET	Brunauer-Emmett-Teller
BLD	Blowdown
BPC	Back pressure controller
CCS	Carbon capture and storage
DFT	Density functional theory
ES	Extended Sips
EQ^d	Depressurization equalization
EQ^p	Pressurization equalization
FIRC	Flow indicator ratio controller
GC	Gac chromatograph
IAST	Ideal adsorption solution theory
LDF	Linear driving force
MFC	Mass flow controller
MFM	Mass flowmeter
MM	Molar mass
MSS	Minimum squares sum
NLDFT	Non-local density functional theory
P	Pressure sensor
PR	Pressurization
PU	Purge
TB	Thermostatic bath
TC	Thermocouple
VSA	Vacuum swing adsorption
VTSA	Vacuum-Temperature swing adsorption

NOMENCLATURES

a_{BET}	Surface area	(m^2)
A	Column surface area	(m^2)
b	Langmuir affinity coefficient	(bar^{-1})
$c_{p,g}$	Gas heat capacity at constant pressure	($J\ kg^{-1}\ K^{-1}$)
$c_{v,g}$	Gas heat capacity at constant volume	($J\ kg^{-1}\ K^{-1}$)
$c_{v,s}$	Solid heat capacity at constant volume	($J\ kg^{-1}\ K^{-1}$)
C_c	Empirical coefficient	(-)
$C_{g,i}$	Gas concentration of component *i*	($mol\ m^{-3}$)
$C_{g,T}$	Total gas concentration	($mol\ m^{-3}$)
D	Internal column diameter	(m)
D_c	Empirical coefficient	(-)
D_m	Molecular diffusivity	($m^2\ s^{-1}$)
D_{ax}	Axial dispersion	($m^2\ s^{-1}$)
d_p	Particle diameter	(m)
E_{ad}	Adsorption Energy	($J\ mol^{-1}$)
F_i	Molar flow rate of component *i*	($mol\ s^{-1}$)
H_{ads}^{int}	Integral heat of adsorption	($J\ mol^{-1}$)
H_{ads}^{d}	Differential heat of adsorption	($J\ mol^{-1}$)
h_w	Heat transfer coefficient between gas and wall	($W\ m^{-2}\ K^{-1}$)
k_{LDF}	Mass transfer coefficient	(s^{-1})
k_s	Dimensionless geometrical factor	(-)
m	Absolute adsorbed concentration	(g)
MM	Molar mass	($g\ mol^{-1}$)
m_{exc}	Excess adsorbed concentration	(g)
m_{sol}	Adsorbent dry mass	(g)
N	Number of points	(-)

N_A	Avogadro number	(-)
n	Effect of surface heterogeneity	(-)
n_{ads}	Adsorbed amount	(mmol g^{-1})
n_m	Adsorbed amount in a monolayer	(mmol g^{-1})
n_μ	Adsorbed amount into microporous	(mmol g^{-1})
n_0	Fitting parameter of Sips equation	(-)
V	Volume	(m^3)
$\dot{V}^0_{inlet}$	Standard volumetric flow rate at column inlet	(m^3 s^{-1})
V_{ads}	Adsorbed phase volume	(m^3)
$\hat{V}_p$	Specific pore volume	(m^3 kg^{-1})
V_{sol}	Solid volume	(m^3)
V_T	Total volume	(m^3)
P	Pressure	(bar)
P_0	Saturation pressure	(Torr)
q	Adsorbed concentration	(mmol g^{-1})
q^*	Adsorbed concentration at equilibrium	(mmol g^{-1})
$\bar{\bar{q}}$	Average concentration of sorbent within the particle	(mmol g^{-1})
Q	Heat of adsorption	(J mol^{-1})
Q_{int}	Integral heat	(J)
Q_d	Differential heat	(J)
q_m	Maximum adsorbed amount coefficient	(mmol g^{-1})
r	Radius	(m)
t	Time	(s)
T	Temperature	(K)
T_0	Standard temperature (298 K)	(K)
u	Gas velocity	(m s^{-1})
U_g	Overall heat transfer coefficient	(W m^{-2} K^{-1})
y	Molar fraction	(-)
x	Molar fraction in adsorbed phase	(-)

ΔH_{ads}	Enthalpy of adsorption	(J mol^{-1} K^{-1})
ΔH_{iso}	Isosteric heat of adsorption	(J mol^{-1} K^{-1})
Δm	Mass difference	(g)
α	Equalization factor	(-)
α_0	Equilibrium pressure of equalization	(Pa)
α_w	Ratio of column internal surface area to volume	(m^{-1})
$\alpha_{w,l}$	Ratio of surface logarithmic mean to volume	(m^{-1})
χ	Fitting parameter of Sips equation	(-)
ε	Bed porosity	(-)
ε_p	Particle porosity	(-)
κ	Fitting parameter of Sips equation	(-)
λ	Axial heat dispersion	(W m^{-1} K^{-1})
θ	Ratio between adsorbed and saturated adsorbed amount	(-)
ρ_a	Tapped density	(kg m^{-3})
ρ_b	Bed density (ratio of adsorbent mass to adsorbent volume in the column)	(kg m^{-3})
ρ_p	Particle density	(kg m^{-3})
ρ_w	Wall density	(kg m^{-3})
μ	Viscosity	(Pa s)
π	Spreading pressure	(bar)
σ	Average surface area occupied by N_2 molecules	(m^2)
Ω	Dimensionless LDF factor	(-)

Subscript nomenclature

μ	Microporous
0	Initial
b	Bulk
bal	Suspended parts of the balance
calc	Calculated
exp	Experimental
g	Gas phase

h	Homogeneous
i	Component
s	Solid
T	Total

SUMMARY

1. INTRODUCTION

The growth in global energy consumption in recent decades has led to a series of environmental concerns caused by the emission of greenhouse gases. Among those gases, CO_2 is considered the main reason for global warming due to the relatively high concentration in atmosphere. Fossil fuels still dominate global energy matrix due to their low cost and high availability (Ling *et al.*, 2015). The majority of CO_2 emissions in the environment comes from the combustion of those fuels. According to IPCC (Intergovernmental Panel on Climate Change) report, the largest sources of greenhouse gases were the energy production, agriculture, forestry, and land-use sectors. Looking at the total of greenhouse gases CO_2 contributes with 76 %; CH_4 with about 16 %, N_2O with about 6 %, and the combined F-gases with about 2 % (Victor *et al.*, 2014). In 2012, the Kyoto protocol was implemented to reduce CO_2 emissions by 2023 (Mendes *et al.*, 2017).

Therefore, to mitigate or control the adverse effects of large CO_2 concentration on the environment, several studies have suggested different technologies aiming to separate and to recover CO_2 from flue gases emitted by power plants (Mulgundmath *et al.*, 2012). Chemical absorption, cryogenic distillation, adsorption processes, and membrane separations are increasingly studied for such a purpose (Kamarudin *et al.*, 2018). Separation processes for CO_2 adsorption in the field of Carbon Capture and Storage (CCS) stand out as a promising technology due to its relatively low cost, low energy consumption and availability (Mondal *et al.*, 2012; Leung *et al.*, 2014; Goel *et al.*, 2016). This kind of process consists of sequestrating CO_2 using porous materials, and it usually is expected to concentrate a CO_2 purity > 95 % and recovery > 90 % (Nikolaidis *et al.*, 2016). Furthermore, this technology has an advantageous potential of reducing the post-combustion CO_2 capture cost when compared to other typical processes such as amine scrubbing (Plaza *et al.*, 2010).

The adsorbent amount to evaluate the performance of gas stream separation is crucial in this kind of process. Most adsorbents have surfaces that interact most strongly with CO_2 than N_2. These materials are commonly referred to equilibrium adsorbents, *e.g.*, activated carbon, zeolites, and metal-organic frameworks (MOFs). Other adsorbents show little difference on the adsorption capacity of both components, but the rates of diffusion are distinct, leading to a kinetic separation nature (Ruthven, 1984). A key requisite for the CO_2 capture by adsorption process relies on finding the proper adsorbent with better separation characteristics. For instance, adsorbents with high equilibrium selectivity, high stability and with low cost are desirable (Lee *et al.*, 2018). Also, to develop an economic adsorption-based separation process, the adsorbent must present aspects of easy regeneration so that the energy consumption does not increase the costs and time consuming of gas stream. Among the adsorbents used for PSA process, activated carbon offers some advantages, when compared to zeolites or silica, due to its applicability, low cost high specific surface area, pore volume, easy regeneration and water resistance (Plaza *et al.*, 2016).

Activated carbon is classified as a porous material, and this kind of adsorbent offers several advantages such as large surface area and high adsorption capacity. They can be synthesized from a variety of low-cost material sources and by several techniques (Goel *et al.*, 2016). The main advantage of activated carbon relies on the large micropores volume which makes its surface area high when compared to other materials (Tien, 1994). They are the most accessible material for separation process. For decades, adsorption using activated carbon has become standard engineering practice in purification process, such as wastewater treatment. In most cases, that sorbent is operated in fixed bed whereas a liquid or gas flow through the column and the separation process occurs. This technique is the most popular way to operate so far (Tien, 1994).

As it is known, to perform and evaluate some cyclic processes experimentally, it may require a high consumption of gases and it is time-consuming. Experimental tests to determine the ideal cycle time, number of steps of the process, and other parameters are unfeasible. However, with a tailored mathematical model capable of describing the experimental data can offer a faster alternative. To be used with confidence, this model must be validated against experimental results, that tested different operating conditions and configurations, at laboratory scale (Marx *et al.*, 2015).

Fundamentals of adsorption and equilibrium models are crucial to design a PSA unit. Numerous models are presented in the literature, and depending on the configurations of the processes the most used ones cannot describe accurately the experimental results. A consistent equilibrium model is the foremost step to start the process design. Furthermore, the column and material properties must be known for a good simulation performance to understand the dynamic behavior of an adsorption process.

In this work, it was used activated carbons in order to evaluate the performance of CO_2 capture by PSA process. It is presented pure component adsorption equilibrium data of CO_2 and N_2 (at 298 K, 323 K and 348 K) as well as binary mixture equilibrium data, for a composition of 85%-15% (N_2/CO_2 at 298 K) that mimics the dry flue gas from coal power plants. Breakthrough curves and PSA experiments at 298 K were performed to evaluate the influence of adsorbent characteristics in CO_2 capture process and to obtain experimental data of the dynamic behavior. The ratio of the mixture N_2+CO_2 was maintained 85:15 for PSA experiments. The minimum pressure of 1 bar was set for blowdown and purge steps. The maximum pressure of 6 bar was set for adsorption step. PSA process simulation using IAST model (Myers & Prausnitz, 1965) was validated comparing to the history of pressure and temperature experimental data as well as the obtained N_2 purity value. In this PSA simulation, dead volume of the column is extremely important to be considered. Depending on how large the dead volume is, it can affect the performance parameters resulting in undesirable values of recovery or productivity. The bench-scale of this unit column presents 43% of dead volume from the total one. Then, a mathematical model considering dead volume coupled with fixed bed was inserted in order to describe satisfactorily all the experimental steps of the PSA experiments.

2. OBJECTIVE

The purpose of this work focuses on to simulate accurately PSA processes for CO_2 capture from binary gas mixture so that it can provide options of how to improve the performance parameters, considering product purity, recovery, and productivity as the key ones. Also, this work intends to determine and assess adequately essential simulation parameters used for modeling PSA processes for N_2/CO_2 separation using activated carbon as adsorbent. In order to obtain these main objectives, specific objectives were set in place, and they are listed below:

i. Evaluation of the relevant properties of commercial activated carbon on static and dynamic tests.
ii. Validation of the single component isotherm equilibrium models for CO_2 and N_2 at different temperatures.
iii. Comparison of the adsorbed amount of each component predicted by the Extended Sips model and Ideal Adsorption Solution Theory (IAST).
iv. Estimation of the mass transfer coefficient with a simple procedure by means of magnetic suspension balance uptake data, obtained during the adsorption equilibrium measurements.
v. Obtaining breakthrough curves data of pure component and binary mixtures.

vi. Evaluation of the heat of adsorption of CO_2 and N_2 on the microporous activated carbons.

vii. Comparison between the simulated results and the experimental data of breakthrough curves and PSA process.

viii. Evaluation of N_2 recovery with the addition of pressure equalization step in the PSA process.

ix. Assessment of the influence of adsorption step time and dead volume on the column in the PSA performance through simulated data.

3. LITERATURE REVIEW

3.1. Adsorption Fundamentals

Adsorption is a physical or a chemical phenomenon, and it occurs when the gas or liquid is exposed to a solid surface. It can be succinctly defined as the increase in the density of the fluid on the adsorbent surface (Rouquerol *et al.*, 2014). In most cases, the adsorption presents itself as a physical and exothermal phenomenon. This phenomenon is considered as a weak interaction between the surface and the molecules adsorbed. The forces involved in it are van der Waals and electrostatic interactions. The van der Waals contributions are almost always present, and the electrostatic ones only appear when the surface is presented as an ionic structure (Ruthven, 1984).

In chemical adsorption, the phenomenon can be exothermic or endothermic, depending on the nature of the sorbent and sorbate. It is denoted chemical adsorption when, in a process it is observed that strong chemical bonds occur between the surface and the molecules to be adsorbed. Another characteristic of chemical adsorption is the high heat of adsorption released in the process (Rouquerol *et al.*, 2014).

The adsorbed species are called as adsorbates. The solid, where the adsorption occurs on its surface, is known as adsorbent. Since adsorption occurs on a surface, the adsorbent must have a high specific surface area (i.e. large surface area per unit mass or volume). Consequently, high-performance adsorbents tend to be microporous materials with large surface areas (Tien, 1994).

3.2. Activated Carbon

The main advantage of activated carbon for adsorption process application relies on the large volume of micropores, high porosity and consequently its interparticulate high surface area (Tien, 1994). Low-temperature nitrogen adsorption at 77 K is generally used as the first step to characterize the surface properties of activated carbon. Progresses on the interpretation of the results obtained by nitrogen adsorption at 77 K have been made since the appearance of computational techniques, such as molecular simulation or density functional theory. However, the characterization by N_2 adsorption at 77 K is still mainly limited to the determination of the surface area by the BET-method (Rouquerol *et al.*, 2014).

The term activated carbon is given to indicate a microporous material produced from carbon-rich raw materials by some form of chemical or physical activation (Rouquerol *et al.*, 2014). The manufacturing process of activated carbon involves a sequence of different steps. The first steps preparation and production with chemical treatment. Then, the production can be largely increased and starts to be produced from cheap and readily available carbon-containing sources, such as coal, peat, petroleum coke, coconut shell and fruit nuts (Yang, 2003; Rouquerol *et al.*, 2014). The following steps are pelletizing low temperature carbonization and activation.

Activated carbon in adsorption processes is used mainly for gas separation or vapor recovery. The main applications in this gas phase are air purification, solvent recovery, flue gas desulfurization and biogas upgrading. As the only commercial adsorbent used for purification or separation processes that does not require moisture removal, it can also be used in processes to treat aqueous solutions (Suzuki, 1990). Activated carbon is also the most appropriate and used adsorbent for cyclic process separation such as PSA.

3.3. CO_2 capture

There is a worldwide concerning among the scientific society about the CO_2 concentration increase over the decades. The CO_2 levels in atmosphere are alarming, and they tend to keep escalating if mitigation solutions are not taken. Therefore, studies are being developed about how to reduce the CO_2 in atmosphere.

Carbon capture and storage has demonstrated to be a feasible solution to mitigate CO_2 emissions. There are two conventional approaches for CO_2 sequestration from industrial power plants; i) Post-combustion, when CO_2 is captured from power plant flue gases before being released in the environment. It is one of the most used strategies for CO_2 sequestration. Chemical aqueous solutions are widely used in the industrial process, although the high energy penalty in these absorption base processes. Plaza *et al.*, (2010) have presented the performance of an activated carbon for post-combustion separation process by adsorption using technology as VSA, TSA and VTSA. They have shown that the adsorbent has enough capacity to purify N_2 from a dry mixture of 83-17% v/v N_2/CO_2 reaching a CO_2 recovery of 97% and a productivity of 1.9 mol CO_2 kg^{-1} h^{-1} (Table 1).

Table 1 ─ Conditions of the TSA, VSA and VTSA adsorption-desorption cycle

Cycle type	P (bar)	CO_2 recovery (%)	Working capacity (mol kg^{-1})	Productivity (mol CO_2 kg^{-1} h^{-1})
TSA	1.3	40	0.17	0.8
VSA	1.3	87	0.40	1.7
VTSA	1.3	97	0.44	1.9

Source: Modified from Plaza (2010)

Moreover, they have noted that the regeneration process is feasible for a cyclic process due to adsorption working capacity do not decay; it has maintained the respective values presented in Table 1 constant along the number of cycles. Nikolaidis *et al.* (2016) have shown, using simulations, an optimum performance separation for CO_2/N_2 at atmospheric pressure. They have shown results using three different adsorbents (zeolite, activated carbon, and metal organic framework) and all showed good performance on N_2 and CO_2 separation regarding the selectivity. Figure 1 shows the mixture selectivity of CO_2 over N_2 for the three materials previously cited.

Figure 1 ─ CO_2/N_2 selectivity at different temperatures for a) Zeolite, b) Activated Carbon and c) MOF.

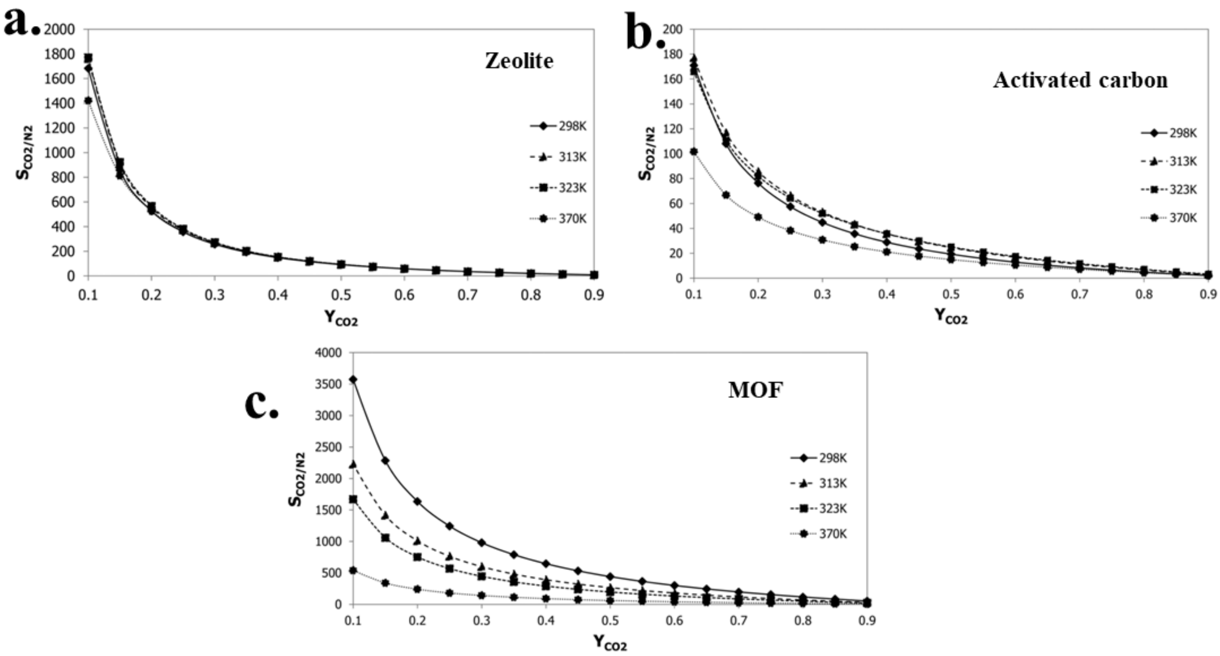

Source: Modified from Nikolaidis (2016)

MOF and zeolites presented better performance and although activated carbon can be used for that separation process, it presented lower selectivity comparing to the other ones. Ben-Mansour *et al.* (2016) have presented also a comparative study using adsorption processes with different adsorbents, such as zeolites, MOF and activated carbon for CO_2 capture from power plants exhaust gases. The activated carbons in the study NCLK3 and NCHA29 have shown a selectivity of 30 and 20, respectively, at 323 K and 1.3 bar. The relative low selectivity for CO_2/N_2 is the main disadvantage of using activated carbon in post combustion adsorption process (Ben-Mansour *et al.*, 2016). However, it is well known that flue gas from coal power plants can present humidity in the gas stream and one of the advantages of using activated carbon as adsorbent for this kind of process is that there is no humidity issue. Conversely, zeolites present great disadvantages, even at very low relative humidity, water molecules interact strongly in this material and it hinders any CO_2 adsorption (Joss *et al.*, 2017).

It can be noted that the authors previously cited presented CO_2 capture studies at low pressures (up to 1.3 bar). This is quite usual due to the exhaust gases are at atmospheric pressure. In that condition, activated carbon does not present a better performance of CO_2 adsorption capacity or selectivity for CO_2/N_2 when compared to others studied materials. However, at higher pressure levels, activated carbon can present promising adsorption performance, even better than zeolites. Activated carbon generally can present higher adsorption capacity at ~310 K at pressures higher than 3.5 bar (Cavenati *et al.*, 2006; Zhang *et al.*, 2009; Grande *et al.*, 2013; Kacem *et al.*, 2015). Hence, activated carbon can have high adsorption capacity for CO_2, presents low cost, little regeneration energy requirement and is insensitive to moisture. ii) Pre-combustion is considered when CO_2 sequestration is performed to upgrade gas fuel, by removing its impurities, increasing its calorific value. Reports have shown that the CO_2 emission could be substantially reduced if the fuel used in power plants was treated before its combustion (Zhao *et al.*, 2017). Schell *et al.* (2013) have presented a promising integrated technology with pre-combustion CO_2 capture in which the emissions levels reach near zero. It is stated that pre-combustion treatment is more adequate to CO_2 capture than post-combustion since, in the latter, the CO_2 adsorption has to be performed at low partial pressure and a large amount of gas has to be treated. Rocha *et al.* (2017) have compared the biogas upgrading (purifying methane) by CO_2 adsorption process using carbon molecular sieve where low, and high pressure processes are compared. It should be noted that high pressure process is advantageous since in most cases, the adsorption capacity of a component increases with pressure. Rufford *et al.* (2012) have reported a review presenting many techniques that can be used to separate carbon dioxide from a gas mixture.

These works describe experiments and simulation of CO_2 capture processes. However, many of them do not make a detailed evaluation of some parameters, such as mass transfer coefficient. For post-combustion analysis, it is quite acceptable to be simulated using empirical models since this kind of process is performed at low pressure (up to 1.2 bar). For pre-combustion CO_2 capture there are many possible pressure levels. Some raw natural gas presents high pressure level at reservoir (40-80 bar), which in this conditions, those empirical and semi-empirical models are not recommended to be used.

3.4. Adsorption Kinetics

Adsorption can be considered a feasible technology for some reasons, including the potential for high capacity and selectivity, fast kinetics, good mechanical properties of sorbents, and stability after repeated adsorption-desorption cycles (Martín *et al.*, 2016). Fast adsorption kinetics is one of the most important features for a dynamic separation process in a fixed bed. The efficiency of a process and the adsorbent loading capacity operating with large adsorbate molar flows are combined with rate of adsorption. Many studies in literature have reported several models to describe the adsorption kinetics of adsorption processes. Due to the complexity involving the phenomenon of kinetics, some approaches were developed to estimate this parameter from experimental data (Serna-Guerrero *et al.*, 2010).

At the microscopic level, the diffusion of the species into the adsorbent structure before the adsorption phenomenon involves in general three different mechanisms (Shafeeyan *et al.*, 2014). Figure 2 shows a schematic illustration of how the molecules should pass through the resistances found in an adsorption process. Firstly, the molecules should flow through an external film that surrounds the adsorbent particle. Depending on the process this resistance can drive a strong influence in fixed bed operations mainly when a low molar flow rate is used. This is known as external fluid film resistance. Then, the molecules must flow through the pores of the particles. The adsorbent can present a structure with several pore size ranges.

Figure 2 – Illustration of the three possible resistances of molecules adsorption into the particle surface.

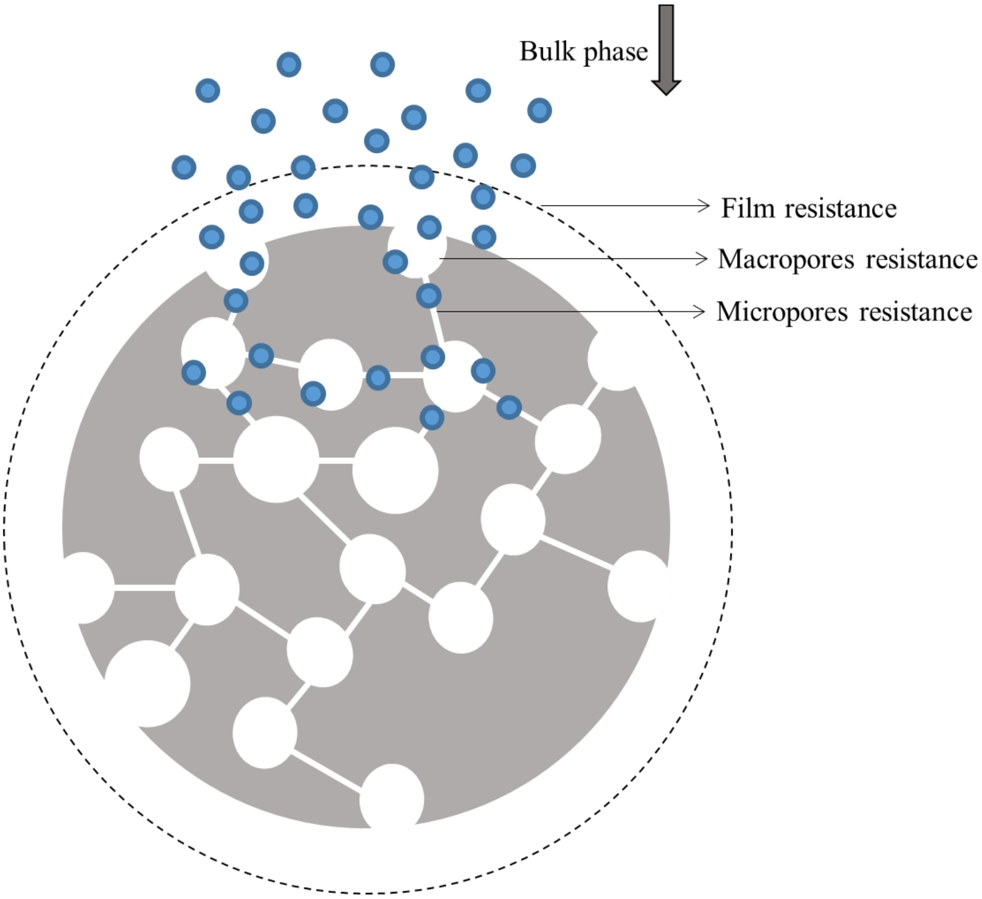

Source: Author

The macropore resistance is defined as the resistance that those molecules acquire through the diffusion into sufficiently large pores. Depending on the size degree of the pores diameter, consequently the mean free path of the adsorbate molecules, transport in a macropore can occur by different mechanisms (Ruthven, 1984). At low pressure, the mean free path of the molecules is larger enough than the pore diameter, so that Knudsen diffusion dominates the transfer mechanism. In this case, the resistance of the mass transfer originates from the collisions between the diffusing molecules and the pore wall. On the other hand, when the mean free path of the molecules is smaller than the pore diameter, the mass transfer resistance is dominated by the molecular diffusion and can be described through Chapman-Enskog equation (Ruthven, 1984; Bird *et al.*, 2006).

Finally, the molecules that have passed through the external film and macropores enter into the micropores of the particle, and another diffusional resistance exists in these pores, called micropore resistance. In these smaller pores, the molecules interact with the particle surface due to the small pore diameter and consequently the force field of the pore wall. For microporous solids, the mass transfer resistance is commonly dominant in those pores. Hence, in those cases, it has been considered that the dominating step for the diffusion of species occurs in this pore size range. The external mass transfer and the resistances in broader pores are therefore neglected (Srinivasan *et al.*, 1995; Cavenati *et al.*, 2006; Delgado *et al.*, 2014).

Although the diffusional models describe a more realistic behavior of the intraparticle adsorption kinetics, simpler mathematical expressions are desirable. Adsorption process simulation needs to be fast and at the same time respond with a good agreement to the experimental results. More straightforward assumptions can make the model more practical and reproduce results with the same accuracy. Linear Driving Force approach was first proposed by Glueckauf & Coates (1947) and still is the most used and acceptable model to describe the adsorption kinetic phenomenon with accurate results. In this approach, the overall resistances (external film, macro, and micro) to mass transfer are lumped into an effective uptake rate coefficient, commonly denoted as k_{LDF}.

3.5. Adsorption Equilibrium Isotherms

Adsorption equilibrium isotherms of species are essential information to understand the adsorption process. They allow the understanding of how the molecules can interact with the adsorbent. Adsorption uptake experiments can be used to study the adsorption equilibria of a single component, as it will be shown later, besides the equilibrium and kinetics of a multi-component system and its selectivity (Do, 1998). Usually, adsorption isotherms are represented by plotting a graphic with adsorbed amount per mass of adsorbent against the total pressure (or concentration) of the components at constant temperature.

The fundamentals of the pure component adsorption rely on the most basic theory in adsorption, known as Langmuir theory. (Langmuir, 1918) has established the monolayer surface adsorption on an ideal surface, as the main hypothesis for his model. Furthermore, the model was defined, based on underlying principles such as adsorption on a plane surface, having only one kind of adsorption site, and each site can hold only one adsorbed molecule on it. So, these molecules are adsorbed in a well-defined localized site, all of them are energetically equivalent, and there is no interaction between the other adsorbed molecules in their vicinity.

3.5.1. Heats of Adsorption

Heats of adsorption derived from calorimetric methods are based on the measurements of the heat released when an amount of molecules is physically adsorbed onto a surface. The most common way to determine the heats involved in the process experimentally is through the measure of the temperature rise of the solid. Moreover, the determination of heat of adsorption in a microcalorimeter does not measure only the magnitude of the released heat but also its variation upon increasing coverage. This is useful to understand the type of adsorbate-adsorbent sites bonding and its evolution according to the surface heterogeneity (Auroux, 2013).

This direct calorimetric method for measuring the heat of adsorption is commonly defined as the integral heat (Q_{int}). It is the heat released when molecules are adsorbed at a constant temperature in a closed gas-solid system. Integral heats normalized to the adsorbed amount (q) can be described according to the following equation:

$$H_{ads}^{\text{int}} = \frac{Q_{\text{int}}}{q} \tag{1}$$

Where H_{ads}^{int} is a heat of adsorption averaged value, and it refers to the thermal response of the all particle surface. By plotting the integral heats according to the adsorbed amount, the so-called integral heats curve can be obtained. This curve is also called by calorimetric isotherm. Hence, differently from equilibrium adsorption isotherm, the curve plotted from the origin up to a measured pressure gives the total heat released since the surface of adsorbent is free of adsorbate.

In case other than this particular one, H_{ads}^{d} can be obtained by differentiating the non-linear integral heat as function of the adsorbed amount. Differential heats represent a reasonable measure of the energy interaction between a molecule and an individual site (Auroux, 2013). The magnitude of the heat evolved in this case depends on the relation between adsorbate-adsorbent sites bonding and varies according to increasing coverage. The results of this differentiation can be observed as a consequence of the presence of the heterogeneous distribution surface sites. Differential heat of adsorption is described from Equation (2).

$$H_{ads}^{d} = \frac{\Delta Q_{\text{int}}}{\Delta q} \tag{2}$$

This method is based on the use of partial molar heat amount, the ratio of the integral heat against the correspondent adsorbed amount for incremental doses of the gas in the system. By plotting the history of heats of adsorption, $\frac{\Delta Q_{\text{int}}}{\Delta q}$ values, as a function of the adsorbed amount, the evolution of the heat of adsorption can be obtained. By taking the middle point of this interval, it means the heat value correspondent to small portions of the surface. This is properly represented as a reasonable measure of heat of adsorption in function of adsorbed amount (Auroux, 2013).

3.6. Fixed Bed

Adsorption process in fixed bed allows understanding the dynamic behavior of separation processes involving gas mixture. The fixed bed consists of a column filled with the solid adsorbent, the gas mixture enters at one end, and the adsorption of the target mixture occurs. However, the adsorbent inside the column must be regenerated first, and be free of any contaminants. If one starts from a bed initially filled with an inert component, the typical dynamic response will be: for a given time no component will leave the column, then the less adsorbed component will start to leave the column at a molar flow-rate higher than its feed molar flowrate (if there is competition), then the bed will be fully saturated, and the outlet stream becomes the same as the feed stream. The response for this process, in terms of concentration against time, is called breakthrough curve.

The breakthrough curve for a gas containing sorbates can be obtained by the solution of the mass, heat and momentum equations for bed and adsorbent particle, with the aid of the adsorption equilibrium isotherm. The shape of the breakthrough curve is determined by the nature of the adsorption isotherm. These elements make the front of concentration less or more dispersed commonly in the axial direction (Yang, 1997). Furthermore, the mass and heat transport process in the bed and the particles can also affect the shape of the curve as the front of concentration passes through the column, the shape changes. The feed is usually stopped when the more strongly adsorbed component breaks through. Important studies about the dynamic behavior of adsorption process by gas mixture have been published by several authors (Dantas *et al.*, 2011; Casas *et al.*, 2012; Mulgundmath *et al.*, 2012; Won *et al.*, 2012;

Rios *et al.*, 2014; Ben-Mansour *et al.*, 2017; Grande *et al.*, 2017; Siqueira *et al.*, 2018a). Recently, Knox *et al.* (2016) studied in more detail the breakthrough curves and their particularities, the results have demonstrated the limitation of the use of these data.

3.7. Pressure Swing Adsorption

Pressure Swing Adsorption (PSA) is a cyclic adsorption process, which allows continuous separation of gas streams. PSA is performed by periodic changes of pressure aiming at the optimization of contaminants removal and is considered viable for capture of CO_2 from flue gases.

As in all adsorption separation processes, the essential requirement for this process relies on the choice of a suitable adsorbent, preferentially adsorbing one component, or a family of related components, from a gas mixture. All the cyclic processes involve two main steps; adsorption and desorption. As most adsorption isotherms present favorable curve shape (as shown in Figure 3), the adsorption process generally occurs at high pressure, in which this condition is beneficial for the adsorption of the target species. The desorption step happens in order to remove the adsorbed components so that the fixed bed reaches a regenerated condition for the next adsorption step.

Figure 3 — Adsorption equilibrium isotherms showing the CO_2 loading according to changes of pressure and temperature.

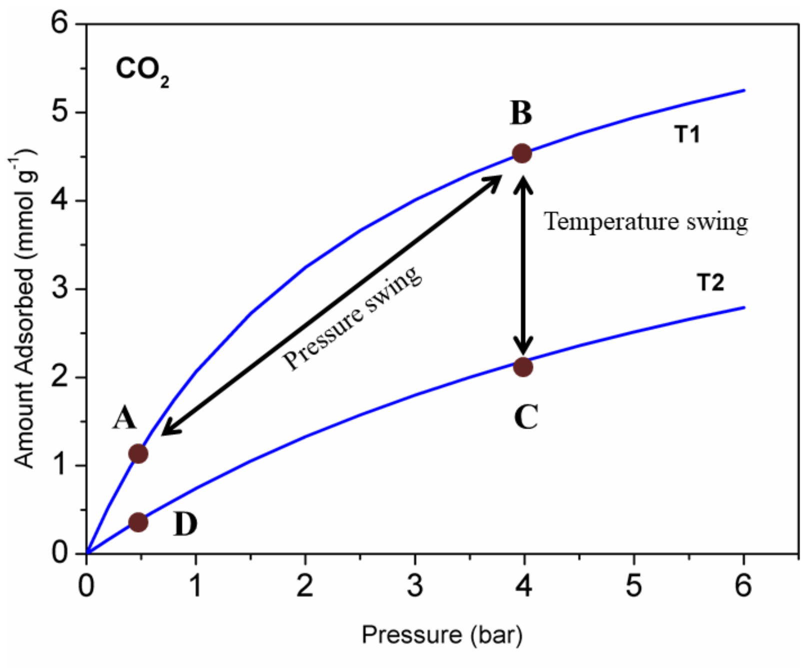

Source: Modified from Siqueira *et al.* (2017)

The basic concept of cyclic process can be seen in Figure 3. Adsorption equilibrium isotherms of CO_2 on activated carbon are presented, at different temperatures, in which T1 < T2. At the beginning of a PSA process, the operating pressure is increased to the high pressure (A to B). Pressurization and feed steps operate at high pressure, and during this steps the light product is produced pure, while the more adsorbed one is retained in the bed. The essential feature of PSA process is that during the regeneration step, at low pressure, the preferential adsorbed specie is removed. That is, when the system changes from point B to A. PSA can be modified by swinging temperature also, to help the efficiency of the regeneration step. As in Figure 3, if the system that is in a certain condition according to point B, cannot be moved to point D by changing pressure only. It will need a temperature rising so that the D condition can be reached. This process is the so-called Pressure Temperature Swing Adsorption (PTSA). Moreira *et al.* (2017) studied a PTSA process to remove CO_2 from natural gas. This approach seems to be very advantageous due to the adsorption and desorption happen in the maximum favorable conditions of both steps. However, this process needs a more sophisticated assessment of the energy requirement to reach the desirable products.

The major advantage of PSA, concerning the other types of separation processes, is that the pressure of the system can be changed faster than the temperature. It makes possible to operate PSA processes on short time cycles. However, PSA has also its limitations. On a large scale PSA unit, it is recommended to operate with adsorbent presenting high selectivity and species strongly adsorbed. However, strong bonds of the adsorbed molecules to the adsorbent make the process economically unfeasible, requiring high energy demand to regenerate the column, such as vacuum application on the system. For this kind of process, temperature swing seems to be the more appropriate process to reach the desirables results.

For air drying, the interesting experiment performed by (Skarstrom, 1960), referred initially as heatless adsorption, uses a two-bed apparatus as shown in Figure 4. The cycle comprises four basic steps and is shown schematically in Figure 5 for better understanding.

I. Pressurization;

II. Feed (Adsorption);

III. Countercurrent depressurization (Blowdown);

IV. Countercurrent purge.

The two beds operate under these four steps and in sequence (Figure 5). They do in such a way that they are well synchronized in order that one is in the production step while the other adsorbent regeneration step. As shown in Figure 5, step 1, bed 1 is pressurized with the feed to the desired operating pressure. The description of each step of the cycle is presented below.

I. Pressurization: This step is commonly performed by the gas mixture to be treated. The column outlet is closed during this step. It is finished when the column pressure reaches the set adsorption pressure (next step), which means that the pressurization time is controlled by the operator. Beside the maximum pressure chosen by the operator, pressurization step duration also depends on the gas mixture molar flow rate.

II. Adsorption (Feed): In this step the column outlet is open and the column continues to be fed with the gas mixture. Adsorption step is performed with constant pressure keeping the feed molar flow rate constant. The pressurization and adsorption flow rate are not necessarily the same; the flow rate can vary if the pressurization step is operated with light product only. Adsorption is the most important step of a 4-step cycle, which is when the separation of the gas occurs. The duration of feed step can be chosen by the operator depending on the affinity between adsorbent and the stronger adsorbate specie.

III. Blowdown: In this step, the column outlet is closed again and the column inlet is kept opened. This time the gas is released to the environment (atmospheric pressure). The velocity of gas flow is too high. For a synchronized PSA process this step must have the same time of the pressurization step. Blowdown aims to remove the heavy product of the column by decreasing the pressure since at the end of the adsorption step the column is practically full of the heavy component (CO_2 in this case).

IV. Purge: The purge step as the name suggests aims to clean the column. Reminiscent impurities left after the blowdown step are removed by the one fraction of the light product, produced in the feed step. The gas flow rate in this step is commonly countercurrent. The column is filled with light product, and the partial pressure of the heavy product is decreased, which promotes its desorption.

The bed to bed equalization step is also one of the most used steps in a PSA process although not essential to perform it. During the equalization step two or more columns are connected together at a moment during the PSA cycle to equalize their pressures between each other. Equalization step is common done after the adsorption step for depressurization equalization and after a regeneration step for pressurization equalization. A history of pressure is presented in Figure 6 when equalization steps are used in a PSA cycle.

Figure 4 ─ Schematic two-bed PSA unit used in Skarstrom cycle.

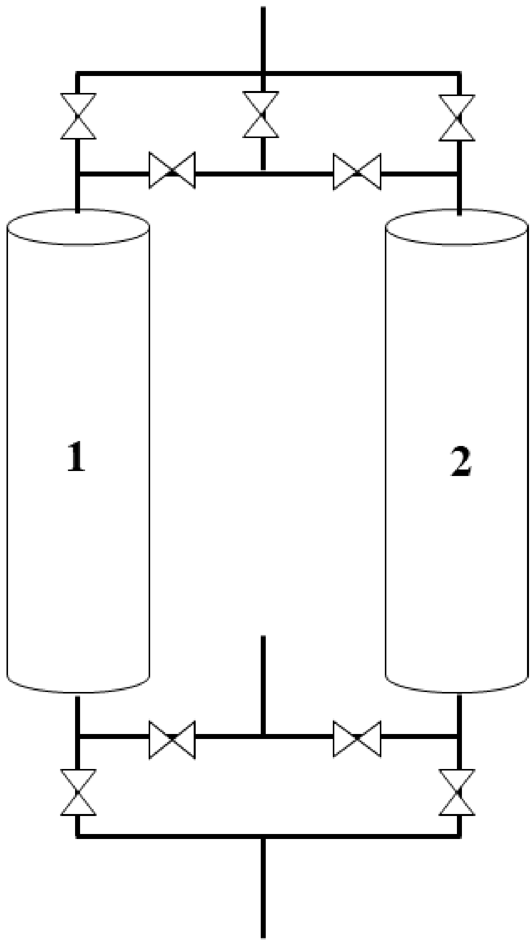

Source: Author

Figure 5 ─ Step sequence of a PSA Skarstrom cycle.

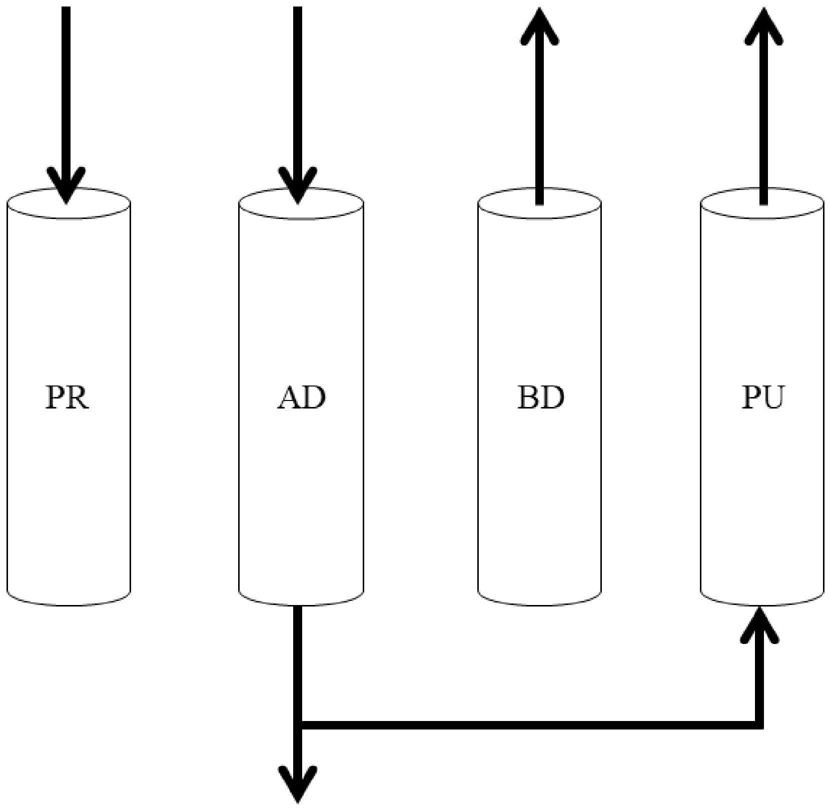

Source: Author

There are three performance parameters, for a PSA system, that evaluate both advantages and limitations of the technology and thus determine the feasibility for a given set of operating conditions.

a. Product Purity: The less adsorbed component can be recovered in its very pure form. The extract product (heavy component) is generally discharged in impure form. The process is commonly used when a high purity light product is desired.

b. Product Recovery: The recovery consists of the fraction of the light component on the feed stream that is recovered as (pure) light product; which is the ratio of the amount of pure product that leaves the column minus the amount of light product used in the purge step to the amount of the same component that enters during the pressurization and feed steps.

Figure 6— Diagram of pressure history in a PSA process with equalization steps.

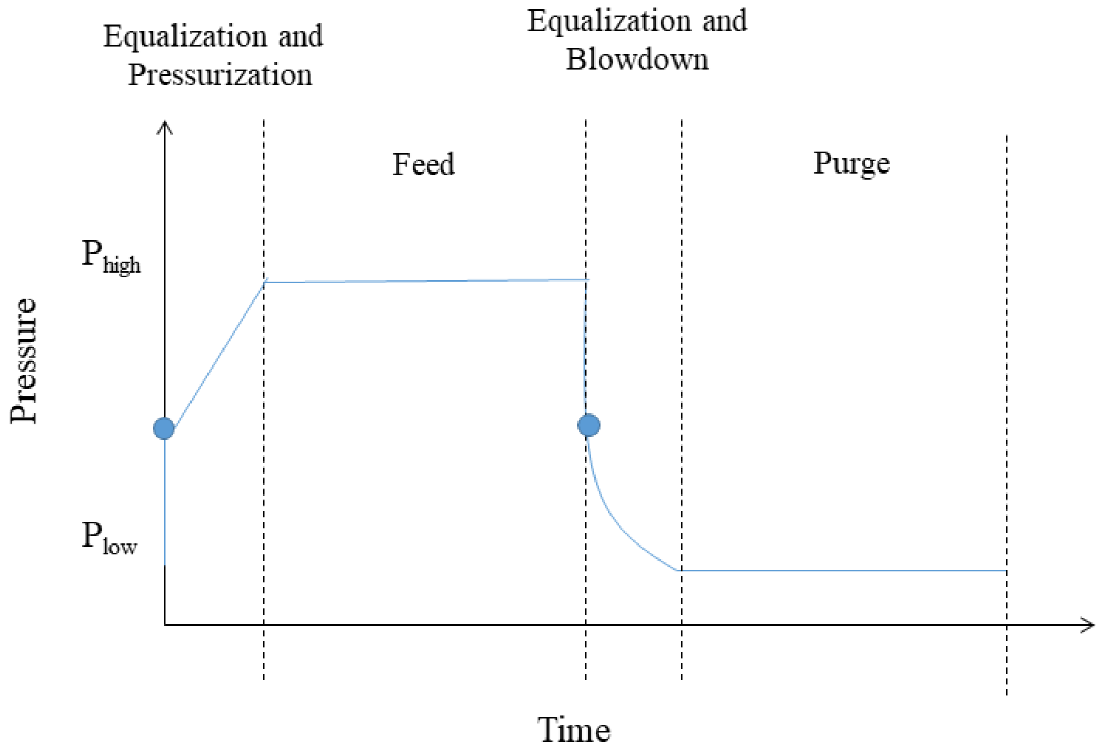

Source: Author

c. Adsorbent Productivity: The productivity is calculated by the amount of product or feed mixture processed per unit of adsorbent mass per unit of time. For a given separation, the size of the adsorbent bed can be inversely proportional to the sorbent productivity (Yang, 1997).

It is important to keep in mind that these parameters are interrelated for any PSA process and the interrelationship can be determine through a process model. Also, it is know that to improve the results of such process, high purity, recovery and adsorbent productivity are desirable. However, it is hardly possible to achieve such performance, since to improve one of these parameters another will be negatively affected.

3.7.1. PSA model

To assess a PSA unit performance at different operating conditions it is necessary to develop a mathematical model so that it can be used to predict the dynamic behavior of the unity accurately. Such procedure in a large scale unit can require large amount of experiments, which can take long time and be expensive. A simulation process of PSA unit uses parameters previously assessed and makes it possible to predict the performance of a PSA process (product purity, product recovery, and productivity) using different operating conditions and different cycles.

A fixed-bed mathematical model, previously validated against breakthrough experimental data, is crucial to develop the PSA mathematical model. This model is capable to estimate the molar concentration of each component at any moment during the PSA cycle. Furthermore, the temperature history observed at the interior of the column can also be predicted.

Generally, the model that describes the dynamic behavior in a fixed bed comprises of several partial differential equations which represent the mass, energy, and momentum balances, coupled with the respective boundary and initial conditions.

3.8. Case study consideration: pressure swing adsorption simulation

Adsorption separation processes involve two basics steps: 1) adsorption, where the gas production is acquired; and b) desorption, where the fixed bed is regenerated in order to start a new adsorption process. The first complete study about PSA was presented by Skarstrom (1960) and it intended to separate O_2 from air. This process is considered the most basic process of a PSA process because involves the minimum number (two) of columns and four steps. Since then, innumerous studies have been developed along the years in order to understand and optimize that cyclic process. Many adsorbents were studied such as, zeolites, activated carbon, metal framework, silica, etc. As well, many processes were also performed for different gas composition; flue gas, dry flue gas, biogas, syngas, etc.

Even the most basic cyclic process evaluation requires a large volume of gas and time consume to be assessed. In this context, it was wisely developed numerical simulations to rapidly represent the experimental behavior of those processes. For such simulations, a variety of experiments and determination of parameters have to be considered. The most important information to start evaluating a PSA process relies on the adsorption equilibrium measurements. To describe such experimental data there are equilibrium models that represent very well the adsorption capacity of a material; Langmuir (Langmuir, 1918), Sips (Sips, 1948) and Toth (Toth, 2001). Then, the kinetics of the adsorption process is also important for simulation, especially when the process separation is not ruled by the equilibrium. The dual process of adsorption and desorption also involves temperature variation, the amplitude of this temperature swing depends on the heat of adsorption. A study about heats of adsorption is also essential to optimize the simulation performance of this process. This may arise in an expansion or pressurization step and also from intrinsic heat of adsorption of the component on the material. These terms appear in the energy balance that is used in simulation. The heat of adsorption information can be useful to schedule operation or to know the regeneration time required for the process (Sundaram & Yang, 1998). The first studies in which investigated the effects of the nonisothermality in these processes were conducted by Chihara & Suzuki (1983). Since then, more realistic simulation to describe PSA processes were performed when energy balance and heats of adsorption are used for such process.

Another important feature to be considered in simulation of dynamic tests in a fixed bed is the dead volume at both feed end and product end of the column. Simulations of breakthrough curves can be erroneous described if the dead volume in the column is large enough. Depend on the system total pressure or gas velocity, a large dead volume interferes on the result of the breakpoint and carries out incorrect responses. Dead volume in PSA columns affects the steps of the cyclic operation in different ways (Ruthven *et al.*, 1994).

In this study, we will demonstrate the relevance of a good determination of the model parameters in order to describe experimental data by simulation process. Different total pressures will be evaluated to guarantee that the simulation can describe the dynamic process in any condition. IAST will be used to predict adsorption of binary mixture. There are very few studies in that IAST model will be directly implemented in gProms avoiding use of empirical and semi-empirical models for binary mixture, in which the latter ones cannot satisfactorily describe the mixture adsorption at some conditions. Dead volume is also applied directly in the software to avoid mistakes in the simulated results. This is an underestimated consideration but extremely relevant to simulate commercial PSA process and it is taken into account in this study to show the influence in the performance parameters of a PSA process.

4. EXPERIMENTAL AND THEORITICAL APPROACH

4.1. Materials

The textural properties of three commercial activated carbons were evaluated in this study; Charbon 500 (*Fábrica Brasileira de Catalisadores, Brazil*), Filtron N and Norit RB4. All of them presenting granular shape, except Norit RB4 (pellets). Firstly, they were characterized by N_2 and CO_2 adsorption-desorption isotherms at 77 K and 273 K, respectively, with the aid of an Autosorb 1-MP instrument (by Quantachrome, USA) in order to determine the specific total pore volume, micropore volume and BET surface area according to the literature (Rouquerol *et al.*, 2014).

N_2 and CO_2 were the adsorptive gases used in the experiments and were provided by *White Martins Praxair Inc. (Brazil)* presenting purities of 99.99% and 99.999%, respectively. Helium was used and is considered a non-adsorptive gas with purity of 99.999%. It was used as a carrier gas in the chromatography analysis and breakthrough curve experiments, also for correction of the buoyancy effects in the magnetic suspension balance.

4.1.1. Specific Total Pore Volume

The specific total pore volume of the particle was calculated by Equation (3) through the N_2 isotherm data at 77 K. To do so, the isotherm measurements were performed up to maximum relative pressure of nitrogen, where $P/P_0 \approx 1$.

$$\hat{V}_p = \left[q\frac{MM}{\rho} \right]_{N_2} \tag{3}$$

Where q denotes the N_2 adsorbed amount per mass unit at the relative pressure, MM is the molar mass and ρ denotes the density of nitrogen at liquid state.

4.1.2. Micropore Volume

The total micropore volume is determined by the Dubinin-Radushkevich model presented in Equation (4) (Rouquerol *et al.*, 2014).

$$\log_{10} n = \log_{10} n_\mu - D\log_{10}^2 \left(P_0/P\right) \tag{4}$$

Where n_μ is the adsorbed amount in the particle micropores. D is an empirical coefficient. P_0 is the saturation pressure of the gas and P denotes the pressure. By plotting $\log_{10} n$ against $\log_{10}^2 \left(P_0/P\right)$, a straight line was obtained with a regression coefficient where the term $\log_{10} n_\mu$ can be found. A range of relative pressure from 10^{-5} to 0.4 is suggested to apply Equation (4) since isotherm data from relative pressure below 10^{-5} can represent the ultramicropore region and above 0.4 the mesoporous one. Then, the total micropore volume can be calculated according to Equation (5).

$$\hat{V}_{\mu} = \left[n_{\mu} \frac{MM}{\rho} \right]_{N_2} \tag{5}$$

Microscopic treatments such as density functional theory (DFT) allow to describe the configuration of the adsorbed phase at molecular levels. They are considered a more reliable approach for providing pore size analysis over their complete range (Thommes *et al.*, 2015). The fluid-solid interaction potential is dependent on the applied pore model. Non-local density functional theory (NLDFT) based methods for pore size analysis of nanoporous materials are available and it was used to obtain the pore size distribution of the activated carbons in study.

4.1.3. Specific Surface Area

The specific surface area was determined through the Brunauer-Emmett-Teller (BET) model (Equation (6)) (Rouquerol *et al.*, 2014).

$$\frac{(P/P_0)}{n_{ads}\left[1-(P/P_0)\right]} = \frac{1}{n_m C_c} + \left(\frac{C_c - 1}{n_m C_c}\right)(P/P_0) \tag{6}$$

Where n_{ads} is the adsorbed amount, n_m denotes the adsorbed amount of nitrogen in a monolayer, C is an empirical coefficient from BET equation and P_0 denotes the saturation pressure at the temperature of the experiment.

Analogous to the Equation (4), by plotting $\frac{(P/P_0)}{n_{ads}\left[1-(P/P_0)\right]}$ against (P/P_0), a straight line was obtained with a regression coefficient where the term n_m can be found. Hence, this parameter is applied in the Equation (7).

$$a_{BET} = n_m N_A \sigma \tag{7}$$

Where a_{BET} denotes the surface area of the adsorbent, N_A represents the Avogadro number and σ is the average area occupied by each molecule of N_2.

4.2. Heats of Adsorption

The determination of CO_2 and N_2 adsorption enthalpy was performed by a Tian-Calvet microcalorimeter (Setaram C80) coupled to a manometric setup. This set-up measures simultaneously the adsorption equilibrium and the differential heat of adsorption with the increasing coverage. The heat measurement data were continuously measured in each increment of pressure added. The differential heat of adsorption data has been plotted by taking the average of the partial molar heat for the different pressure steps as a function of the adsorbed amount (Bolis *et al.*, 2004; Auroux, 2013). The experiments were carried out at 298 K in a pressure range of 0.05 to 1 bar after outgassing under high vacuum at 393 K.

4.3. Equilibrium and uptake measurements

4.3.1. Experimental

The static adsorption experiments of pure CO_2 and N_2 at 298 K, 323 K and 348 K were performed using a *Rubotherm* (Bochum, Germany) magnetic suspension balance equipped with a gas dosing unit. The experimental setup (Figure 7) consists of a balance coupled with a measuring cell, a data acquisition system, a thermocouple, a thermostat bath (temperature controller), and a vacuum pump. An adsorbent mass of around 0.65 g was used per sample. Prior to each measurement, samples were outgassed at 423 K for 6 hours (heating rate of 2 K min^{-1}) under vacuum (0.001 bar).

Figure 7 ─ Schematic illustration of the magnetic suspension balance.

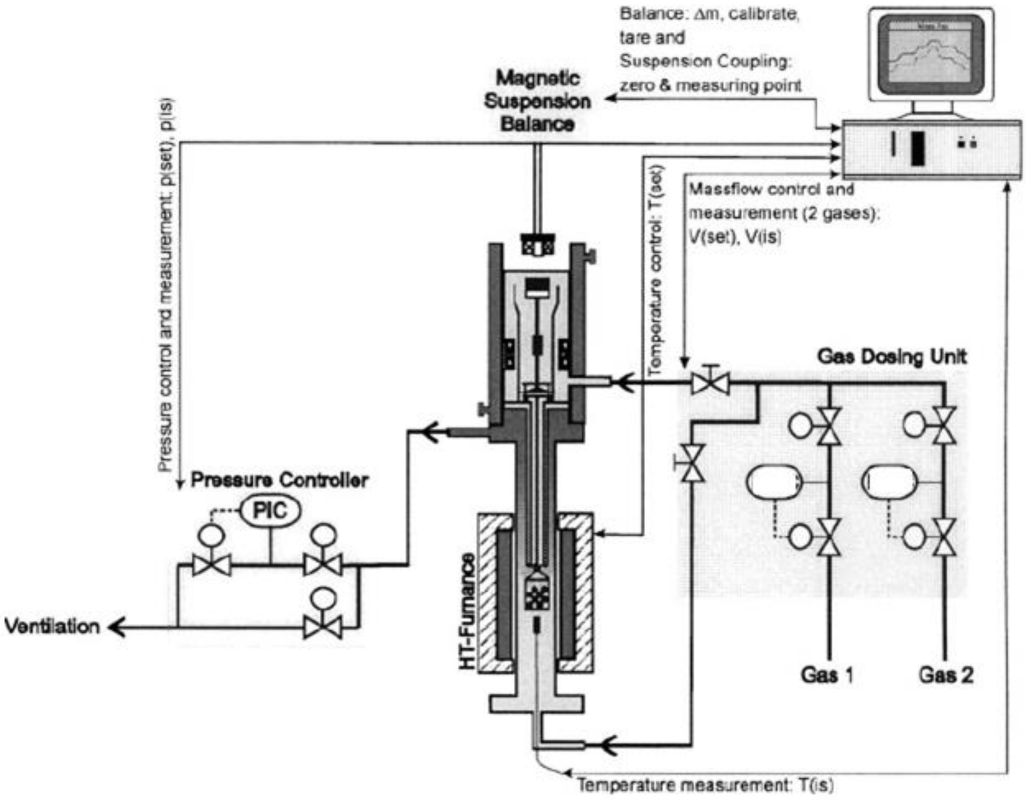

Source: Keller & Staudt (2005)

For each pressure step, sample mass variation was continuously measured until equilibrium was reached, which was considered, by reasonable assumption, when a mass variation of less than 1×10^{-4} g for at least 30 min was observed. The data for mass variation with time was used to estimate mass transfer coefficients, as to be described later.

Due to gas density variations with pressure increase, buoyancy effects acting on the suspended components and sample solid phase (+ adsorbed phase) inside the measuring cell were taken into account. This was done by previous calibration measurements with helium at 298 K in the pressure range of 0–12 bar with and without adsorbent sample. The absolute component adsorbed concentration (mmol per g of adsorbent mass) was determined according to Equation (8) (Murata *et al.*, 2002; Brandani *et al.*, 2016).

$$m\left(P,T\right) = m_{exc}(P,T)+\frac{\rho_b\left(P,T\right)V_{ads}}{m_{sol}\ MM} \tag{8}$$

Where m and m_{exc} are the absolute adsorbed amount and the excess adsorbed amount (mmol per g of adsorbent mass) at each measured point at current pressure, respectively. The calculation of excess adsorbed amount per mass unit is often used in literature and the detailed equation can be found elsewhere (Dreisbach *et al.*, 1999; Bastos-Neto *et al.*, 2005; Keller & Staudt, 2005), ρ_b is the bulk density (at a fixed pressure and temperature) of the fluid phase surrounding the adsorbent. Bulk density was obtained experimentally by direct measurement with the same apparatus. V_{ads} represents the volume of the adsorbed component in the pores, that was here considered equivalent to the micropores volume, MM represents the molar mass of the component and m_{sol} denotes the dry adsorbent mass.

4.3.2. Equilibrium Isotherm Model

Differently from Langmuir's theory, according to Freundlich, the total amount adsorbed in the particle will increase as long as the pressure increases, that is, the maximum loading in the particle depends on the pressure and consequently the temperature. Sips proposed a model following Freundlich assumptions but also according to Langmuir's theory, in which there is maximum adsorbed amount independent of pressure. Hence, Sips equation (Equation (9)) is also known as Langmuir-Freundlich, since he lumped the two theories in one equation. This model is simple and vastly used to describe the adsorption equilibrium model. Sips model can be described as follows.

$$\theta = \frac{(bP)^{1/n}}{1+(bP)^{1/n}} \tag{9}$$

$$b = b_0 \exp\left(\frac{\Delta \mathrm{H}_{ads}}{RT}\right) \tag{10}$$

Where θ has the same meaning from the Langmuir equation and $1/n$ is related to the surface heterogeneity. Although Sips equation was originally proposed as an empirical equation, it is derived from theoretical assumptions (Do, 1998). The Sips model parameters b, q_m and $\frac{1}{n}$ was determined as follow Equations (10) (11) and (12), respectively.

$$q_m = q_{m,0} \ \exp\left[\chi\left(1-\frac{T_g}{T_0}\right)\right] \tag{11}$$

$$\frac{1}{n} = \frac{1}{n_0} + \kappa\left(1-\frac{T_0}{T_g}\right) \tag{12}$$

The model parameters were determined by a solver tool from Microsoft Excel to give the best fit to the experimental adsorbed amount at each pressure by minimizing the sum of the relative errors as the objective function (Equation (13)).

$$\%E = \frac{100}{N}\sum_{i=1}^{N}\left|\frac{q_{exp} - q_{calc}}{q_{exp}}\right| \tag{13}$$

where q_{exp} and q_{calc} denote the experimental and calculated adsorbed amount of the component, respectively, N is the number of measured points. The fitting procedure was performed simultaneously for the three temperatures.

However, the most reliable method to determine the multi-component equilibrium relations from single component isotherm is the Ideal Adsorption Solution Theory (IAST). It was first introduced by (Myers & Prausnitz, 1965) and may be used to predict the competing adsorption behaviors at equilibrium of multicomponent gas mixture. The theory is based on the concept of an ideal adsorbed solution analogous to Raoult's law (Clarkson & Bustin, 2000).

$$P\,y_i = P_i^0(\pi)\,x_i \tag{14}$$

Where P is the total pressure, y_i is the molar fraction of component i in the bulk phase, P_i^0 denotes a hypothetical pressure in the standard state of component i that results in the spreading pressure (π) of the mixture, x_i represents molar fraction of the component in the adsorbed phase.

In order to determine the spreading pressure for pure component in its standard state, an expression derived from the Gibbs free energy is developed as follows (Myers & Prausnitz, 1965; Buss, 1995).

$$\frac{\pi A}{RT} = \int_0^{P_i^0} \frac{q_i^0}{P} dP \qquad (15)$$

In Equation (15), q_i^0 is the adsorbed amount of pure component, A is the adsorbent surface area. In the standard state, the surface potential of the mixture is equal to the surface potential of each single component (Rudziński *et al.*, 1995; Do, 1998).

The spreading pressure must be the same for each component and q_i^0 can be expressed by an adsorption equilibrium equation as Sips, Toth, Langmuir, etc. The solution for that equation allows to find a relation between spreading pressure (π) and the standard pressure of each component (P_i^0).

For an ideal solution, the total amount adsorbed in the mixture can be determined by the expression (Equation (16)) (Do, 1998; Clarkson & Bustin, 2000).

$$\frac{1}{q_T} = \sum_{i=1}^{n} \frac{x_i}{q_i^0} \qquad (16)$$

In Equation (16), q_T is the total loading of the mixture. It is possible to calculate the adsorbed molar fraction when the total pressure, temperature and molar fraction of each component in a mixture are known. A system of equations involving the single component isotherm model and Equations (14), (15) and (16) are required to find the values of adsorbed amount of each component. Then, at equilibrium, the adsorbed concentration can be found by the expression:

$$q_i^* = x_i \, q_T \qquad (17)$$

The main concern about IAST application regards the sensitivity to the accuracy of pure component isotherms used to fit experimental data. At low pressure a little variation on the slope of the isotherm can result in a very different result when the integration of the equation is solved. Therefore, it is crucial to obtain reliable experimental measurements of adsorbed amount for single component isotherm at low pressures (Rota *et al.*, 1993).

4.3.3. Adsorption kinetic model

For microporous solids, the mass transfer resistance is commonly dominant in the micropores. Thus, it has been assumed that the controlling step for the diffusion of species occurs in this pore size range and the external mass transfer resistances are therefore neglected (Srinivasan et al., 1995; Cavenati et al., 2006; Delgado et al., 2014; Shafeeyan et al., 2014). The mass transfer coefficient was described by the LDF approach as shown in Equation (18).

$$k_{LDF} = \frac{\Omega D_\mu}{r_\mu^{\ 2}} \tag{18}$$

where k_{LDF} is the LDF mass transfer coefficient, Ω is the dimensionless LDF factor, D_μ and r_μ denote the micropore diffusivity and radius, respectively.

Equation (19) was used to describe mass transfer inside an adsorbent particle subject to a given bulk gas phase pressure and temperature. It is analogous to the approach proposed by Glueckauf & Coates (1947), by averaging radial gradients based on a linear driving force (LDF) approximation (Chatterjee & Schiewer, 2014; Yao & Chen, 2015).

$$\frac{\partial \overline{\overline{q}}_i}{\partial t} = k_{LDF}\left(q_i^* - \overline{\overline{q}}_i\right) \tag{19}$$

where $\overline{\overline{q}}_i$ is the volume-averaged adsorbed concentration and q_i^* is the adsorbed concentration in equilibrium with the gas phase concentration.

Pressure variation of the system was constantly measured with the aid of sensors. Equation (20) was used to describe the pressure history after each gas pressure increment. The initial condition is assumed equal to the equilibrium condition of the previous experimental data.

$$P(t) = \frac{P_f - P_0}{\Delta t} \tag{20}$$

where P_f and P_0 is the final and initial pressure, respectively, and Δt is the time variation between both pressures.

By integrating Equations (19) together with the isotherm equation (Equation (9)) and a suitable initial condition, it is possible to estimate the k_{LDF} parameter by matching the calculated adsorbed concentration history with the experimental uptake data obtained gravimetrically (Siqueira *et al.*, 2018b).

4.4. Fixed bed

4.4.1. Experimental

A fixed bed unit was used to perform the breakthrough curves experiments at different pressures, which is presented in Figure 8. The gas mixture composition at the bed outlet was measured by a Gas Chromatograph 580 Series (Gow-Mac Instruments Co., USA).

Figure 8 ─ Schematic diagram of the fixed bed unit (MFC: Mass Flow Controller; TC: Thermocouples; BPC: Back-Pressure Controller; MFM: Mass Flow meter; P: Pressure Sensor; GC: Gas Chromatograph).

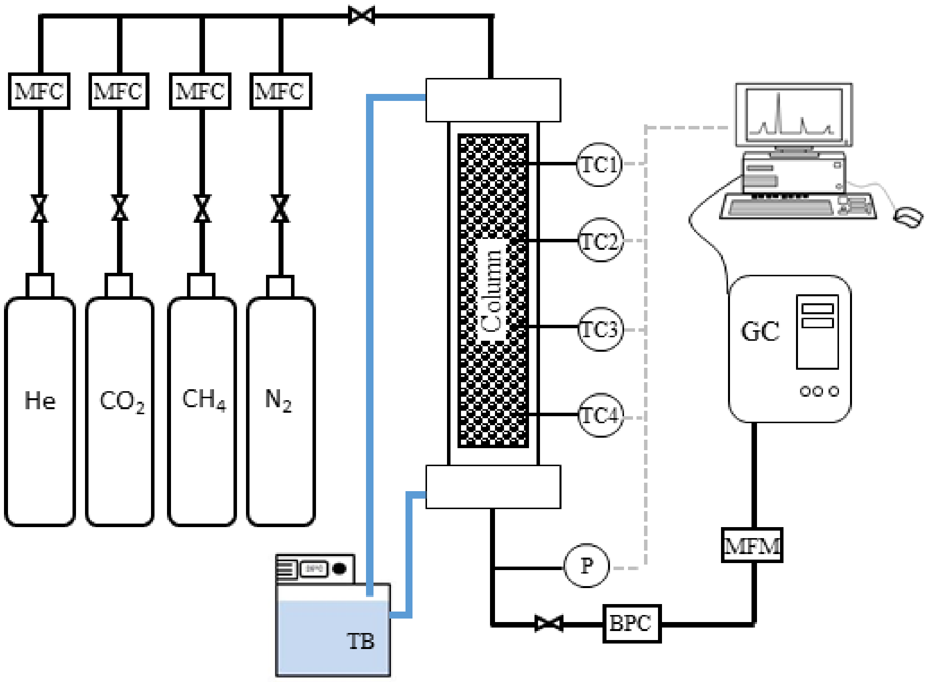

Source: Author

The pressure inside the system was measured at the bed outlet. A back-pressure controller (BPC) was used to keep the pressure constant inside the column. The bed was kept at a constant temperature of 298 K by a thermostat water bath (TB) with a continuous flow rate. Four K-type thermocouples (TC1 – TC4) are distributed along the column in equal distances (0.150 m, 0.275 m, 0.400 m, 0.525 m) to measure the temperature inside column in order to obtain the temperature distribution during the experiment. Features of the packed column is presented in Table 2.

Table 2 ─ Properties of the fixed bed.

Column length	0.955 m
Inner diameter	0.028 m
Wall thickness	2.8×10^{-3} m
Wall density	7400 kg m^{-3}
Wall specific heat capacity	470 J kg^{-1} K^{-1}

Source: Author

Before all the experiments, the fixed bed was heated to around 423 K under vaccuum (2 Pa) for six hours in order to regenerate the solid adsorbent. Initial condition was established by flushing the column with Helium at a constant flow rate and constant pressure for each experiment. Table 3 summarizes the operating conditions of the tests, which were also used in the model to simulate the breakthrough curves. Mass flow controllers (MFC) were used to control individually the flow of CO_2, N_2 and He, keeping a constant ratio of mixture gas in the column inlet.

Table 3 ─ Operation conditions for breakthrough curves inlet of the column for all pressures investigated (6, 12 and 18 bar).

Binary mixture	Ratio	Total Volumetric Flowrate
$N_2 + CO_2$	85:15	4.25 SLPM
Single component	**Composition**	**Total Volumetric Flowrate**
CO_2	10%	5.8 SLPM
N_2	10%	5.8 SLPM

Source: Author

All the gas mixtures were diluted in helium, where for single component analysis its concentration was 90%. An additional of 90% of inert gas, in this case, maintains the total pressure of the column constant during the input of CO_2 or N_2. In experiments where total pressure of 12 bar is set, for example, the column should be pressurized before the CO_2 flow rate enters in it. That is why the experiments need an inert gas. Thus, it helps to keep high pressure in the beginning of each experiment and avoids any pressure variance during it. For gas mixture, helium composition was set 28.2%, following by nitrogen 61% and carbon dioxide 10.8% maintaining the N_2/CO_2 ratio of 85:15.

4.4.2. Mathematical Model

The mass, energy balance and momentum equation used to describe the breakthrough curves in a fixed bed, as well as the boundary conditions are amply known on literature (Ribeiro *et al.*, 2008; Grande *et al.*, 2013; Schell *et al.*, 2013; Silva *et al.*, 2013; Rios *et al.*, 2014; Ferreira *et al.*, 2015; Luberti *et al.*, 2015; Marx *et al.*, 2015; Ntiamoah *et al.*, 2015; Campo *et al.*, 2016). The nonisothermal mathematical models used to describe the dynamic behavior of adsorption in the fixed bed are presented in this section. The assumptions for the equations development in this study are listed below:

1. Ideal gas behaviour;
2. Mass, energy and momentum gradients only in the axial direction (z) is considered;
3. Mass transfer into the particle according to the Linear Driving Force approach;
4. Mass adsorbent well distributed along the column, resulting in a constant void and bed density;
5. Axial mass dispersion $D_{ax}(Re, Sc)$ calculated according to Knox *et al.* (2016);
6. Constant mass and heat coefficients;
7. The temperature of the gas and solid phases is the same;
8. The temperature of the wall is only in function of time.
9. The pressure drop is calculated from Ergun equation (Bird *et al.*, 2006);

Based on those model assumptions above, the partial differential equations of the fixed bed can be written for total mass balance of the gas phase as:

$$\frac{\partial}{\partial z}\left(\varepsilon D_{ax} C_{g,T} \frac{\partial y_i}{\partial z}\right) - \frac{\partial}{\partial z}\left(u\, C_{g,i}\right) - \varepsilon \frac{\partial C_{g,i}}{\partial t} - \rho_b \frac{\partial \bar{\bar{q}}_i}{\partial t} = 0 \tag{21}$$

Where the term of loading capacity ($\bar{q}_i$) is a function of time. The total molar concentration of gas phase is denoted by $C_{g,T}$, the molar concentration of component i is $C_{g,i}$, u is the gas velocity, ε is the bed porosity and ρ_b is the bed density. The correlation for D_{ax} can be found in Appendix A.

The gas phase energy balance according to the assumptions can be described as follows:

$$\frac{\partial}{\partial z}\left(\lambda\frac{\partial T_g}{\partial z}\right)-\frac{\partial(u\ C_{g,T}\,c_{p,g}\,T_g)}{\partial z}+\varepsilon RT_g\frac{\partial C_{g,T}}{\partial t}-4\left(\frac{h_w}{D}\right)(T_g-T_w)-$$
$$\left(\varepsilon C_{g,T}\,c_{v,g}+(1-\varepsilon)\left(\varepsilon_p\,\Sigma(C_{g,i}\,c_{v,g_i}\right)+\rho_p\Sigma\bar{\bar{q}}_i\,c_{v,s}+\rho_p\,c_{p,s}\right)\frac{\partial T_g}{\partial t}+(1-\varepsilon)\,\varepsilon_p\frac{\partial C_{g,T}}{\partial t}RT \tag{22}$$
$$+\rho_b\,\Sigma\left(-\Delta H_{iso,i}\frac{\partial\bar{\bar{q}}_i}{\partial t}\right)=0$$

Where ΔH_{iso} is the isosteric heat of adsorption, h_w is the heat transfer coefficient, c_p and c_v denote the heat capacity at constant pressure and volume, respectively. The axial heat dispersion is λ and ρ_b is the bed density.

The isosteric heat of adsorption was calculated according to Clausius-Clapeyron equation and an average value was chosen in order to perform the simulation process (Ruthven, 1984; Lopes *et al.*, 2009; Casas *et al.*, 2012; Shafeeyan *et al.*, 2014).

$$\frac{\Delta \mathrm{H}_{iso}}{RT^2}=\left(\frac{\partial \ln P}{\partial T}\right)_q \tag{23}$$

The energy balance of the column wall is also considered in the simulation. The heat transfer is assumed as forced convection from gas phase to the inner area of the column wall. The equation is described as follows:

$$\rho_w\,c_{p,w}\frac{\partial T_w}{\partial t}=\alpha_w\,h_w\left(T_g-T_w\right)-\alpha_{wl}\,U_g\left(T_w-T_\infty\right) \tag{24}$$

Where subscript w means wall, U_g is global heat transfer coefficient, α_w and α_{wl} are the ratio of column internal and external surface area to volume, respectively.

The pressure drop along the column can be calculated according to Equation (25) (Bird *et al.*, 2006).

$$-\frac{\partial P}{\partial z}=\frac{150\mu\left(1-\varepsilon\right)^2}{\varepsilon^3 d_p^2}u\ +\frac{1.75(1-\varepsilon)\rho_a}{\varepsilon^3 d_p}u^2 \tag{25}$$

In order to solve the partial differential equations system, boundary and initial conditions are required. Such conditions vary depending on the experimental procedure. In the case of breakthrough curves experiments the boundary and initial conditions used are presented in Table 4. The parameters values used in simulation can be found in Appendix B.

Table 4 ─ Initial and boundary conditions for breakthrough curves simulation

t = 0	
$y_i = 0$ $T = T_w = 298\,K$ $\dfrac{dq_i}{dt} = 0$	
z = 0	**z = L**
$\dot{V}^0_{inlet}\left(\dfrac{P^0}{RT^0}\right)\dfrac{y_{i,0}}{A} = \left(u\,C_{g,i}\right)\Big\vert_0 - D_{ax}\,\dfrac{\partial C_{g,i}}{\partial z}\Big\vert_0$	$\dfrac{\partial C_{g,i}}{\partial z}\Big\vert_L = 0$
Amount of component i in molar basis entering and its variation leaving the column	
$\dot{V}^0_{inlet}\left(\dfrac{P^0}{RT^0}\right)\dfrac{1}{A} = \left(u\,C_{g,T}\right)\Big\vert_0$	$\dfrac{\partial C_{g,T}}{\partial z}\Big\vert_L = 0$
Total amount of gas in molar basis at the inlet and outlet of the column in across surface	
$P\vert_0 = \left(C_{g,T}\,RT\right)\Big\vert_0$	$P\vert_L = P_{set}$
Pressure of the system at the inlet and outlet of the column	
$\dot{V}^0_{inlet}\left(\dfrac{P^0}{RT^0}\right)\dfrac{1}{A}c_{p,g}\,T_0 = \left(u\,C_{g,T}\,c_{p,g}\,T_g\right)\Big\vert_0 - \lambda\,\dfrac{\partial T_g}{\partial z}\Big\vert_0$	$\dfrac{\partial T_g}{\partial z}\Big\vert_L = 0$
Energy quantity of the gas stream that enters and leaves the column in across surface	

Source: Author

The gProms software (Process System Enterprise, UK) was used to solve the system of partial differential equations. The numerical method used to discretize the axial domain was the second order orthogonal collocation over thirty finite elements. Thirty finite elements were the minimum number to lead an efficient solution procedure, not changing the simulation performance for higher number of elements. The embedded solver of the gProms software used a value of 1×10^{-5} for absolute error tolerance. The simulations were performed in a personal computer with an Intel® Core i5-4440@ 3.1 GHz processor. All reported simulations took about thirty seconds to finish the execution output.

4.4.3. Dead Volume

The dead volume in this study is a particularity in the developing of the model that should be considered. The PSA unit was acquired from the company L&C Science and Techonology (USA). In previous section, it was shown the properties of the column used for experiments; the bed length (0.955 m) presented in Table 2 denotes the filled and unfilled parts of the column by adsorbent. In order to suit the packed adsorbent inside the column, some apparatus were put in the ends of the column such as two cylinders at each end of the column that sustain the adsorbent material inside the bed. Also, there are two filters in each end of the packed bed to avoid trespassing powder. One spring was put in the top of the column to guarantee the package of the material and avoid it to be free inside the column. In consequence, the entire volume of the column then presents a large void space which consists of 43% of total volume.

Hence, the domain of the column to apply the model equations was divided in three parts (Figure 9).

Figure 9 ─ Schematic illustration of the column domain division for simulation processes.

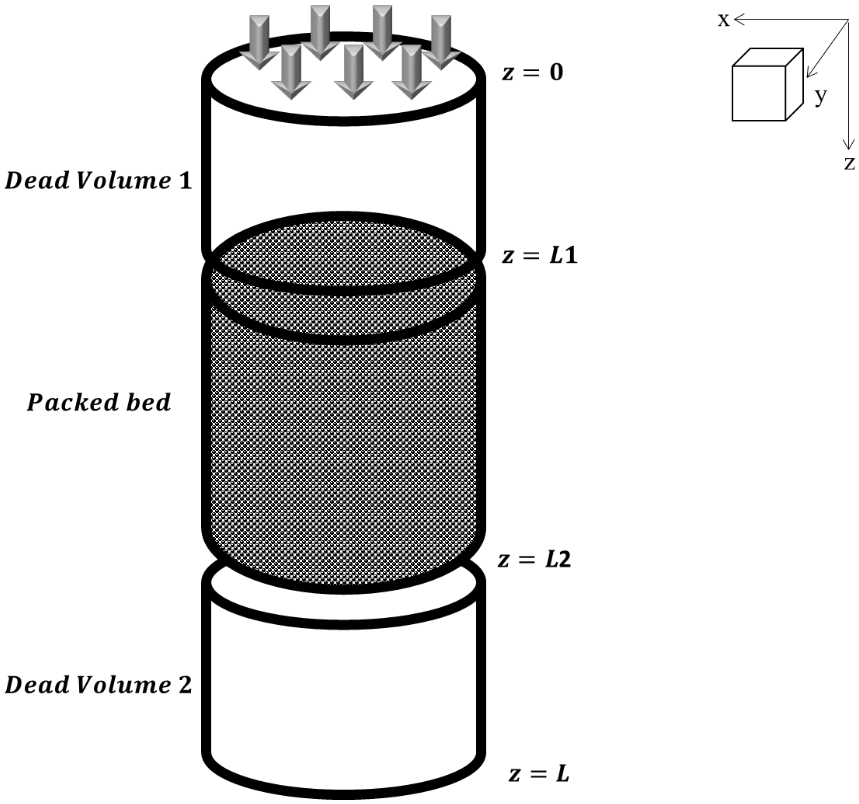

Source: Author

As mentioned before, the mass, energy and momentum balances are considered only in axial dimension. Then, the equations were maintained the same for all column (from z = 0 to z = L). However, in the first (Dead Volume 1) and third (Dead Volume 2) parts of the domain of the column, since there is no adsorbent in it, some terms were removed from equations and the mass balance in dead volumes become:

$$\frac{\partial}{\partial z}\left(D_m C_{g,T}\frac{\partial y_i}{\partial z}\right)-\frac{\partial}{\partial z}\left(u\,C_{g,i}\right)-\frac{\partial C_{g,i}}{\partial t}=0 \tag{26}$$

Where D_m is the molecular diffusion of the gas. The term of porosity as well as loading capacity are removed from the balance since there is no mass transfer between gas and solid.

Analogously, the energy and momentum balances in dead volumes become:

$$\frac{\partial}{\partial z}\left(\frac{\partial T_g}{\partial z}\right)-\frac{\partial(u\ C_{g,T}\, c_{p,g}\, T_g)}{\partial z}+RT_g\,\frac{\partial C_{g,T}}{\partial t}-4\left(\frac{h_w}{D}\right)(T_g-T_w)=0 \quad (27)$$

$$-\frac{\partial P}{\partial z}=u\ \delta \quad (28)$$

The pressure drop in the dead volume is considered negligible and the constant coefficient δ was selected so that the pressure drop become almost null. All the others terms of the Equations (26), (27) and (28) were kept unchanged. The boundary conditions were also maintained the same as previously presented.

4.5. PSA Process

4.5.1. Experimental

The experimental setup described in breakthrough curve section is adapted from the PSA unit. The whole unit is illustrated in Figure 10. It consists of two beds system connected to the gas chromatograph, as cited before.

Figure 10 — Schematic diagram of the bench-scale PSA unit.

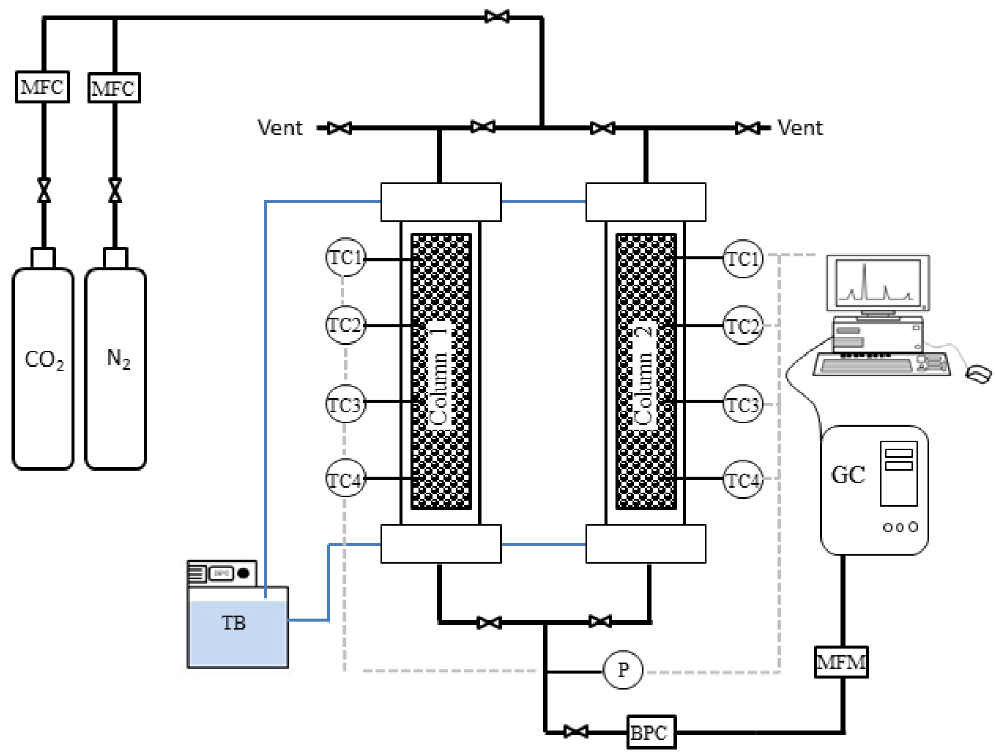

Source: Modified from Siqueira *et al.* (2017)

The configuration used for experiments in the PSA unit is well known as Skarstrom cycle (Skarstrom, 1960). This is the most elemental PSA cycle and can be described by the following steps: Adsorption, Blowdown, Purge and Pressurization (Figure 11). In this process, the temperature of the column, 298 K, is kept constant with the aid of the thermostatic bath. The upper pressure was set for 6 bar and the lower one for 1 bar.

Figure 11 — Graphical schedule of a 4 steps / 2-bed synchronized PSA cycles.

	t_ads	t_bld	t_pu	t_pr
BED 1	ADSORPTION	BLOWDOWN	PURGE	PRESSURIZATION
BED 2	PURGE	PRESSURIZATION	ADSORPTION	BLOWDOWN

Source: Author

The PSA process started with a co-current pressurization step (PR) at the top of the bed, fed with the gas mixture in a set volumetric flow rate of 4.7 SLPM. Pressurization time depends on the maximum pressure set for adsorption step. The pressurization ends when the pressure in the column reaches a tolerance of 0.1 bar (~60 seconds) from the maximum value set. In adsorption step (AD), CO_2 is captured by the adsorbent as long as the gas mixture flows through the column (70 seconds). The adsorption process is performed at the highest constant pressure, 6 bar in this case. Adsorption step time was chosen so that its duration was not lower than pressurization step. Blowdown (BD) is the third step (~60 seconds); a rapid counter-current depressurization is performed until the column reaches the lowest pressure of the entire cycle, 1 bar. A small amount of CO_2 is removed in this step. Finally, the cycle ends in the purge step (PU) (70 seconds) where a small volumetric rate of the light product (N_2 in this case) flows counter-current through the fixed bed at the lowest constant pressure, 1 bar. Purge aims to clean the column removing all CO_2 adsorbed remained after blowdown step. All steps are synchronized in a way that while one operates adsorption the other is in the purge step. When the pressurization is running in one column, the other one operates in the blowdown. All process is finished when the unit reaches the cyclic steady state.

The whole procedure was monitored and operated through an interface created in LabView software (National Instruments Corp.), including control of valves, MFCs and BPC. The gas mixture composition was measured using the gas chromatograph.

4.5.2. Mathematical Model

A mathematical model was developed to better understand and predict the dynamics of PSA separation processes. Material, energy and momentum balances were the same applied to breakthrough curves simulation as well as the assumptions made. Boundary conditions differs the PSA simulation from the fixed bed experiments. Table 5 describes the boundary condition used for PSA process simulation in this work.

Table 5 ─ Boundary conditions used in the simulation of the PSA process.

z = 0	**z = L**
Pressurization	
$\dot{V}_{inlet}^{0}\left(\frac{P^0}{RT^0}\right)\frac{y_{i,0}}{A}=\left(u\,C_{g,i}\right)\Big|_0-D_{ax}\left.\frac{\partial C_{g,i}}{\partial z}\right|_0$	$\left.\frac{\partial C_{g,i}}{\partial z}\right|_L=0$
$\dot{V}_{inlet}^{0}\left(\frac{P^0}{RT^0}\right)\frac{1}{A}=\left(u\,C_{g,T}\right)\Big|_0$	$u\big|_L=0$
$\dot{V}_{inlet}^{0}\left(\frac{P^0}{RT^0}\right)\frac{1}{A}c_{p,g}\,T_0=\left(u\,C_{g,T}\,c_{p,g}\,T_g\right)\Big|_0-\lambda\left.\frac{\partial T_g}{\partial z}\right|_0$	$\left.\frac{\partial T_g}{\partial z}\right|_L=0$
Adsorption	
$\dot{V}_{inlet}^{0}\left(\frac{P^0}{RT^0}\right)\frac{y_{i,0}}{A}=\left(u\,C_{g,i}\right)\Big|_0-D_{ax}\left.\frac{\partial C_{g,i}}{\partial z}\right|_0$	$\left.\frac{\partial C_{g,i}}{\partial z}\right|_L=0$
$\dot{V}_{inlet}^{0}\left(\frac{P^0}{RT^0}\right)\frac{1}{A}=\left(u\,C_{g,T}\right)\Big|_0$	$\left.\frac{\partial P}{\partial t}\right|_L=0$
$\dot{V}_{inlet}^{0}\left(\frac{P^0}{RT^0}\right)\frac{1}{A}c_{p,g}\,T_0=\left(u\,C_{g,T}\,c_{p,g}\,T_g\right)\Big|_0-\lambda\left.\frac{\partial T_g}{\partial z}\right|_0$	$\left.\frac{\partial T_g}{\partial z}\right|_L=0$
Blowdown	
$\dot{V}_{inlet}^{0}\left(\frac{P^0}{RT^0}\right)\frac{y_{i,0}}{A}=\left(u\,C_{g,i}\right)\Big|_0-D_{ax}\left.\frac{\partial C_{g,i}}{\partial z}\right|_0$	$\left.\frac{\partial C_{g,i}}{\partial z}\right|_L=0$
$P\big|_0=\left(P_{AD}-P_{PU}\right)\,\exp\left(0.2t\right)+P_{PU}$	$u\big|_L=0$
$\dot{V}_{inlet}^{0}\left(\frac{P^0}{RT^0}\right)\frac{1}{A}c_{p,g}\,T_0=\left(u\,C_{g,T}\,c_{p,g}\,T_g\right)\Big|_0-\lambda\left.\frac{\partial T_g}{\partial z}\right|_0$	$\left.\frac{\partial T_g}{\partial z}\right|_L=0$

Purge	
$\left.\dfrac{\partial C_{g,i}}{\partial z}\right\|_0 = 0$	$-\dot{V}^0_{PU,inlet}\left(\dfrac{P^0}{RT^0}\right)\dfrac{y_{PU\_i,0}}{A} = \left.\left(u\,C_{g,i}\right)\right\|_L - D_{ax}\left.\dfrac{\partial C_{g,i}}{\partial z}\right\|_L$
$\left.\dfrac{\partial C_{g,T}}{\partial z}\right\|_0 = 0$	$-\dot{V}^0_{PU,inlet}\left(\dfrac{P^0}{RT^0}\right)\dfrac{1}{A} = \left.\left(u\,C_{g,T}\right)\right\|_L$
$\left.P\right\|_0 = P_{PU}$	$\left.\dfrac{\partial P}{\partial z}\right\|_L = 0$
$\left.\dfrac{\partial T_g}{\partial z}\right\|_0 = 0$	$-\dot{V}^0_{inlet}\left(\dfrac{P^0}{RT^0}\right)\dfrac{1}{A}c_{p,g}\,T_0 = \left.\left(u\,C_{g,T}\,c_{p,g}\,T_g\right)\right\|_L$

Source: Author

In addition, when equalization step was performed, the boundary conditions was inserted as following:

Table 6 ─ Boundary conditions used in PSA simulation process with equalization step.

Equalization depressurization	
z = 0	**z = L**
$\left.\dfrac{\partial C_{g,i}}{\partial z}\right\|_0 = 0$	$\left.\dfrac{\partial C_{g,i}}{\partial z}\right\|_L = 0$
$\left.u\right\|_0 = 0$	$\left.P\right\|_L = a_0 + (P - a_0)\exp(-\alpha t)$
$\left.\dfrac{\partial T_g}{\partial z}\right\|_0 = 0$	$\left.\dfrac{\partial T_g}{\partial z}\right\|_L = 0$

Equalization pressurization	
z = 0	**z = L**
$\left.\frac{\partial C_{g,i}}{\partial z}\right\|_0 = 0$	$-F_{i_{EQ^d}} \frac{1}{A} = \left(u\, C_{g,i}\right)\big\|_L - D_{ax} \left.\frac{\partial C_{g,i}}{\partial z}\right\|_L$
$u\|_0 = 0$	$-\sum F_{i_{EQ^d}} \frac{1}{A} = \left(u\, C_{g,T}\right)\big\|_L$
$\left.\frac{\partial T_g}{\partial z}\right\|_0 = 0$	$-\sum F_{i_{EQ^d}} \frac{1}{A} c_{p,g}\, T_0 = \left(u\, C_{g,T}\, c_{p,g}\, T_g\right)\big\|_0 - \lambda \left.\frac{\partial T_g}{\partial z}\right\|_L$

Source: Author

where α_0 is the equilibrium pressure in the end of equalization step. The molar flow rate (F_i) in equalization pressurization denotes the ratio of component amount *i* that leaves the column during the depressurization equalization step to the time of this step. The specie amount from depressurization step was calculated according to Equation (29).

$$F_i = (C_{g,i}\, u\, A)\big|_L \tag{29}$$

Table 7, Table 8 and Table 9 show the definition of each term in the boundary conditions for mass balance, energy balance and momentum balance used in simulations of breakthrough experiments and PSA process.

Table 7 ─ Terms definition from boundary conditions for mass balance

$\dot{V}^0_{inlet} \left(\frac{P^0}{RT^0}\right) \frac{1}{A}$	Molar flow rate.
$\left(u\, C_{g,T}\right)\big\|_0$	Rate of z-molar in across surface at z = 0.
$-D_{ax} \left.\frac{\partial C_{g,i}}{\partial z}\right\|_0$	Diffusive z-molar flux in across surface at z = 0.
$\left.\frac{\partial C_g}{\partial z}\right\|_L = 0$	Variation of molar concentration across surface at z = L.
$P\|_0$ *and* $P\|_L$	Pressure at z = 0 and z = L, respectively.

Source: Author

Table 8 — Terms definition from boundary conditions for momentum balance

$P\big\|_0$ and $P\big\|_L$	Pressure at z = 0 and z = L, respectively.

Source: Author

Table 9 — Terms definition from boundary conditions for energy balance

$\dot{V}^0_{inlet}\left(\frac{P^0}{RT^0}\right)\frac{1}{A}c_{p,g}\,T_0$	Energy flow rate.
$\left(u\,C_{g,T}\,c_{p,g}\,T_g\right)\Big\|_0$	Rate of z-energy in across surface at z = 0.
$-\lambda\frac{\partial T_g}{\partial z}\Big\|_0$	Diffusive z-energy flux in across surface at z = 0.
$\frac{\partial T_g}{\partial z}\Big\|_L = 0$	Variation of gas temperature across surface at z = L.

Source: Author

The performance of a PSA process is commonly evaluated through the product purity, product recovery and productivity. Those three parameters for N_2 can be calculated according to Equations (30)-(32).

$$Purity = \frac{\sum_{AD}\left(\int_0^{t_{AD}} F_{N_2,out}dt\right)}{\sum_{AD}\left(\int_0^{t_{AD}} F_{N_2,out}dt + \int_0^{t_{AD}} F_{CO_2,out}dt\right)} \tag{30}$$

$$Recovery = \frac{\sum_{AD}\left(\int_0^{t_{AD}} F_{N_2,out}dt\right) - \sum_{PU}\left(\int_0^{t_{PU}} F_{N_2,in}dt\right)}{\sum_{AD}\left(\int_0^{t_{AD}} F_{N_2,in}dt\right) + \sum_{PR}\left(\int_0^{t_{PR}} F_{N_2,in}dt\right)} \tag{31}$$

$$Productivity = \frac{\sum_{AD}\left(\int_0^{t_{AD}} F_{N_2,out}dt\right) - \sum_{PU}\left(\int_0^{t_{PU}} F_{N_2,out}dt\right) - \sum_{PR}\left(\int_0^{t_{PR}} F_{N_2,in}dt\right)}{mass\,of\ dry\,adsorbent\ \ t_{cycle}}\, n^{\circ}\,beds \tag{32}$$

Where AD, PR, BD and PU are the steps of the PSA cycles previously denoted. The samples of the gas mixture leaving the column in PSA process were manually captured and stored into the GC loops for posterior analysis.

5. RESULTS

5.1. Textural Properties

The textural properties of all three adsorbents are listed in Table 10.

Table 10 ─ Properties of the adsorbents.

	Filtron N	**Norit RB4**	**Charbon 500**
Specific Surface Area [m^2 g^{-1}]	905	907	1025
Pore Specific Volume [cm^3 g^{-1}]	0.42	0.39	0.46
Micropore Specific Volume [cm^3 g^{-1}]	0.34	0.37	0.39
Solid Specific Volume [cm^3 g^{-1}]	0.46	0.48	0.49
Particle Radius [m]	5×10^{-4}	3.5×10^{-3}	5×10^{-4}
Bed density [kg m^{-3}]	385	471	485
Microporosity fraction [a] [-]	0.809	0.949	0.848

[a] Ratio of micropore volume to the total pore volume
Source: Author

Figure 12 and Figure 13 show the adsorption-desorption isotherm measurements of N_2 and CO_2 at 77 K and 273 K, respectively, for all adsorbent studied. In Figure 12, Filtron N presented the lowest value of N_2 quantity adsorbed at 77 K. Norit RB4 and Charbon 500 presented almost the same characteristics. None of them presented hysteresis during the adsorption equilibrium measurements.

In Figure 13, Norit RB4 presented a lower value of CO_2 quantity adsorbed. Charbon 500 and Filtron N presented higher values of CO_2 adsorbed. It suggests that Charbon 500 presented a higher micropore volume due to the high CO_2 adsorbed amount.

However, it can be assumed that none of the materials presented significant difference in equilibrium isotherms at 77 K and 273 K results, respectively.

Even Charbon 500 presenting high micropore volume it also has high pore volume. Norit RB4, in this case, presented relatively lower micropore characteristics, but this volume is approximated to the total pore volume, which explain the high microporosity fraction presented in Table 10.

Figure 12. N_2 adsorption-desorption at 77 K of a) Filtron N, b) Norit RB4 and c) Charbon 500

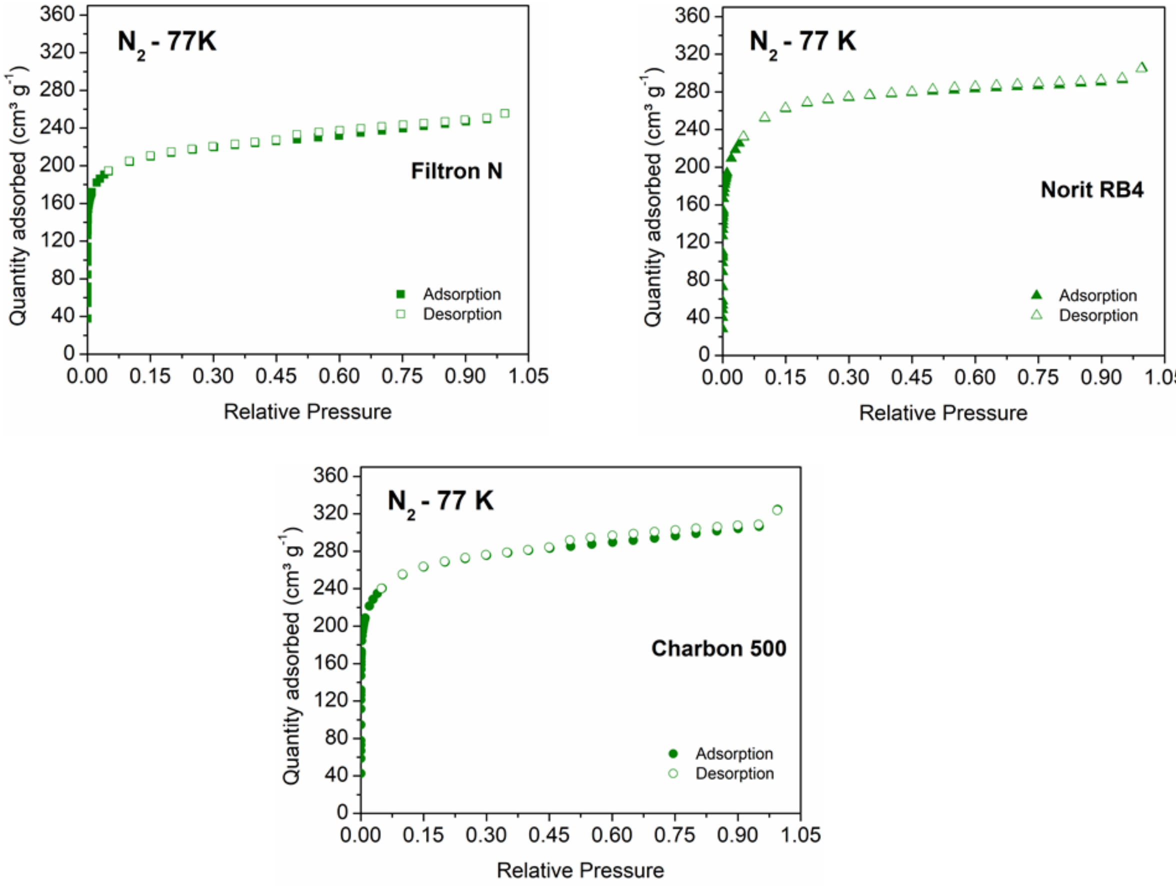

Source: Author

Figure 13. CO_2 adsorption-desorption at 77 K of a) Filtron N, b) Norit RB4 and c) Charbon 500

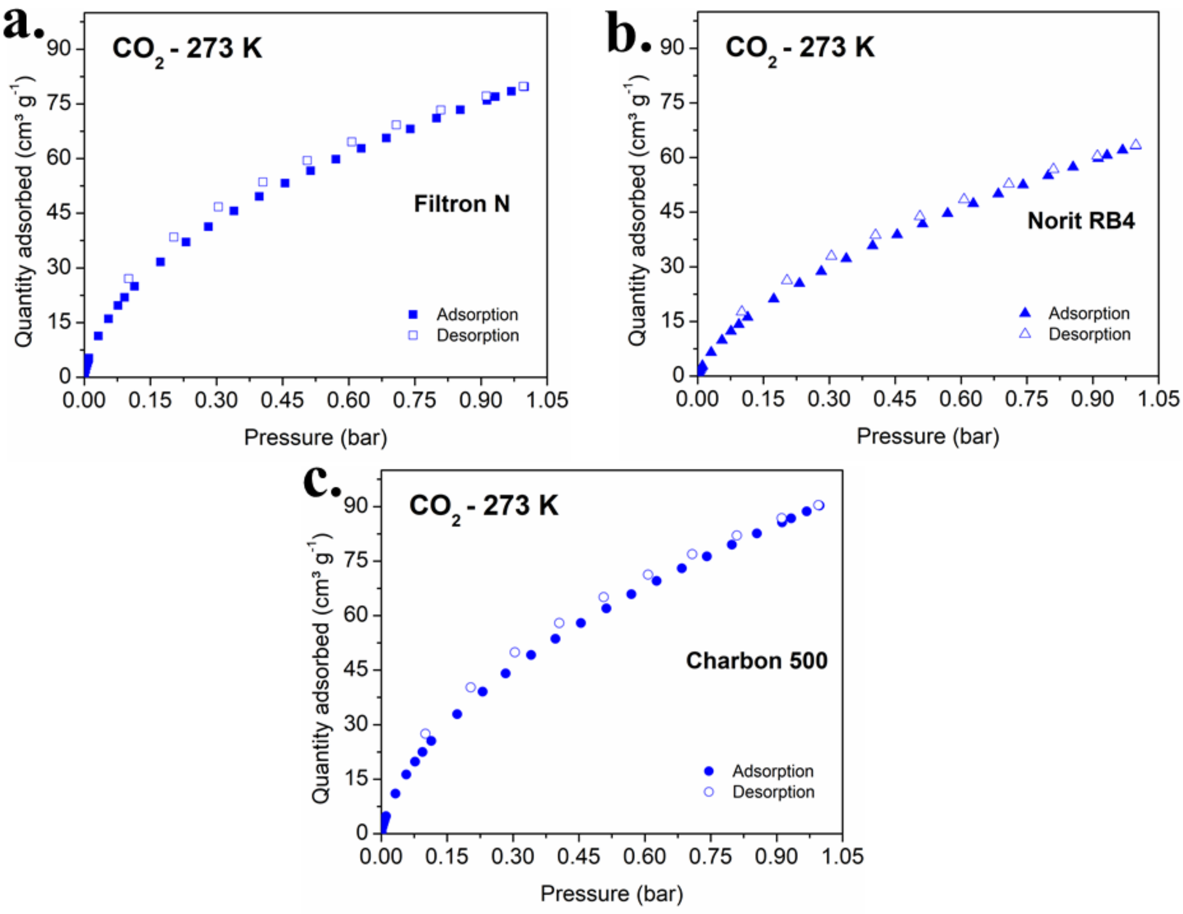

Source: Author

Figure 14 shows the pore size distribution of the activated carbons according to the gas used to obtain it.

Figure 14– Pore size distribution of the activated carbons obtained by NLDFT using CO_2 and N_2 ; a) Filtron N, b) Norit RB4 and c) Charbon 500.

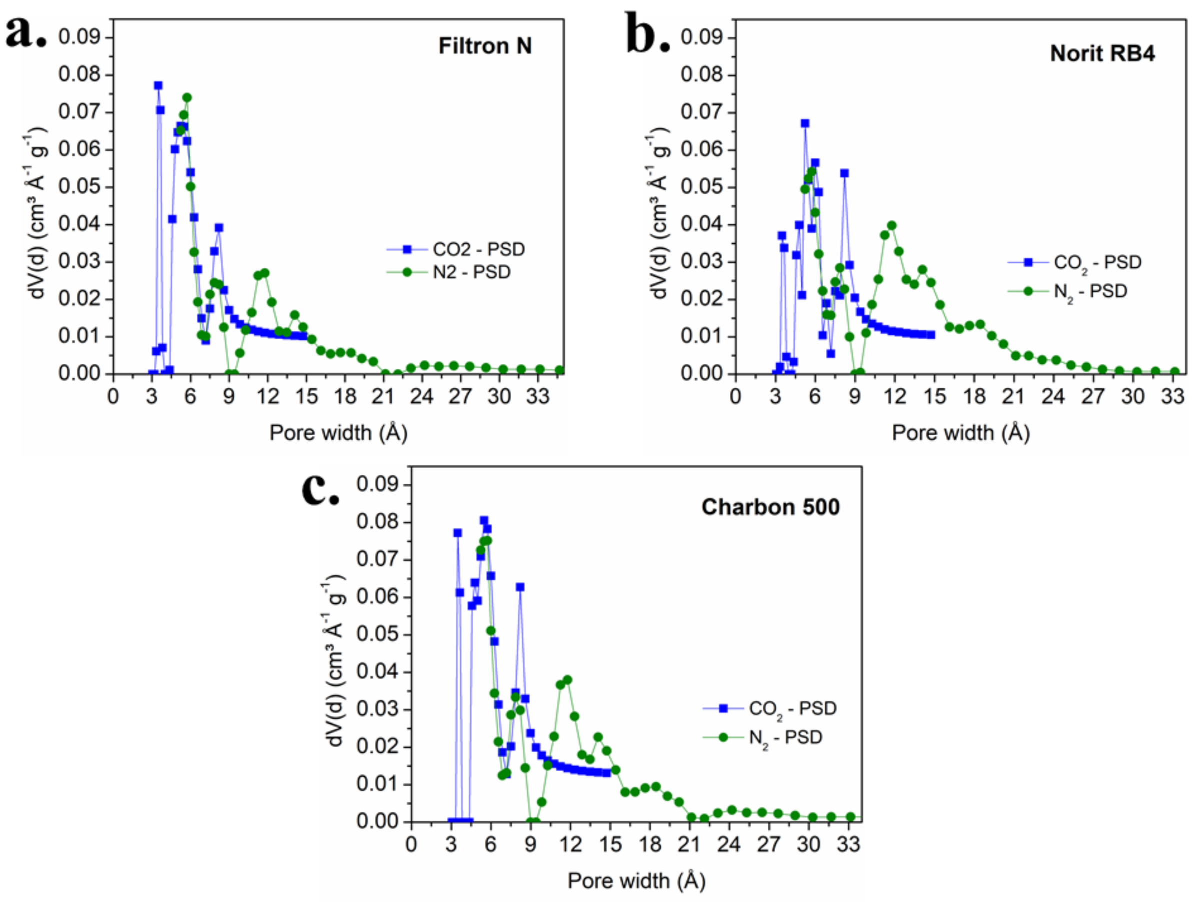

Source: Author

It is noteworthy that this study covers only materials with high microporosity fraction, in which the mass transfer resistance should be considerable in that range of pores. Those adsorbents with high microporosity fractions and BET surface area were previously selected to evaluate the adsorption capacity and applicability of the approach to estimate the mass transfer coefficient and assess the equilibrium model for each of them.

5.2. Adsorption Equilibrium Isotherms

Experiments in the magnetic suspension balance are performed in order to determine the equilibrium isotherm and the parameters of Sips isotherm equation of each component. The fitting of the Sips model, cited in Section 4.3.2., was limited to the selected data of the three isotherms at three different temperatures. The constant model parameters of CO_2 and N_2 for each adsorbent are summarized in Table 11 and Table 12.

Table 11 ─ Model parameters of Sips equation for CO_2 adsorption equilibrium isotherm.

	CO_2					
Adsorbent	$q_{m_0}\left(mol\,kg^{-1}\right)$	$b_0\left(bar^{-1}\right)$	χ	κ	n_0	$Q\left(J\,mol^{-1}\right)$
Charbon 500	11.2282	0.1238	1.6984	1.0589	0.6697	17890
Filtron N	10.9813	0.1102	0.7929	1.8481	0.6530	17236
Norit RB4	12.6522	0.0777	0.6474	0.5097	0.7493	17341

Source: Author

Table 12 ─ Model parameters of Sips equation for N_2 adsorption equilibrium isotherm.

	N_2					
Adsorbent	$q_{m_0}\left(mol\,kg^{-1}\right)$	$b_0\left(bar^{-1}\right)$	χ	κ	n_0	$Q\left(J\,mol^{-1}\right)$
Charbon 500	4.5962	0.0538	0.5328	0.2631	0.8805	12206
Filtron N	4.3029	0.0456	0.2668	0.3794	0.9196	12111
Norit RB4	4.3085	0.0455	0.2422	0.3729	0.9190	12201

Source: Author

Since CO_2 is more preferential adsorbed into activated carbon, the model parameters also tend to be higher due to the adsorption capacity into the adsorbent. For CO_2, the maximum adsorbed amount parameter q_{m_0} dependent on temperature, the affinity coefficient b_0 and the heat of adsorption Q presented higher values when comparing to those of N_2. Unlike in Langmuir equation, the later parameter represents the measurement of heat of adsorption and it is not equal to the isosteric heat invariant with the loading. The parameter of heat of adsorption Q in this study is used only as an empirical coefficient model. The similarity among the studied activated carbons can also be seen by the model parameters values; being all the parameters of the materials for CO_2 and N_2 very similar when comparing to each other. Maximum adsorbed amount ($q_{m,0}$) and heat of adsorption (Q), for instance, are approximate values. They suggest that a textural properties comparison among the materials do not influence on different adsorption performance. However, for similar adsorbents, the bed density of the carbons is an important parameter to assess, especially in case of PSA performance. The adsorbent mass capacity, in order to fill an entire column, can simplify the analysis of which activated carbon can be promising for such operation.

A comparison about the model used and the experimental data of equilibrium isotherm of the three adsorbent equilibrium data are presented in Figure 15. The adsorbed amount per mass unit of single component (CO_2 and N_2) according to the increasing total pressure of the system is presented in one graphic for each studied adsorbent.

Figure 15 ─ Adsorption equilibrium isotherms of pure components (CO_2 and N_2) up to 12 bar and at 298 K, 323 K and 348 K for the three carbons used in the study.

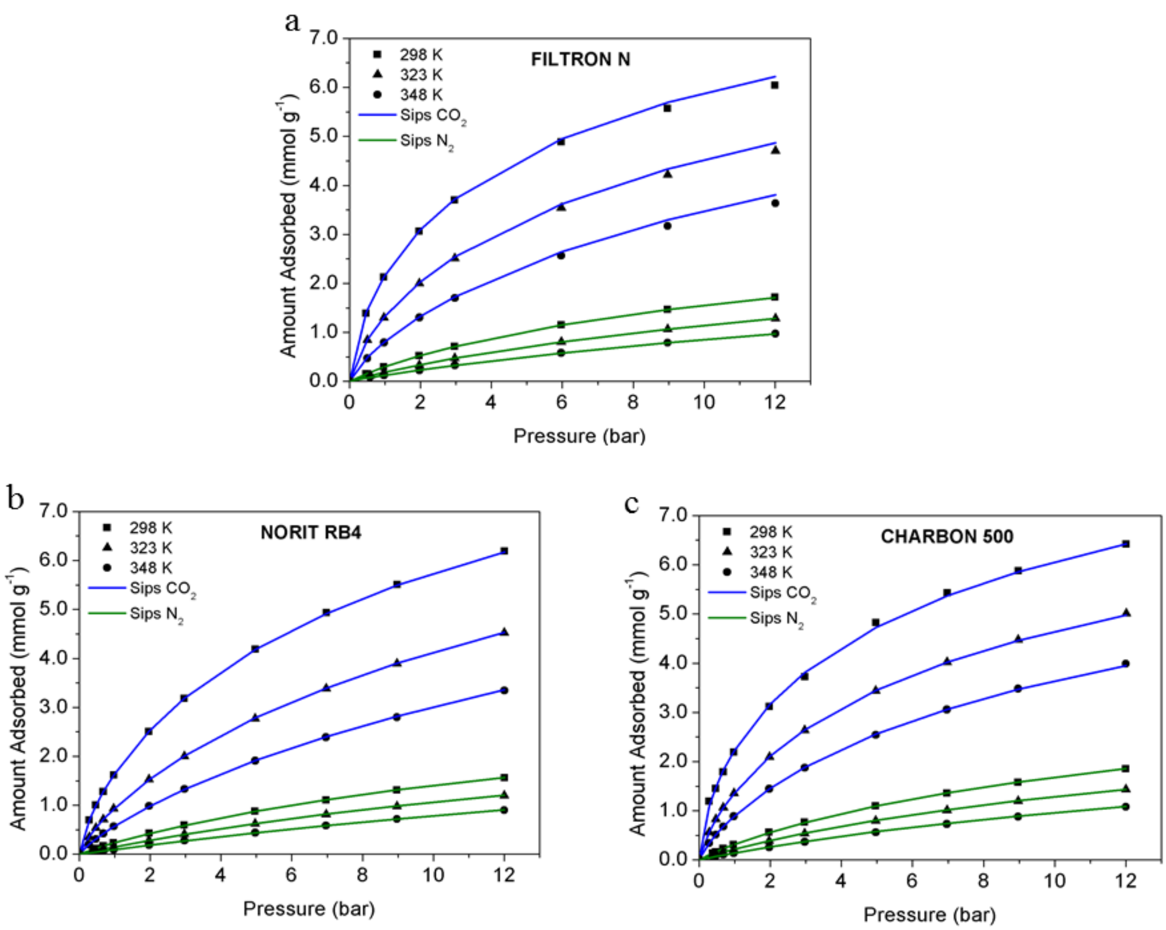

Source: Author

As it can be seen in Figure 15, the adsorbed amount of pure components presented very similar values when compared to each other. In this section, Sips model was chosen due to its high degree of agreement with the experimental data, as it can be observed in Figure 15. The %E (Equation (13)) for the activated carbons presented results below 0.1% for all temperatures investigated. Moreover, Sips equation better describes the adsorption behavior on energetically heterogeneous adsorbents (Ruthven, 1984; Do, 1998). Once the activated carbon presents such characteristics, in order to select a representative equilibrium model, it is worth not considering this material as a homogeneous particle. Sips equation differs from

Langmuir model by presenting an additional parameter in which it can be regarded as the system heterogeneity parameter. Theoretically, the parameter n then suggests system heterogeneity from the solid, or the adsorbate, or both of them. The larger that parameter is, the more heterogeneous the surface is. Considering a homogeneous particle, the parameter suggests being equal to unity, which reduces the equation to the well-known Langmuir model.

Binary mixture isotherms were also measured, at 298 K, in a range of pressure up to 12 bar. Figure 16 shows the experimental data and model fitting of a binary mixture N_2 + CO_2 (85% - 15% v/v) equilibrium isotherm. At first, the model used to represent the adsorption data was the Extended Sips (ES) equation. As it can be seen in Figure 16, using ES model, some materials did not show totally agreement with the experimental results. The equilibrium mixture isotherm model for Norit RB4 presented a little discrepancy at low pressures. Conversely, equilibrium model for Filtron N presented different results from experimental data at higher pressures. On the other hand, the model for Charbon 500 totally agrees with the experimental data for all pressure range. It can take us to believe that ES model is reliable for such binary separation experiment analysis at any pressure range. It is not entirely true and it will be demonstrated forward.

It is noteworthy that in this procedure, each measurement of the experimental data was obtained at equilibrium condition, i.e. when the mixture in the gravimetric balance reached the composition N_2/CO_2 85:15 and there was not variation in adsorbed amount along time. The balance can only measure the total adsorbed mass of the gas mixture. Hence, it is quite difficult to measure the exact adsorbed amount of each component in the mixture. Then, empirical models such as Extended Sips are used as a tool to represent the adsorption equilibrium data of binary mixture and to calculate the adsorbed amount of each component.

However, these empirical binary isotherm models for some material can present discrepancies in a range of pressure, as it was seen in this case for Filtron N and Norit RB4. It is recommended that a large number of experimental measurements should be obtained at very low pressure to avoid discrepancies and to have a good model representation. The absence of experimental data at low pressures can vary the model solution in a large scale due to the difference of slope of the isotherm curve. For another reason, some models cannot describe properly the experimental data when the pressure is increased, which suggests that this difference can be caused not because of missing data but by the solution of empirical model used.

A very good agreement of the equilibrium isotherm model to the experimental measurements is essential for a performance analysis in a fixed bed separation process and, consequently, in a PSA unit. The accuracy of the model parameters influences directly the description of the simulated results. As an important key role in the simulation of a PSA process, for instance, the equilibrium mixture isotherm fitting requires an excellent agreement with the experimental data. In order to guarantee reliable simulation results, it is crucial for others simulation processes to describe well the dynamic experiments.

Figure 16 ─ Adsorption equilibrium isotherms of mixture CO_2+N_2 (15-85%) at 298 K.

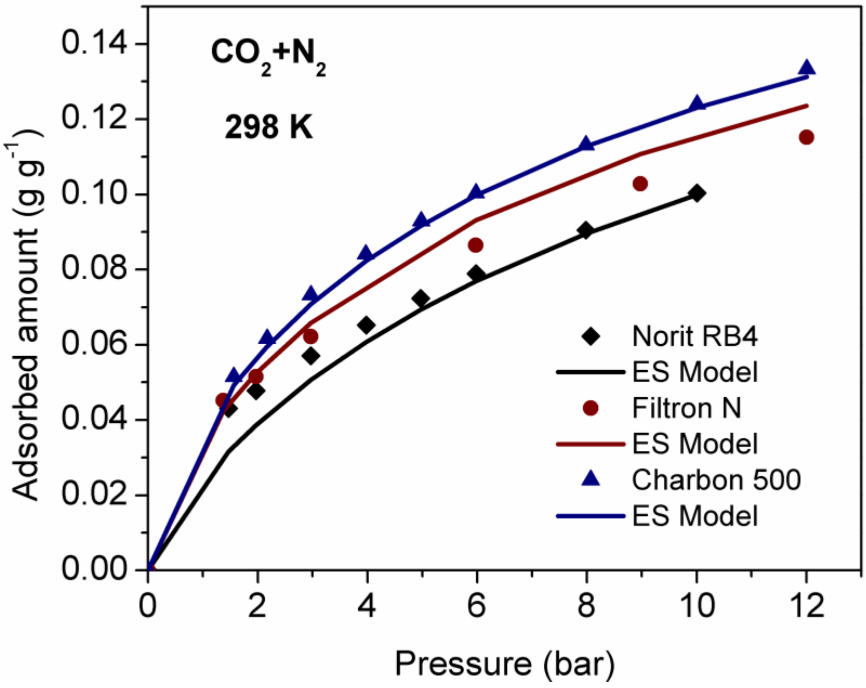

Source: Author

Although the ES model represents the total adsorbed amount experimental data quite well for Charbon 500, as it can be observed in Figure 16; in a binary mixture, the adsorption competition between the CO_2 and N_2 at high pressures may not be satisfactorily well represented, as it can be seen for Filtron N and Norit RB4. This observation was taken into account and a more detailed analysis of the adsorbed amount for each component in a binary mixture was evaluated. As it can be observed in Figure 16, the adsorbed amount of gas in the figure is presented as g g^{-1} since the experimental setup measures only the total gas amount adsorbed into the material (Equation (8)). In this work, the amount adsorbed of each component in the mixture could not be measured. Another reason for such assessment was the discrepancies of the isotherm model for Filtron N presented in Figure 16, when the pressure is increased.

Figure 16 shows that some empirical or semi empirical equilibrium models are not well representative when estimated parameters from single adsorption data are used. Then, the Ideal Adsorption Solution Theory model was used, as presented in Section 3.5, in order to evaluate these discrepancies. It was firstly presented by Myers & Prausnitz (1965) to describe adequately the adsorbed amount in multicomponent mixture and was used in this work to evaluate the adsorbed amount or the adsorbed fraction of each component in a binary mixture.

The experimental adsorption equilibrium isotherms for the N_2/CO_2 mixture (85:15 on molar basis) on activated carbon Charbon 500 at 298 K and 0.01 to 12 bar was taken as an example so that we can compare both models. They are presented in Figure 17, along with the experimental data.

Figure 17 ─ Binary isotherm (CO_2+N_2 – 15/85% on molar basis) on Charbon 500. Scatters for experimental data and lines for model fitting.

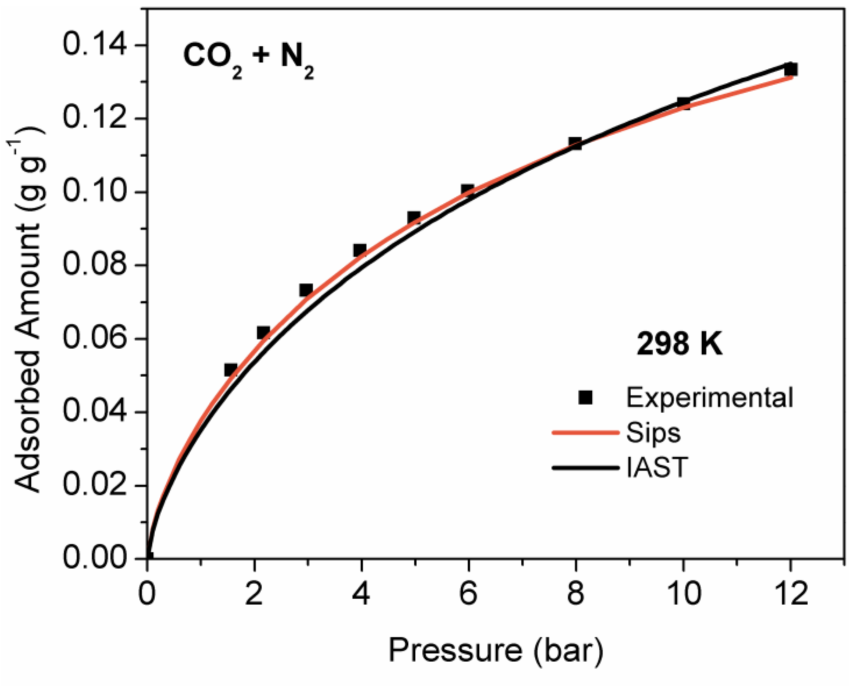

Source: Author

The symbols are the experimental data and the lines represent the predictions obtained from the extended Sips (ES) and IAST model. As it can be seen, both multicomponent adsorption models (IAST and ES) predict approximately the same total loading up to 12 bar. Thus, by evaluating the total adsorbed amount of the gas mixture in Figure 17, both isotherm models apparently are satisfactory to describe the experimental data in those conditions.

However, in Figure 18, it is shown the estimated individual loadings for the N_2/CO_2 mixtures with 85:15 of molar concentration. Black scatters denote the CO_2 and N_2 adsorbed amount when calculated by Extended Sips Equation. Red scatters represent the adsorbed amount of each component calculated by IAST. At low pressure, both models can represent the total loading of the binary isotherm. Nonetheless, as the pressure increases, a meaningful discrepancy between model predictions is observed. IAST model predicts a larger adsorbed concentration of CO_2 and a lower adsorbed concentration of N_2, as compared to ES model. This difference can directly impact on selectivity calculation depending on the model used. It is noteworthy that the parameters used for simulations are the same for both models. They can be found in Table 11 for CO_2 and Table 12 for N_2.

Figure 18 — Models representation of adsorbed amount of each component (CO_2 and N_2) in the binary isotherm – 85% N_2 – 15% CO_2.

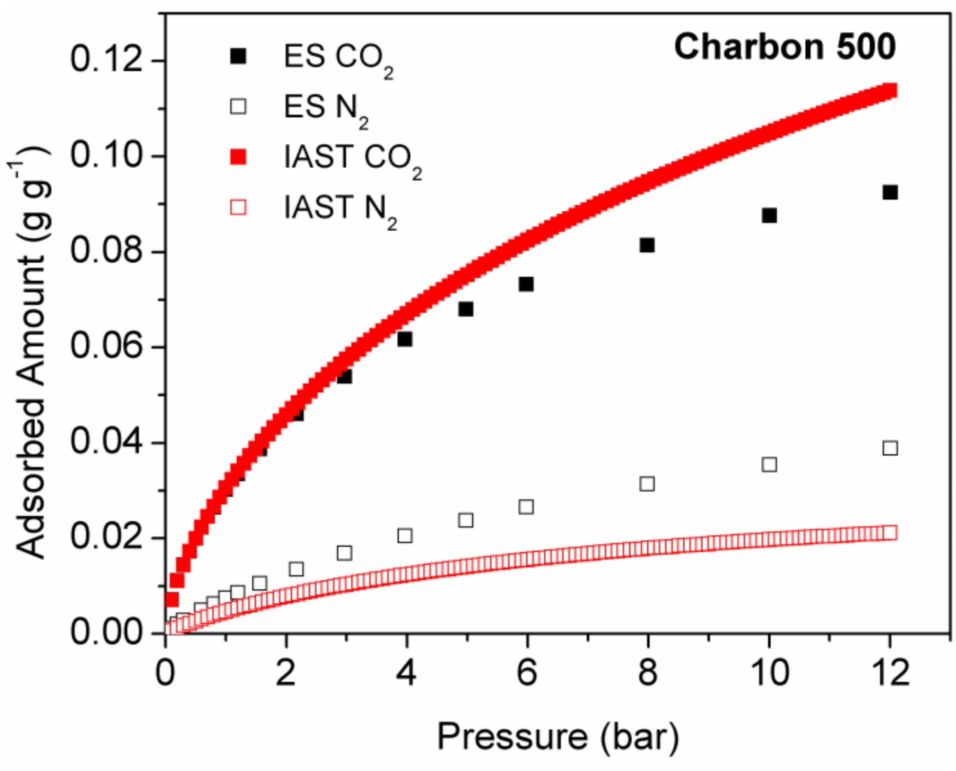

Source: Author

The difference of the adsorbed amount of each component in Figure 18 can be explained due to the IAST model suggests a realiable result since its approach has physical meaning and it is based on Gibbs excess formalism. The model was developed taking into account the application of the thermodynamics of the solution to adsorption. The proposed definition of an ideal adsorbed solution in porous material considers the chemical potential of the component (Myers, 2002).

It is noteworthy that in particular cases, as dilute CO_2, ES model can represent a mixture isotherm with a good agreement. Rocha *et al.* (2017) showed by means of breakthrough curves that the Extended Sips model may be satisfactorily used to simulate CH_4/CO_2 separation in a fixed bed packed with carbon molecular sieves at high pressure. They reported good agreement between simulated and experimental results even at 7000 kPa, yet with a feed of 90% CH_4 and 10% CO_2. The preferentially adsorbed gas (CO_2) is much more diluted than in the present work (60:40), which may suggest that the accuracy of models is a function not only of total pressure, but also of the relative fraction of gases in the mixture.

Isotherms models of gas mixture are considered more important than single isotherms when it is needed to improve a separation process by adsorption. Isotherms of binary mixture described more realistic the equilibrium selectivity in the studied conditions of temperature and composition. Equilibrium selectivity can be responded with very different values depending on the model utilized. When adsorbed amount of individual gases under competitive conditions are compared, IAST and Sips models predict increasingly different values as pressure increases.

According to the textural properties similarity presented among the activated carbon it was decided to evaluate the PSA experiments and simulation of one material only. Since one of the goals of this work relies on determining the appropriate k_{LDF} parameter and, in this case, it is related to the micropore resistance in the particle. Then, Norit RB4 was selected to be experimentally analyzed in PSA unity due to its high microporosity. Furthermore, Norit RB4 is the only one in pellet shape, which allowed considering homogeneity in distribution of the adsorbent particle size. Moreover, during the developing of the model, several experiments of fixed bed and PSA had to be performed to improve the simulation. These experiments were performed using Norit RB4. Also, the PSA unit presents two columns with large volume which became economically unfeasible the performance of several PSA experiments for all activated carbon. Then, the PSA experimental data using Norit RB4 to develop the model were considered and used to present the comparison to the simulated results in this work.

5.3. Adsorption Kinetics

For determination of the kinetic parameter, the experimental adsorption isotherms were performed measuring the adsorbed amount according to time when the total pressure was changed. They were plotted during pressure intervals of around 0.5 (for low pressures) and 1 bar or more (for high pressure). They were recorded so that it was possible to evaluate the pressure changing during the adsorption process. In all experiments, even for different intervals, the pressure of the experiment increased linearly.

Figure 19 and Figure 20 show CO_2 and N_2 uptake during pressure change. As a result of the good fitting of the Sips model to the equilibrium data and the accurate description of pressure change in each experiment, the estimated k_{LDF} value provides an excellent agreement between the simulations of CO_2 and N_2 uptakes and respective gravimetric uptake data.

Figure 19 — Uptake data of CO_2 on Norit RB4 with k_{LDF} = 0.1 s^{-1}.

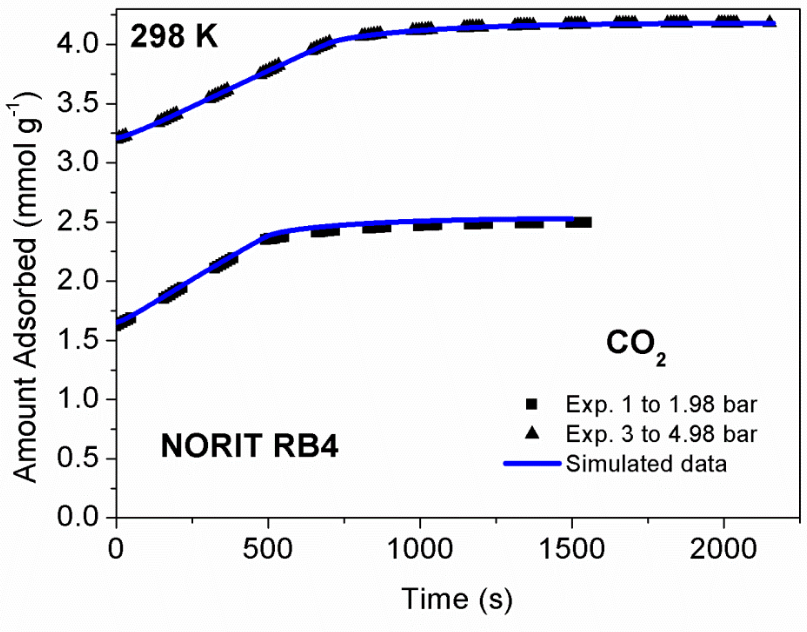

Source: Author

Figure 20 — Uptake data of N_2 on Norit RB4 with k_{LDF} = 0.05 s^{-1}.

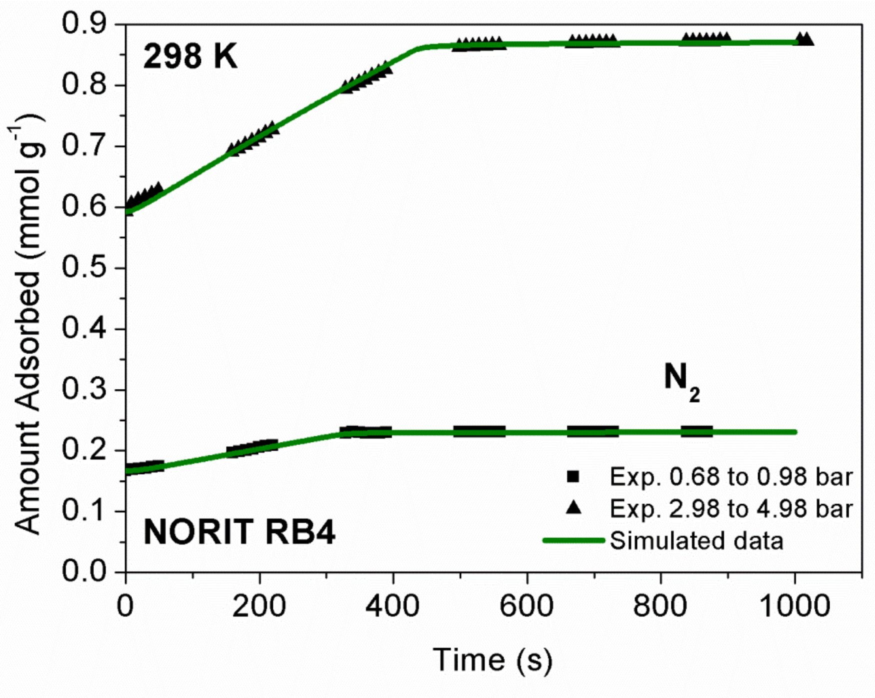

Source: Author

Due to their similarity, for all the three activated carbons, the k_{LDF} value found that best fits the experimental data was 0.1 s^{-1} for CO_2 and 0.05 s^{-1} for N_2. It was considered that the estimated k_{LDF} value is independent from the pressure step (variation) and assumed the same value regardless of the pressure used for a given adsorbate. It suggests, as expected, that the mass transport phenomena into the micropores of the particle are dominant over the film and macropore resistance.

In order to validate the procedure presented in this study, Figure 21a shows a simulated breakthrough curve of CO_2, diluted in Helium, onto Norit RB4 with three different values of k_{LDF}. It can be observed that the best value for k_{LDF} to fit the experimental data in this case was 0.1 s^{-1}. When this coefficient is ten times higher than 0.1, which is the minimum estimated, the breakthrough curve presents a different shape but approximate to the best fit result. Conversely, when a lower k_{LDF} value is used, in the range of 0.01 s^{-1}, the simulated curve tends to unreal results comparing to experimental data. The later coefficient value suggests a very slow gas mass transfer into the particle; which is represented by the dispersive breakthrough curve. For temperature assessment, it was chosen only one thermocouple in order to have a representative visualization of the effects on the temperature. The mass transfer coefficient influence can also be seen in Figure 21b (history of temperature).

According to it, a higher coefficient value tends to increase the temperature during the adsorption. The mass transfer coefficient fitted only by the breakthrough curve shape can be erroneous. In some case, in simulation process, an overestimated coefficient can still represent the experimental breakthrough curve. To avoid this erroneous analysis of mass transfer coefficient, the assessment of history of temperature is also necessary. By doing that, Figure 21b helps to understand when the mass transfer coefficient can be over or underestimated. When a very low coefficient is used in the simulation process, besides the unreal breakthrough shapes, the history of the temperature presents a very low temperature increasing. When a higher k_{LDF} value is set, it indicates that the mass transfer happens very quickly. Since physical adsorption is an exothermically process, when the gas adsorption occurs in such condition, the temperature tends to rapidly increase.

Figure 21 ─ (a) CO_2 Breakthrough curves and (b) history of temperature during CO_2 dynamic adsorption on Norit RB4. Scatters for experimental data, lines for simulated data.

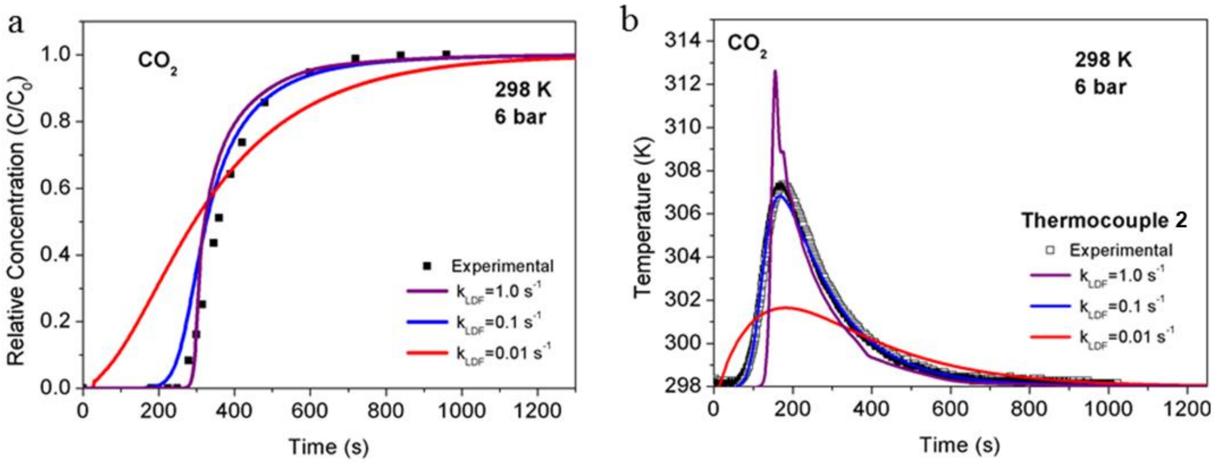

Source: Siqueira *et al.* (2018b)

Although the CO_2 mass transfer coefficient is higher than N_2, the adsorption process of CO_2 takes a longer time to reach the equilibrium in comparison with N_2 because the amount of CO_2 adsorbed is relatively higher than that of N_2 in the same conditions of pressure and temperature. The adsorption of these gases on ordinary hydrophobic activated carbons (without any chemical groups on the surface) is known to be a physical process. Under these conditions and given the higher critical temperature of CO_2 in comparison with N_2, the first is more likely to behave as a condensable vapor than as a supercritical gas, being less volatile and more easily adsorbed (Rios *et al.*, 2014). This selectivity for CO_2 indicates that these adsorbents may be suitable for the capture of CO_2 from mixtures such as exhaust gases. Furthermore, the interactions of CO_2 with the particle surface tend to be higher due to the smaller molecular diameter and its quadrupole moment (Pillai *et al.*, 2008; Liu *et al.*, 2011). For lower values of k_{LDF}, the simulated results underestimate the experimental data. For higher k_{LDF} values than the optimal estimated ones, the shape of the uptake curves becomes sharper, overestimating the uptake for a given time.

In a fixed bed experiment, other factors besides mass transfer coefficient may influence the shape of the breakthrough curve (i.e., axial dispersion and heat effects). Such factors can be significant and lead to discrepancies in the estimation of the mass transfer coefficient, if they are not properly addressed or measured. The approach presented here has the advantage of avoiding or minimizing such effects by using a gravimetric batch system. With the proposed procedure, one may obtain fast and reliable results in a more efficient way than those obtained by model matching with column dynamics experiments (Siqueira *et al.*, 2018b).

5.4. Heats of Adsorption

Figure 22 shows the experimental differential heat of adsorption measured according to the CO_2 and N_2 loading for all adsorbents in study. It can be noted that the differential heat of adsorption, for both components, presents higher values in the region of low pressure in the experimental data. The higher values of CO_2 and N_2 heat of adsorption at low coverage can be attributed to the sites more preferential for adsorption, i.e. the first molecules are more energetically attracted by the sites, although the difference between the values of heat of adsorption at low and high coverage is not so large. This relative low values and not so large difference of heat of adsorption can be attributed to the predominance of physical adsorption in the system. According to the literature, heat of adsorption when chemical adsorption is performed presented values in a range 90 – 140 kJ mol^{-1} for CO_2 (Serna-Guerrero *et al.*, 2010).

Figure 22 ─ Differential heat of adsorption of each component (CO_2 and N_2) varying according to the adsorbed amount on activated carbon, a) Norit RB4, b) Filtron N and c) Charbon 500

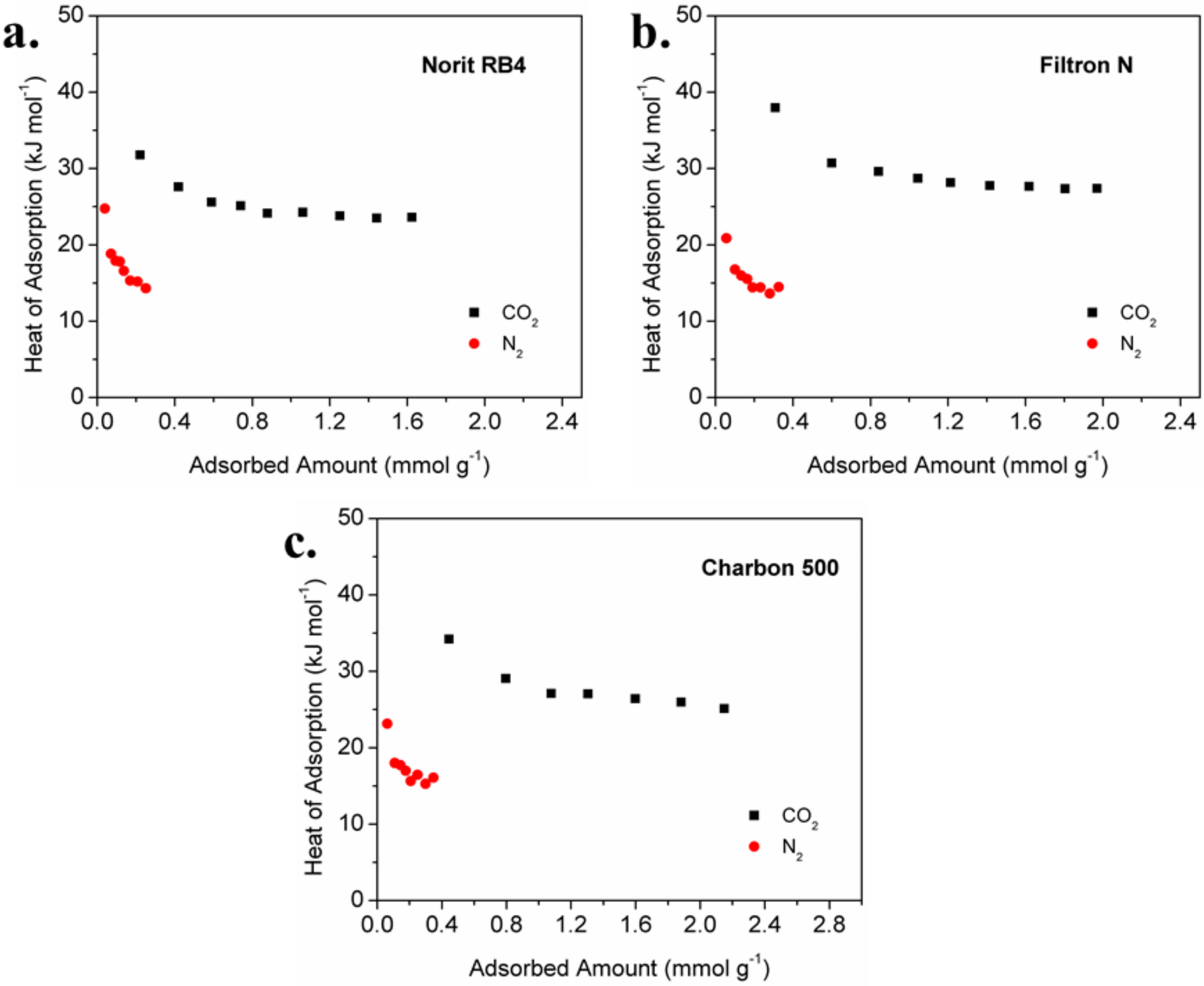

Source: Author

In simulation process, the heat of adsorption was calculated using Equation (23). The calculation of heat of adsorption of CO_2 and N_2 by Clausius-Clapeyron equation was performed in order to compare the values to the experimental data from calorimetry (differential heat of adsorption) and find an average value for using in energy balance equation.

In Figure 23 and Figure 24, it is presented the CO_2 and N_2 differential and isosteric heat of adsorption according the each component loading. The Clausius-Clapeyron equation results showed good agreement with the experimental data for all activated carbon. As the difference of heat of adsorption at low and high coverage is not so significant, the isosteric heat of adsorption used in simulation process can be considered constant and they were selected for CO_2 and N_2 as 25 kJ mol^{-1} and 15 kJ mol^{-1}, respectively.

Figure 23 ─ CO_2 differential and isosteric heat of adsorption varying according to the adsorbed amount on activated carbon, a) Norit RB4, b) Filtron N and c) Charbon 500

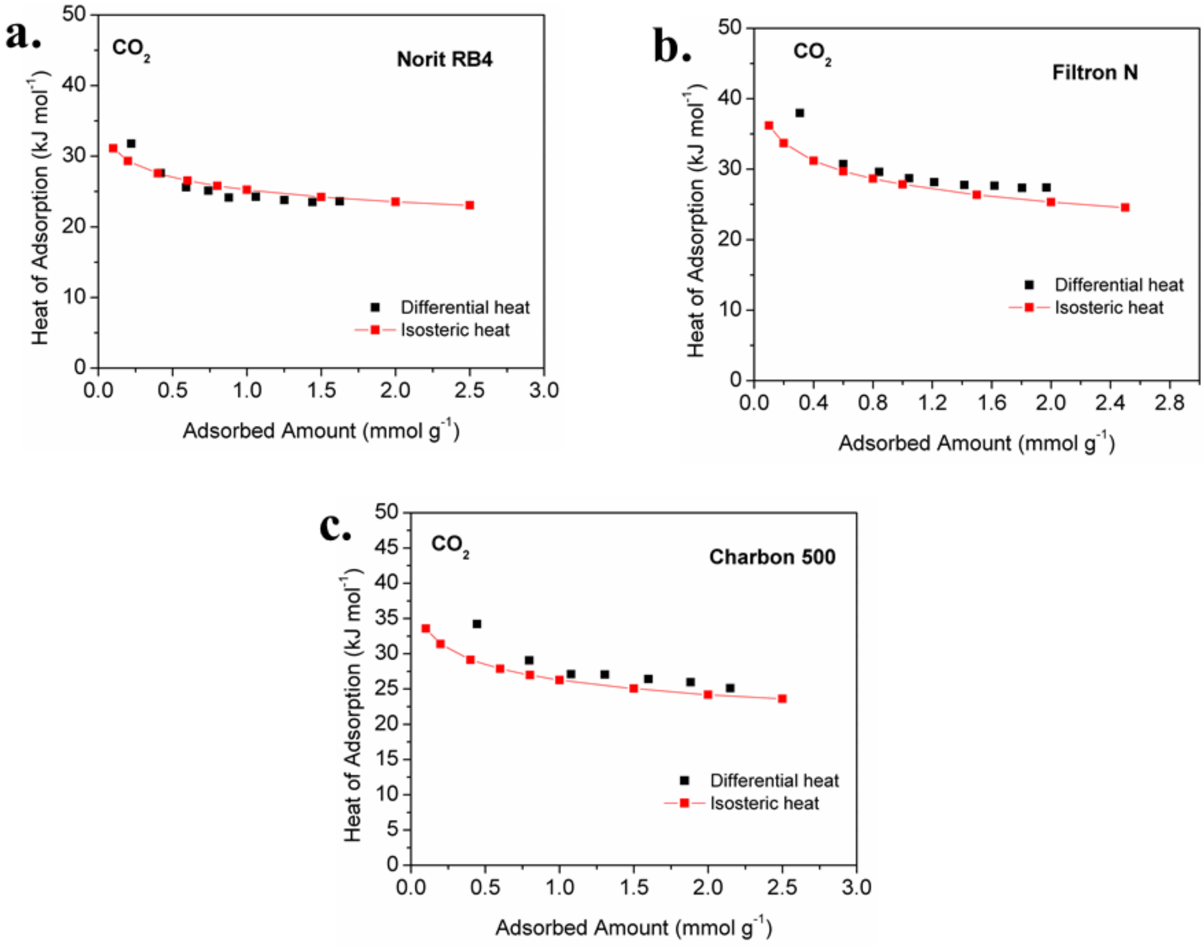

Source: Author

Figure 24 — N_2 differential and isosteric heat of adsorption varying according to the adsorbed amount on activated carbon, a) Norit RB4, b) Filtron N and c) Charbon 500

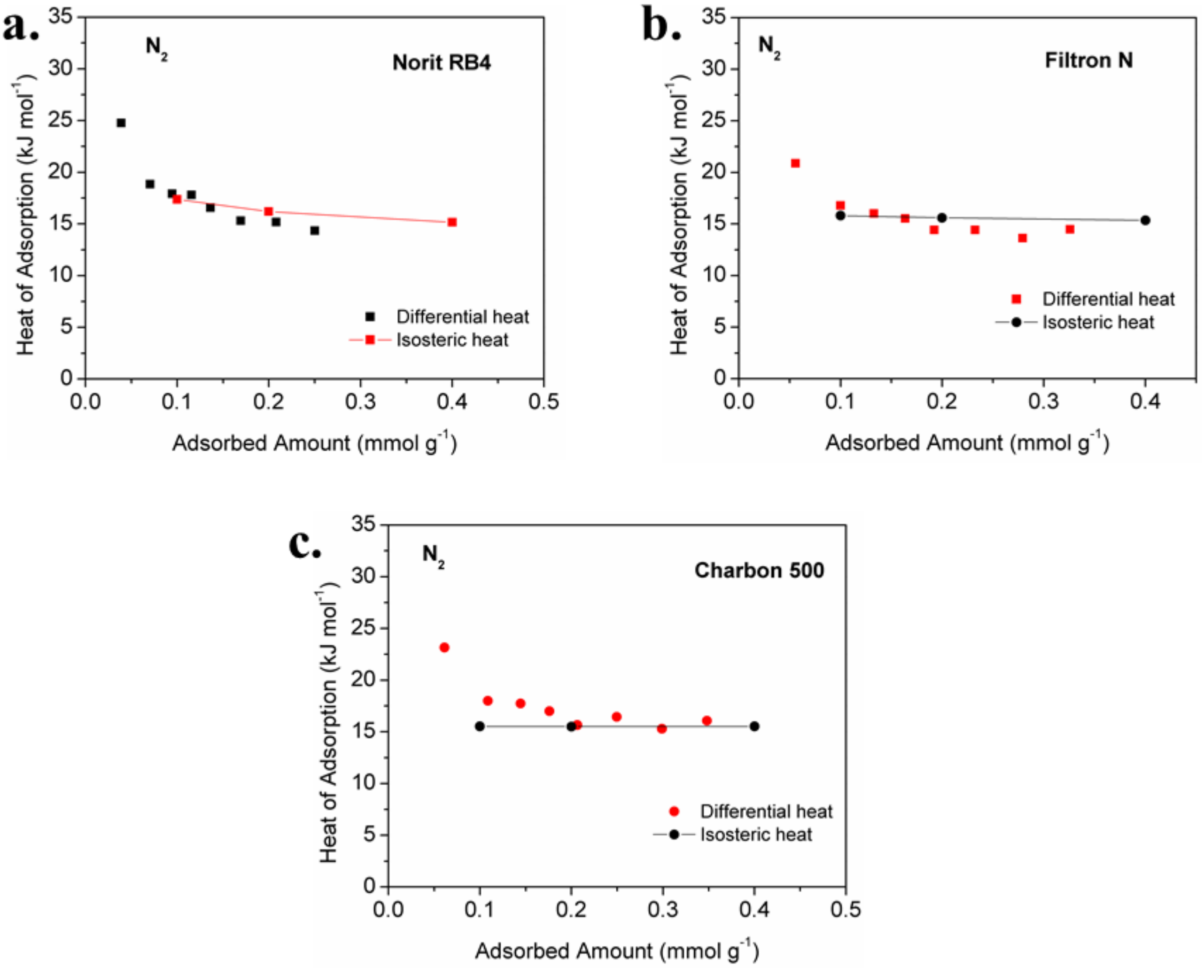

Source: Author

5.5. Breakthrough Curves

5.5.1. Single component

Breakthrough curves were performed in order to validate the simulation of the adsorption process in a fixed bed. Experimental data are compared to the simulation of CO_2 and N_2 adsorption diluted in He. Figure 25 and Figure 26 show the breakthrough curves of 10% CO_2 and 10% N_2 in helium, respectively. The breakthrough tests were assumed as pure component once He is considered an inert gas. The breakthrough curves were performed at 6, 12 and 18 bar for all the three adsorbents. For all of them, the simulated results described quite well the concentration profile (C / C_0).

According to the shape of the equilibrium isotherm, the time of breakpoint increases because the adsorbed amount is higher when pressure is increased. However, on the limits of the isotherm curve, the gas adsorbed amount tends to be constant or have an insignificant mass variation. Even when the pressure applied is on this limit region of the isotherm curve, the time of breakpoint also will tend to increase due to the velocity of the gas inside the column influenced by the system pressure. Hence, the interpretation of the late or early breakpoint time in a breakthrough curve has to be considered by the factor of the lumped of those two phenomena; system pressure and equilibrium isotherm.

As observed in Figure 25, Charbon 500 exhibited the largest breakpoint time for CO_2 at the highest pressure (CO_2 partial pressure of 1.8 bar), followed by Filtron N and then by Norit RB4, which displayed the lowest CO_2 adsorbed amount. Those differences in the breakthrough time can be noticed at higher pressures. For such CO_2 partial pressure and temperature at 298 K, according to Figure 25, in those conditions, Norit RB4 is clearly the adsorbent that adsorbs the least (lower breakpoint time) and Charbon 500 adsorbs the most (higher breakpoint time) indicating that besides the similarity among the textural properties the activated carbon, Charbon 500 in some way presented higher CO_2 adsorbed amount. The previous conclusion can be explained by the bed density influence. The density of the carbons is different and the mass of adsorbent that fills the column is a crucial parameter to be evaluated in the studied cases for gas separation in fixed bed. Charbon 500 and Filtron N presented approximated CO_2 adsorbed amount in adsorption equilibrium isotherm. However, in the fixed bed experiment, Charbon 500 had higher mass inside the column (see Table 13), which allows increasing the CO_2 adsorbed amount, (i.e., the larger the mass of the adsorbent packed in the column, the larger the adsorbed amount). The adsorbent mass in the column used in all dynamic experiments for each material is presented in Table 13.

Table 13 ─ Mass of adsorbent inside the column

	Filtron N	**Norit RB4**	**Charbon 500**
Adsorbent mass [kg]	0.136	0.166	0.171

Source: Author

Figure 26 suggests that Charbon 500 also adsorbed higher amounts of N_2 than the other two adsorbents. Besides the relative concentration curves, the history of temperature was also checked during the fixed bed experiments.

Figure 27 presents the history of temperature related to the experimental data of CO_2 showed in Figure 25, only at 6 bar. Figure 28 shows the history of temperature of the experiments with N_2 (Figure 26) also at 6 bar for all adsorbents. The temperature data of each thermocouple can be found individually in Appendix C and D for clear observation.

During the CO_2 adsorption, a temperature increase of around 20 K can be observed, except for Norit RB4. In Figure 27, the smaller temperature increment (~10 K) during the breakthrough experiments for Norit RB4 confirms its poorer performance for CO_2 adsorption. For the case of N_2, the temperature did not exhibit a large rising (i.e., 4 K of temperature difference). This little difference between the temperatures, in Figure 27 and Figure 28 (20 K and 10 K, respectively), may be explained by the preferential adsorption of CO_2 molecules onto the activated carbon porous structure in comparison with N_2. Moreover, the superior attraction for CO_2 can be confirmed by the difference in the values of the isosteric heats of adsorption between CO_2 and N_2 in all the adsorbents (as seen in Figure 23 and Figure 24), which are estimated according to the isotherms data at different temperatures. Heat of adsorption of N_2 adsorption on activated carbon is much lower than that of CO_2.

Figure 25 ─ Relative concentration history of CO_2 on fixed bed at 6 bar, 12 bar and 18 bar. (a) Filtron N, (b) Norit RB4 and (c) Charbon 500

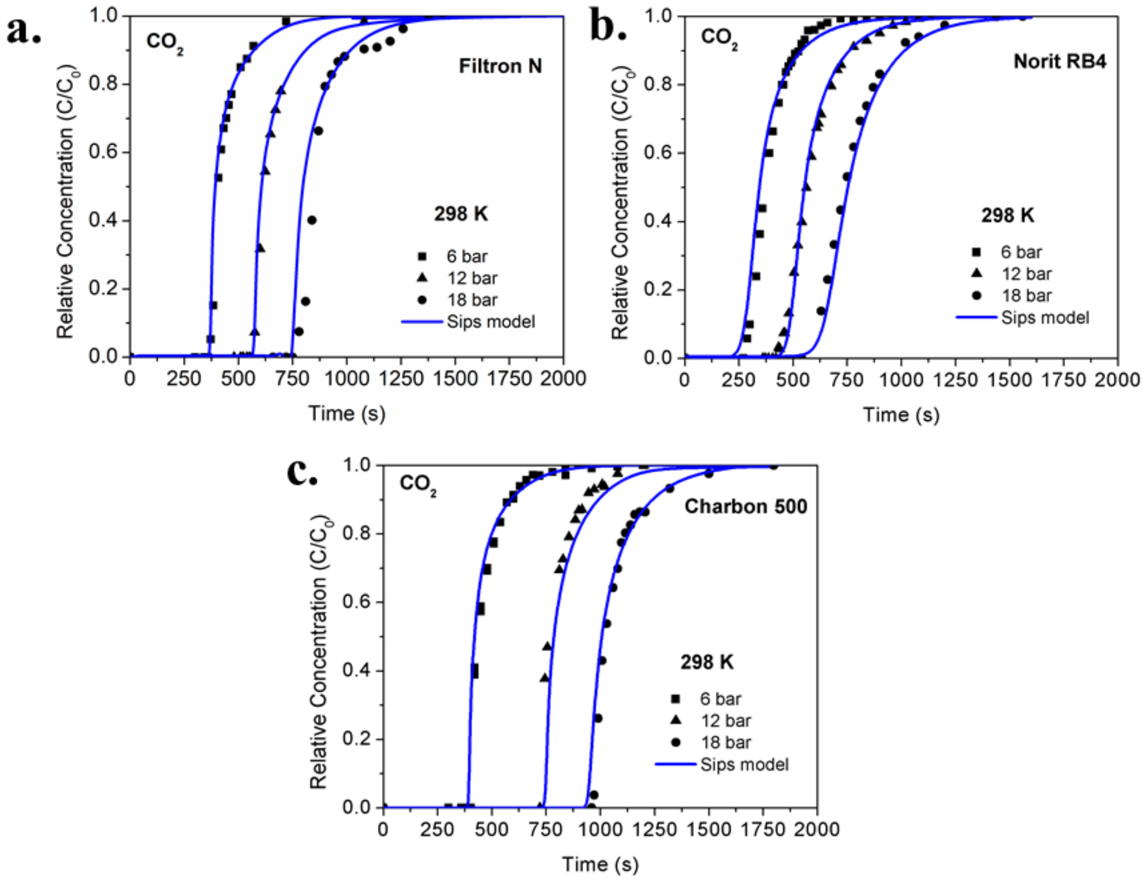

Source: Author

Figure 26 ─ Relative concentration history of N_2 on fixed bed at 6 bar, 12 bar and 18 bar. (a) Filtron N, (b) Norit RB4 and (c) Charbon 500

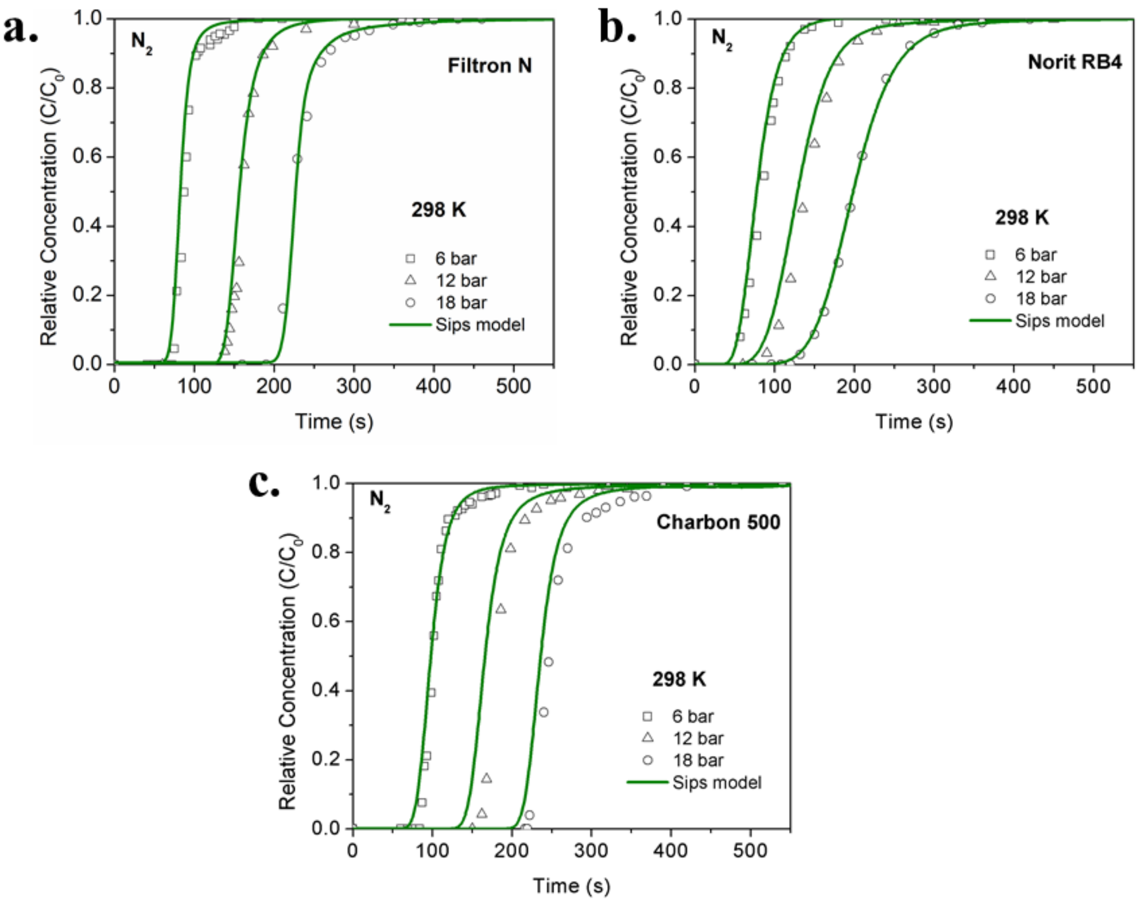

Source: Author

Figure 27 ─ History of temperature of CO_2 on fixed bed at 6 bar, 12 bar and 18 bar. (a) Filtron N, (b) Norit RB4 and (c) Charbon 500

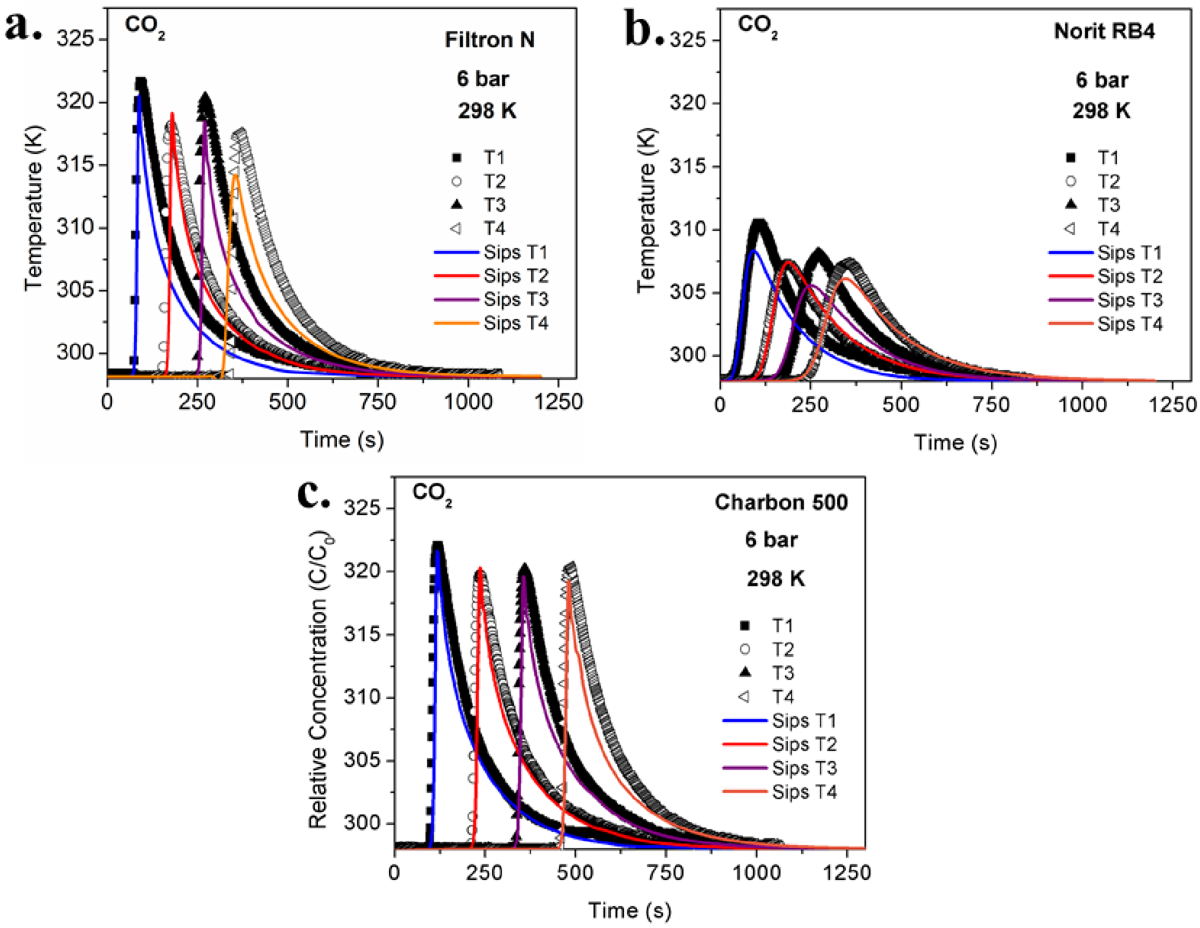

Source: Author

Figure 28 ─ History of temperature of N_2 on fixed bed at 6 bar, 12 bar and 18 bar. (a) Filtron N, (b) Norit RB4 and (c) Charbon 500

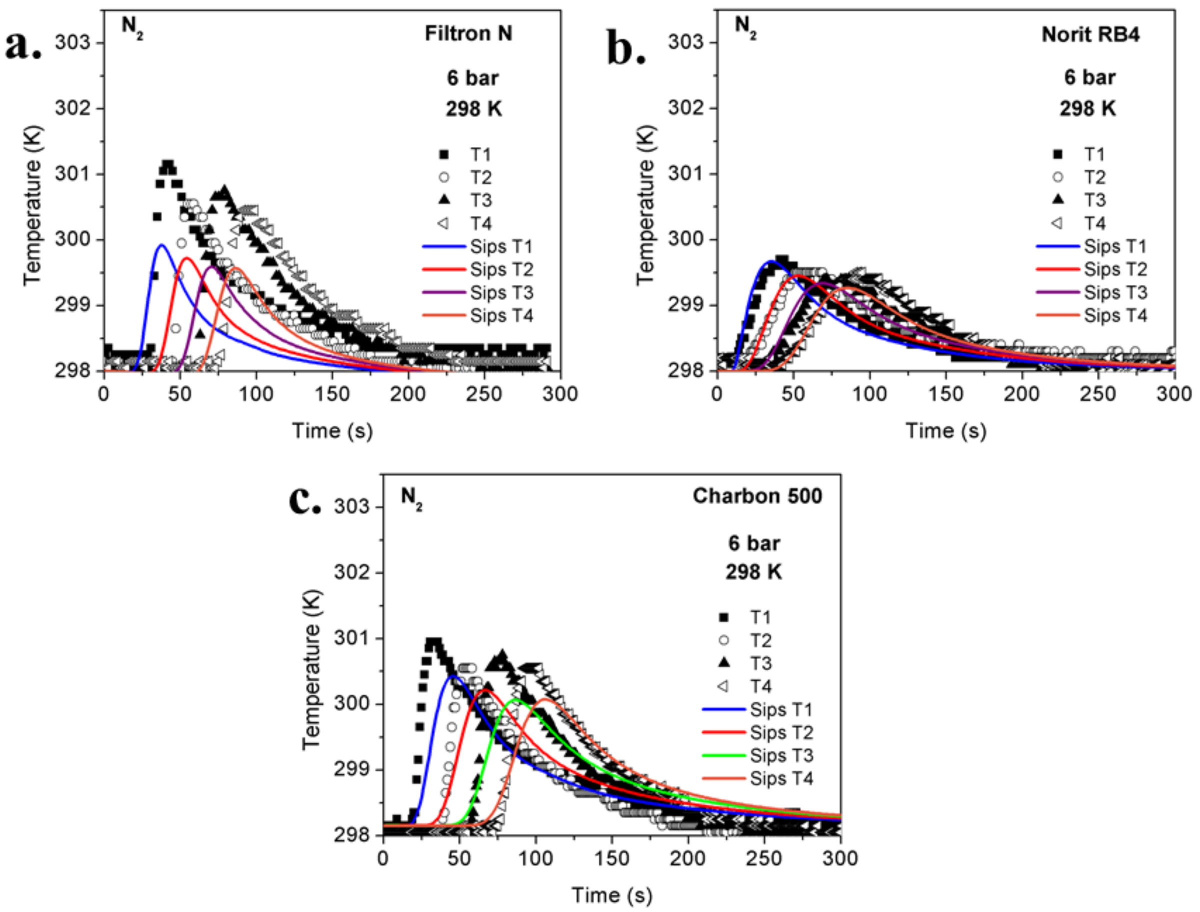

Source: Author

It can be noted that Sips model can describe the experimental data for pure components for all pressures set in the dynamic test. Similarly, the history of temperature is satisfactorily described by the model for all adsorbents at all range of pressure investigated.

In order to study the behavior of the CO_2 adsorption from a gas mixture with other components, such as CO_2+N_2, binary mixture breakthrough curves were performed. In this case, a study of CO_2 capture from a typical dry flue gas composition was used. The model was validated by varying the pressure values.

5.5.2. *Binary mixture (CO_2+N_2)*

As previously reported, all the activated carbons presented similar results of equilibrium adsorption isotherm and breakthrough curves for single gas tests. Correspondingly, the simulated results exhibited good agreement with the experimental data for all adsorbents studied. In order to assess only the appropriate mixture model comparing to Sips Extended, the evaluation of the IAST model for binary mixture at different pressures was applied for one activated carbon (Norit RB4).

Figure 29 shows the breakthrough curves at different pressures for the Extended Sips model used to simulate CO_2/N_2 mixture in a fixed bed. It was observed that, using this model, it did not agree with the experimental data, mainly when pressure was increased. It can be noted that at the lower total pressure (6 bar), CO_2 concentration profile still agrees with some experimental data. However, when pressure was increased the simulated curve did not represent the experimental data quite well.

Figure 29 ─ Breakthrough curve of binary mixture (CO_2+N_2) in Norit RB4 at (a) 6 bar, (b) 12 bar and (c) 18 bar. All experiments performed at 298 K. Experimental data (scatters) and ES model (line).

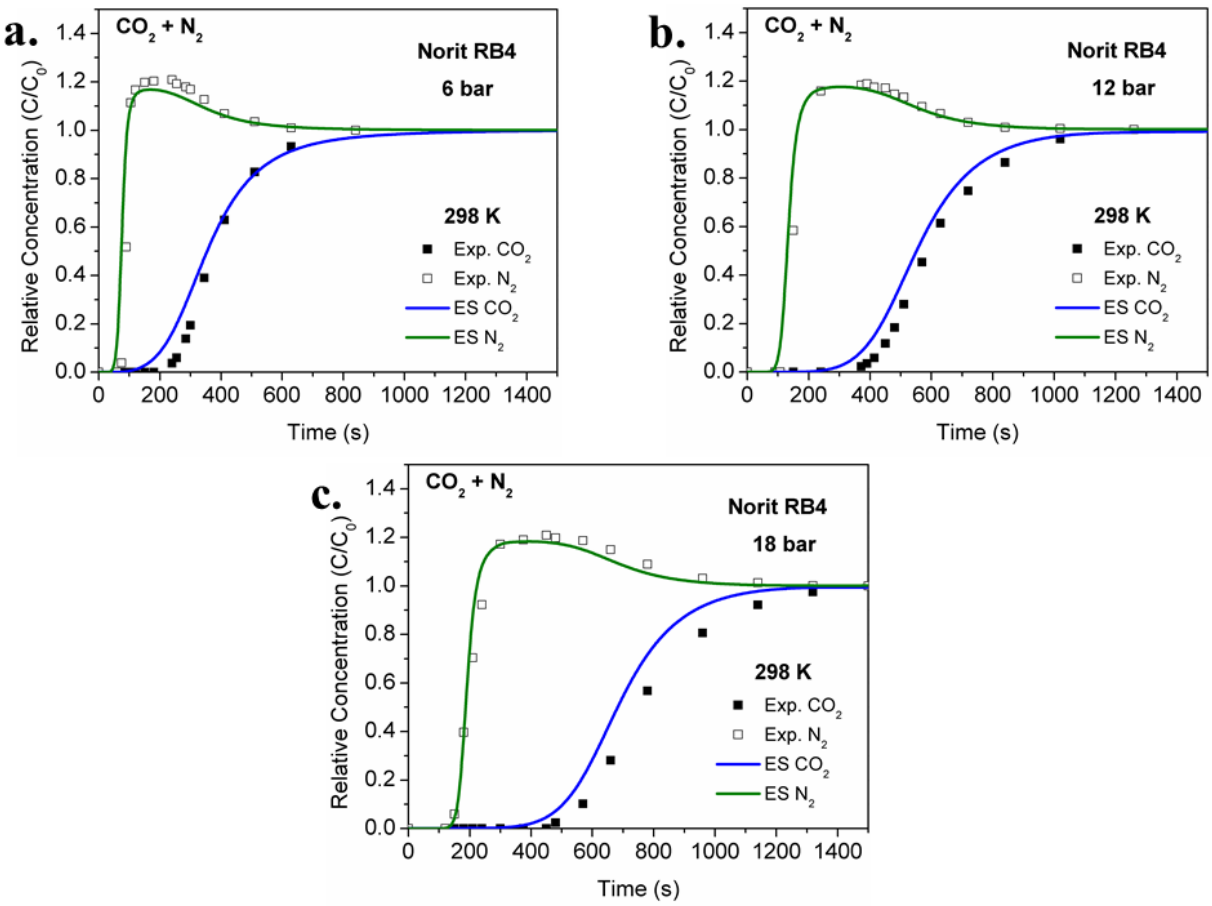

Source: Author

Due to the similarity in static measurements results between the activated carbons studied herein and the approximated values of model parameters, it is likely that their simulated results for breakthrough curves were similar to the ones found in Figure 29 using Extended Sips model.

Taking as example the Figure 29c, it can be noted that the breakthrough curve of CO_2 is significant far from the experimental data. It suggests that ES model underestimated the CO_2 adsorbed amount since the area above the curve represents the amount adsorbed in the fixed bed at the equilibrium condition. The concentration profile for N_2 agrees with experimental data up to the roll-up. The roll-up in fixed bed experimental data observed for N_2 is a typical behaviour of the less adsorbed component in a binary non-linear adsorption equilibrium. This phenomena is caused by a displacement of the weaker adsorbate (N_2) by the stronger one (CO_2). That is why at a specific time, nitrogen relative concentration at the bed outlet exceeds unity. It can be observed that the simulated curve of N_2 is quite below the experimental data. It suggests that ES model describes a system where N_2 quantity is more retained in the fixed bed, i.e. less nitrogen amount leaves the surface of adsorbent and less CO_2 amount takes its place. The latter statement can also explained why the model described a lower CO_2 adsorbed amount.

In Figure 30, it is shown the breakthrough curves at different pressures for IAST model used to simulate CO_2/N_2 mixture adsorption in a fixed bed. It can be observed that the IAST model predict very well the experimental data. Also, the simulated data of temperature history have a good agreement with the experimental temperature measured by thermocouples. For that reason, IAST model showed to be the most adequate equation model to predict the dynamic separation of a gas mixture. It is here proved that this model describes better what happens experimentally during the process.

Figure 30 ─ Breakthrough curve of binary mixture (CO_2+N_2) in Norit RB4 at (a) 6 bar, (b) 12 bar and (c) 18 bar. All experiments performed at 298 K. Experimental data (scatters) and IAST model (line).

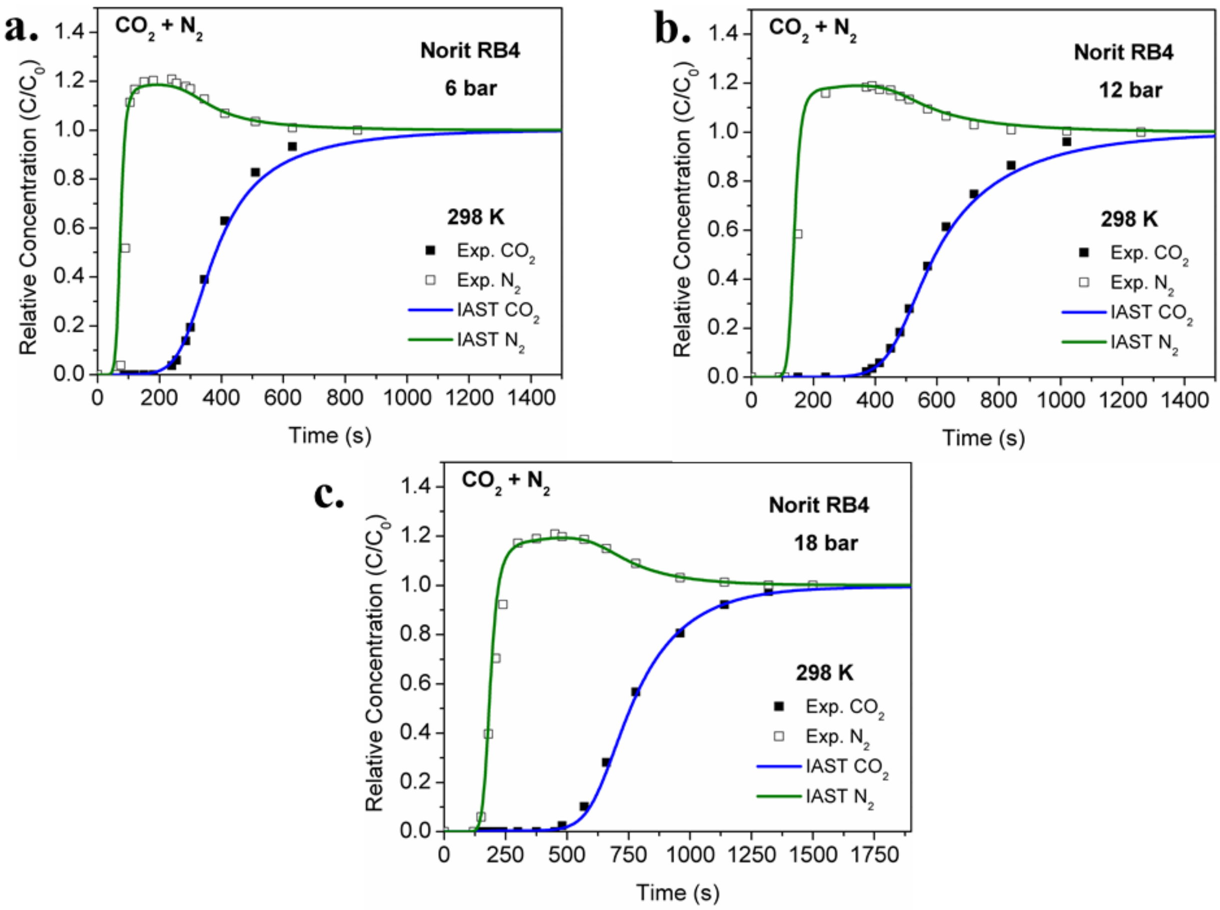

Source: Author

Figure 31 ─ Histories of temperature of binary mixture (CO_2+N_2) in Norit RB4 at (a) 6 bar, (b) 12 bar and (c) 18 bar. Experimental data (scatters) and IAST model (line).

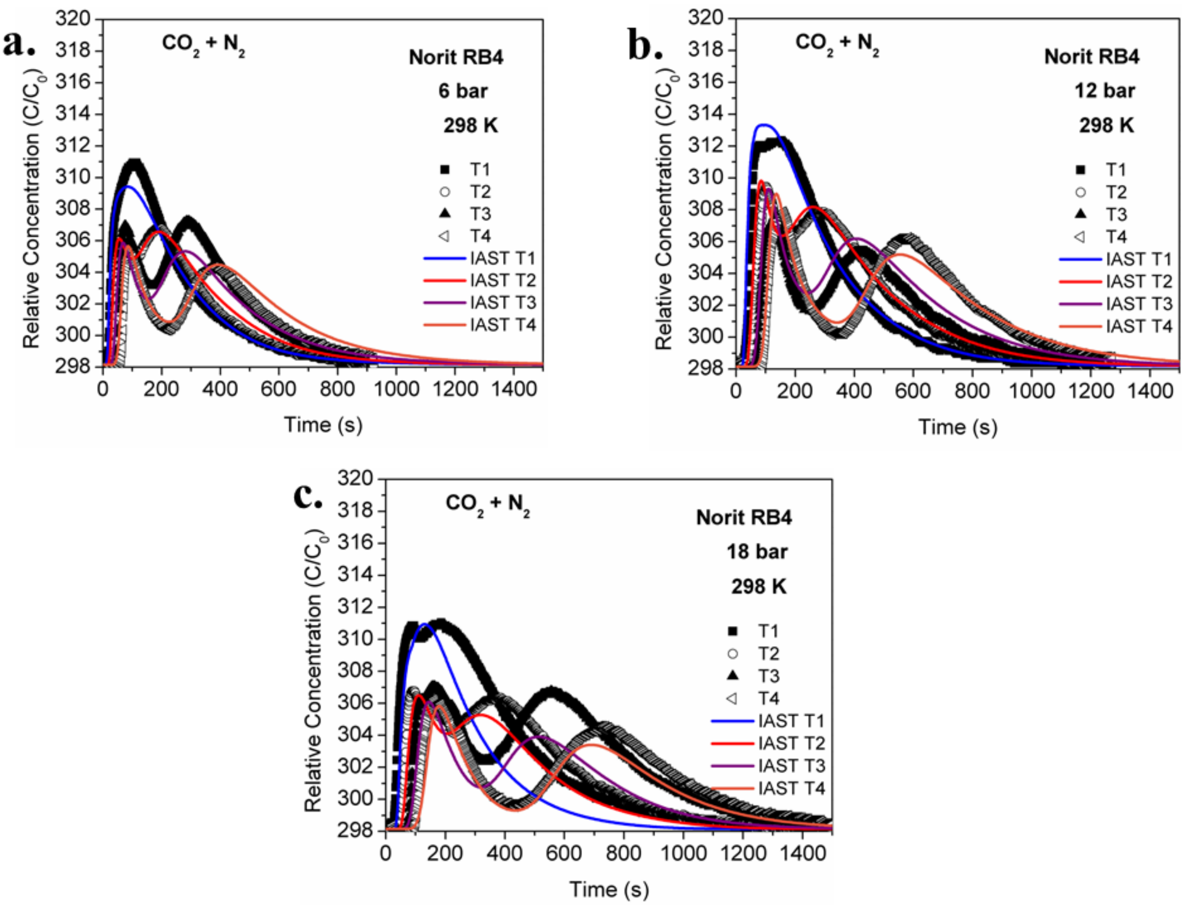

Source: Author

The history of temperatures measured by the probes placed along the column were also compared to simulated results for the breakthrough curves at the low and high total pressures (Figure 31). Each thermocouple indicates two temperature peaks corresponding to the net heat generated by the adsorption of both components during the breakthrough experiment. As the gas mixture enters the column and adsorption takes place, heat is generated and conducted through the bed. Since CO_2 is preferebly adsorbed in comparison to N_2, the concentration front of the latter moves faster throughout the bed allowing its adsorption as soon as free adsorption sites are reached. The greater the distance from the bed inlet, the higher the separation between both components, which is noted by observing the increasing gap between the peaks in the same experimental run. Analysing the thermocouple 4 in Figure 31 (each thermocouple data can be seen individually in Appendix E), the first temperature peak indicates the heat generated by local N_2 adsorption while the second one corresponds to the local CO_2 adsorption. Although the heat of adsorption of CO_2 is higher than that of N_2, one can note that the second peak is lower than the first. This can be attributed to the combination between the lower CO_2 concentration (10.8%) and the desorption of N_2 (cooling effect) caused by CO_2 displacement, as previously explained. Also, the higher peak for N_2 shown by each TC can be attributed to the sum of its local adsorption and the CO_2 adsorption heat generated that was carried by the gas stream. This phenomenum cannot be seen only in results of thermocouple 1. This thermocouple is placed in the bed inlet. It is the first to sense the effects of the adsorption in the column. In bed inlet, the properly separation did not occur since there is no bed length for such operation. Hence, the CO_2 and N_2 adsorption occur simutaneously in this region of the column and the desorption effects are almost null. Then, it explains the first temperature peak be much higher when comparing to the other ones.

5.6. PSA process

After the fixed-bed model validations the next step was to simulate PSA cycles as described in the previous section. As mentioned before, nitrogen and carbon dioxide were dosed to the PSA unit in a composition ratio similar to typical values for dry flue gases (i.e. 85% of N_2 and 15% of CO_2). With a pressurization time around 60 seconds, the PSA process was performed in 25 cycles, reaching the cyclic steady state (CSS) around the 10^{th}. Adsorption time was set to 70 seconds so that it does not have a time step lower than pressurization. Due to the results of the models comparison seen in previously section, IAST was then selected to be used as the appropriate model to simulate the PSA process.

5.6.1. Pressure history

The pressure profile inside the adsorption bed of the cycles and the simulated pressure data are displayed in Figure 32, showing good agreement between each other. The pressure changing from 1 to 6 bar denotes the pressurization. It is followed by adsorption step where the dynamic separation occurs by means of adsorption. In this step the pressure was kept constant by the backpressure controller and its time was selected for duration of seventy seconds. This step time was chosen to be larger than the time of pressurization step since adsorption is the main step of the cyclic process and it was aimed a relative N_2 high productivity. After that it starts blowdown step; there was a counter-current depressurization and a quick drop of pressure from 6 to 1 bar was presented. Blowdown aims to remove the high concentration of impurities inside the column, such as CO_2, since after adsorption process the column is filled with high CO_2 content. The CO_2 removal was chosen to be applied counter-current so that the CO_2 do not contaminate the product in the bed outlet. Also, the blowdown step goals to decrease the pressure in order to improve the gas desorption and prepare the column to receive the following step. When blowdown reached the lower pressure of PSA cycles (1 bar), the purge was started with pure N_2 until the cycle reinitiate. The goal of blowdown and purge steps is to clean the entire fixed bed. The purge step with pure N_2 after blowdown then aims to decrease even more the CO_2 partial pressure. Since the pressure of column after blowdown is the lower one, when fixed bed is filled with 100% of N_2 at 1 bar (purge), the partial pressure of CO_2 decrease to the minimum.

It is worth noting that the pressurization step simulation is according to time of the experiment. The pressurization step in simulation is guided by the molar flow rate, kinetic of adsorption and time of the step. This time was set by information from experimental data. It shows that simulation is well validated when even the duration of column pressurization coincides with the experimental data besides all estimated parameters that can influence this step. If not, even the time chosen equal to the experimental pressurization, the increasing be inside the column could be erroneous and could larger or insufficient to reach 6 bar.

Figure 32 ─ Pressure history of PSA process. Experimental and simulated data.

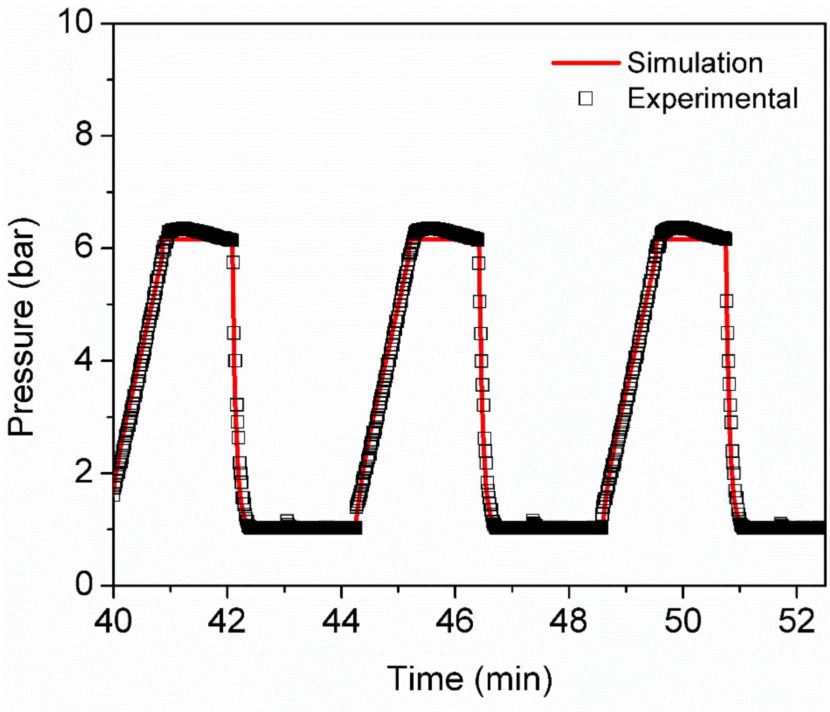

Source: Author

Other results were assessed to evaluate the simulation validation of a PSA process to separate N_2 and CO_2. Histories of temperature were recorded by the thermocouple positioned along the column. As experimental performance, simulated data were assessed according each thermocouple as shown in Figure 33. All the simulated results had good agreement with the experimental one for each thermocouple.

5.6.2. Temperature history

The results shown in Figure 33 were plotted when the PSA process reached the cyclic steady state. It shows a variation of temperature about 10 K between the adsorption and desorption steps. It can be noted that the simulated temperature data coincides quite well with the experimental when pressurization and adsorption steps are performed. These steps can be seen by the history of temperature when a larger temperature variation occurred. When pressurization occurs the fixed bed is receiving the gas mixture and at this step the adsorption process is already happening. It explains the increase of temperature. Then, when the adsorption happens, the temperature continues to increasing up to the maximum value and then starts to smooth decrease due to the fixed bed is being saturated. The history of temperature of the adsorption step is similar to that one observed in the breakthrough curves, but can be less noticeable in the PSA experimental data due to the quick procedures of this process.

The rapidly decreasing of temperature indicates the blowdown step since the pressure swing at this step occurs abruptly. The pressure increasing improves desorption and since it is an endothermic process the temperature then will diminish. The difference between simulated and experimental results can be seen in the history of temperature at this step. As it can be observed in Figure 33, simulated results of blowdown step describe larger decreasing of temperature when compared to the experimental results. There are at least three reasons for that discrepancy. Firstly, it could be explained by the constant isosteric heat of adsorption set in the parameters of the simulation. The isosteric heat of adsorption is a loading dependent parameter which can vary between 35 – 21 kJ for these activated carbon, as it has been previously seen. Since the isosteric heat is denoted by an average value, it was assumed to be reliable using it in adsorption step experiments due to the heats of adsorption experimental data recorded 34 kJ for zero loading and 21 kJ for saturated conditions. These values are considered approximated and its change may not cause such difference to describe the heats of adsorption. In blowdown step, where the simulated temperature differs from experimental, it must be considered that not all adsobate is removed due to the very short time to do so. Then, the adsorbed amount would vary from saturated condition to one in which the coverage is not even close to zero loading since blowdown cannot desorb all CO_2 adsorbed in bed. Hence, it makes the isosteric heat of adsorption be acceptable to perform this experiment. Hence, this hypothesis can be discarded.

Figure 33 ─ Temperature history for a PSA process in cyclic steady state (a) Thermocouple 1, (b) Thermocouple 2, (c) Thermocouple 3, (d) Thermocouple 4.

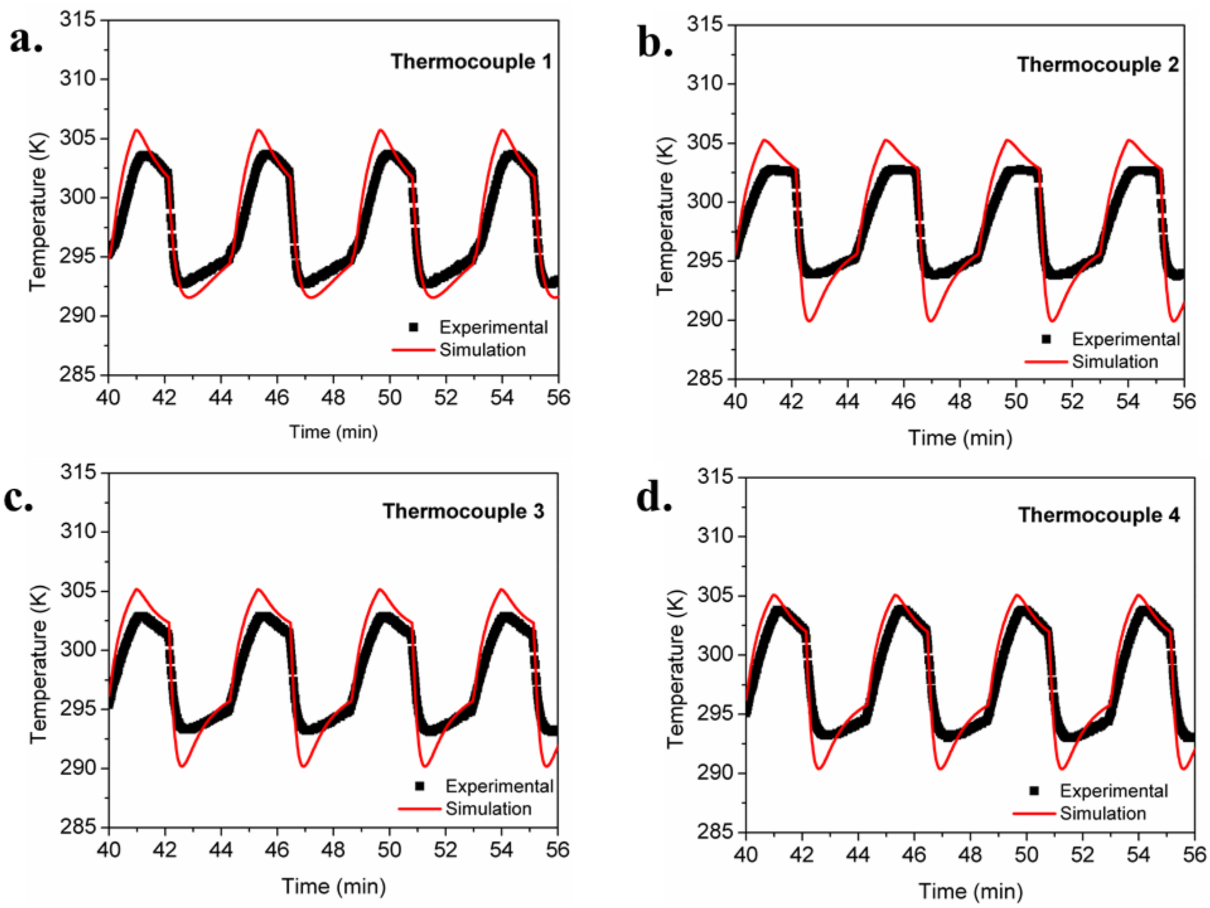

Source: Author

Second reason is linked to the mass transfer coefficient. Rigorously the k_{LDF} is a temperature dependent parameter. However, the mass transfer coefficient was determined only by adsorption experiments and simulation validations, and according to the dynamic results, the constant k_{LDF} value was satisfactorily acceptable. The k_{LDF} describes the gas diffusivity into the micropores of the particle and it is considered that this parameter is the same for adsorption and desorption since the molecules that enters or leave the adsorbent particle do not know if they are entering or leaving it. A more rigorous description of kinetic could be developed and a mass transfer parameter varying according to the gas loading would be more capable to describe an adsorption and desorption phenomena into an adsorbent particle.

The third hypothesis is that there is no isotherm model for lower temperature than 298 K. The model parameters fitting were performed between 298 K and 348 K. Simulation of the adsorbed amount at equilibrium at temperatures above or below that range will extrapolate the adsorbed amount and could not well describe such operation in that condition. As it can be seen in Figure 33, the discrepancy appears when the temperature is below 298 K.

5.6.3. PSA performance

The gas chromatograph attached to the experimental apparatus allowed analyzing the composition of gas mixture that leaves the column at the bottom. Due to the PSA process takes a very long time and the main goal of the experiment is to evaluate the N_2 purity of the process, the gas samples were collected in the adsorption step. Gas phase samples were collected at the end of the adsorption along the PSA cycles. Then, the achieved N_2 purity according to the number of cycles was then plotted in Figure 34.

Figure 34 – N_2 purity along the cycles of the PSA process.

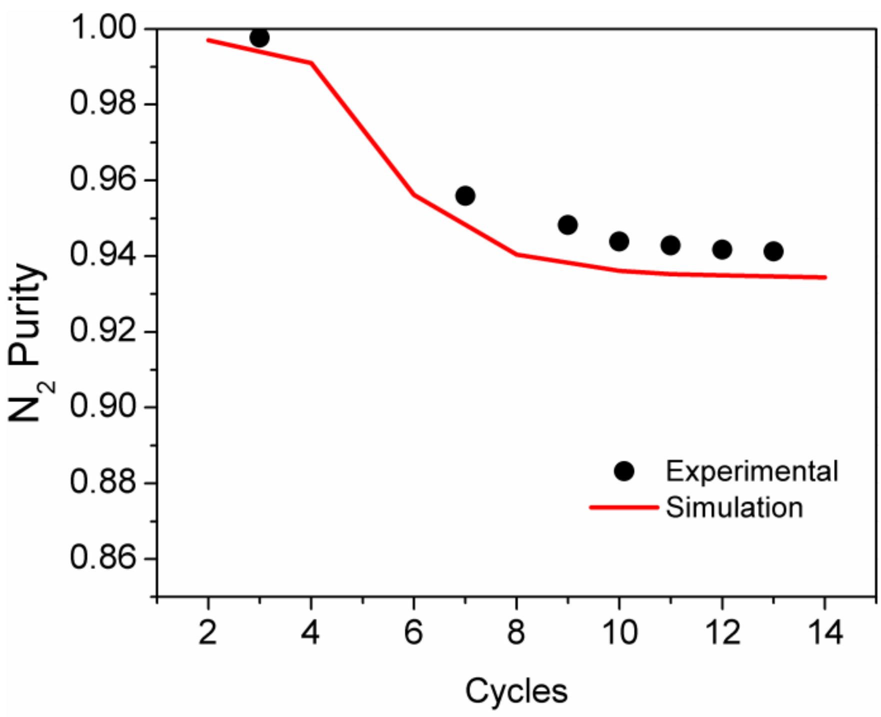

Source: Author

In the very early phase of the process the cyclic steady state was not reached yet. In the beginning of the experiment the packed bed is still filled with N_2 and free of CO_2, the most adsorbed gas in the mixture. Meanwhile the experiment is running the CO_2 concentration is filling the column. Even after the regeneration steps of Skarstrom cycle, the CO_2 concentration moves forward through the column. It is known that the most basic cycle of PSA is not capable to totally regenerate the activated carbon in a fixed bed during the experiment; blowdown and purge steps in short time are not sufficient to remove all CO_2 from the adsorber. So, as long as the CO_2 is flowing through the column the purity of N_2 was decreasing up to reach a cyclic steady state. This PSA experiment condition is noticeable when the entire column is operating repeatedly. It can be seen by the history of temperature in which present a uniform profile along the number of cycles and by the parameters performance such as purity. About the 10^{th} cycle, purity results suggest that the PSA process started the cyclic steady state since its value starts to be constant. Simulation data using adsorption step time of seventy seconds described quite well the values of N_2 purity along the PSA cycles according to the experimental data. It started from 100% then decrease to a constant value about 93.8% meanwhile the experimental results responded a purity of N_2 about 94.1%.

Figure 35 shows the CO_2 concentration at the column outlet with different time of adsorption step. It was chosen to be analyzed times from 50 to 175 seconds. As it was expected as much time the adsorption step occurs more contaminated the product will be. The higher value of N_2 purity was reached when feed operation was set on 50 seconds. It is noteworthy to mention that all the others parameters as molar flow rate in all the steps were kept constant, as well as maximum and minimum pressure. By doing that, the time of pressurization was kept the same and the CO_2 molar fraction was analyzed just by the influence of adsorption step time (Figure 35). It is shown the CO_2 concentration profile in the gas phase inside the column at the end of the adsorption time in the 25^{th} cycle, in which the cyclic steady state was already reached. CO_2 molar fraction can be an indirect evaluation of purity since its calculation is related to the fraction molar between CO_2 and N_2.

Figure 35 – Simulation of CO_2 molar fraction along the column with different time of adsorption step in a PSA process for CO_2/N_2 separation.

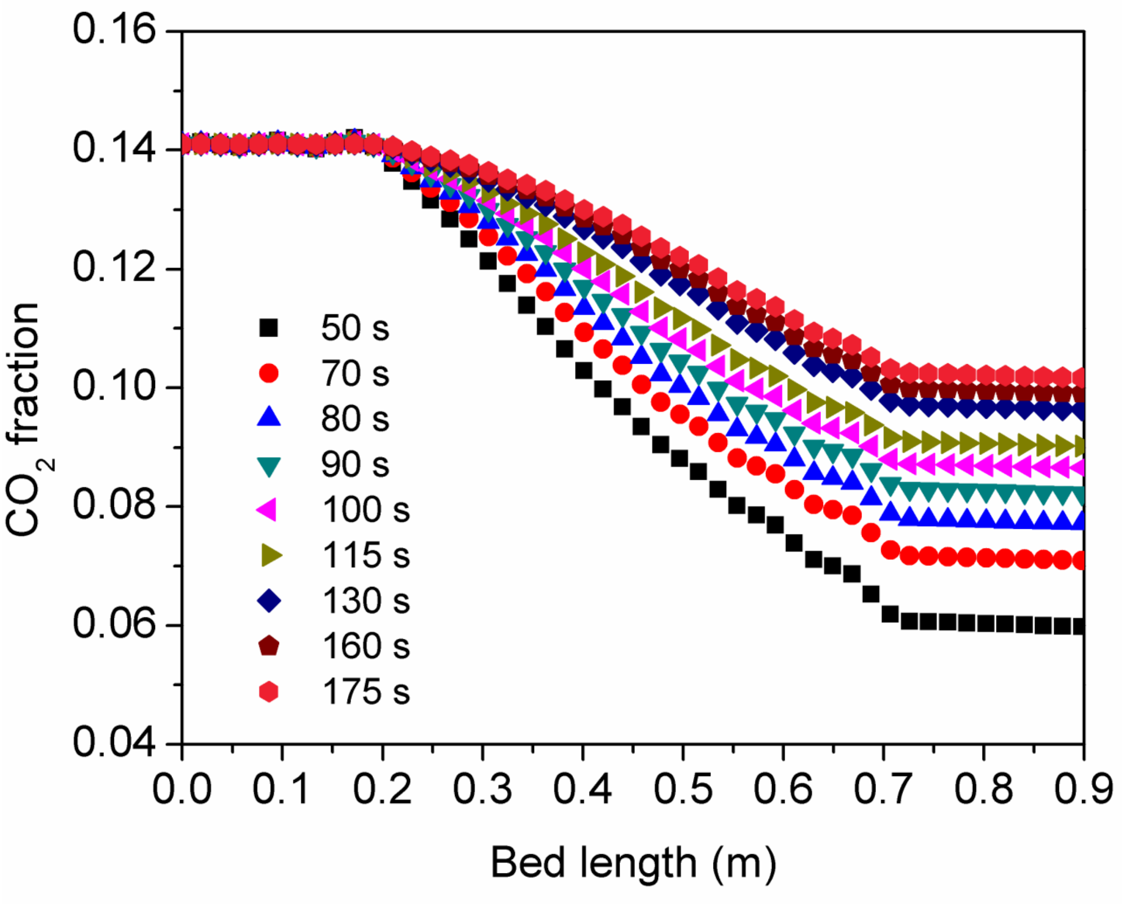

Source: Author

It can be noted that the CO_2 molar fraction is kept constant along 0.2 m of column and then start to decrease. It is explained by the dead volume before the packed bed, then when the gas mixture enters the adsorber the concentration of CO_2 in the gas phase starts to decline. At the end of the column the CO_2 molar fraction also presented a constant behavior, which represents the other dead volume in the end of the column. A minimum of CO_2 molar fraction was obtained using an adsorption time of 50 seconds due to the time of separation is lower and avoid contamination as showed conversely by the molar fraction when 175 seconds are set.

An appropriate time of adsorption can be selected by analyzing Figure 35. Choose the time of adsorption is an arbitrary task since it depends on the result you are keen on to achieve. It is also important to remember that the purity, recovery and productivity are dependent on each other. Increase purity values decreasing the time of adsorption will also result in a low productivity since it is related to time of adsorption step.

The PSA experimental setup unfortunately was not designed to measure experimental results of product recovery and productivity. However, since previous simulated results such as pressure history, temperature history and product purity were presented in good agreement with the experimental data, it was here assumed then that simulations of N_2 recovery and productivity data are adequate. Considering that, it was calculated the N_2 recovery along the process according to Equation (31) when it was and was not used equalization step. The result is presented varying with the number of cycle (Figure 36).

Figure 36 ─ N_2 purity and recovery, with and without equalization step, along the cycles of the PSA process.

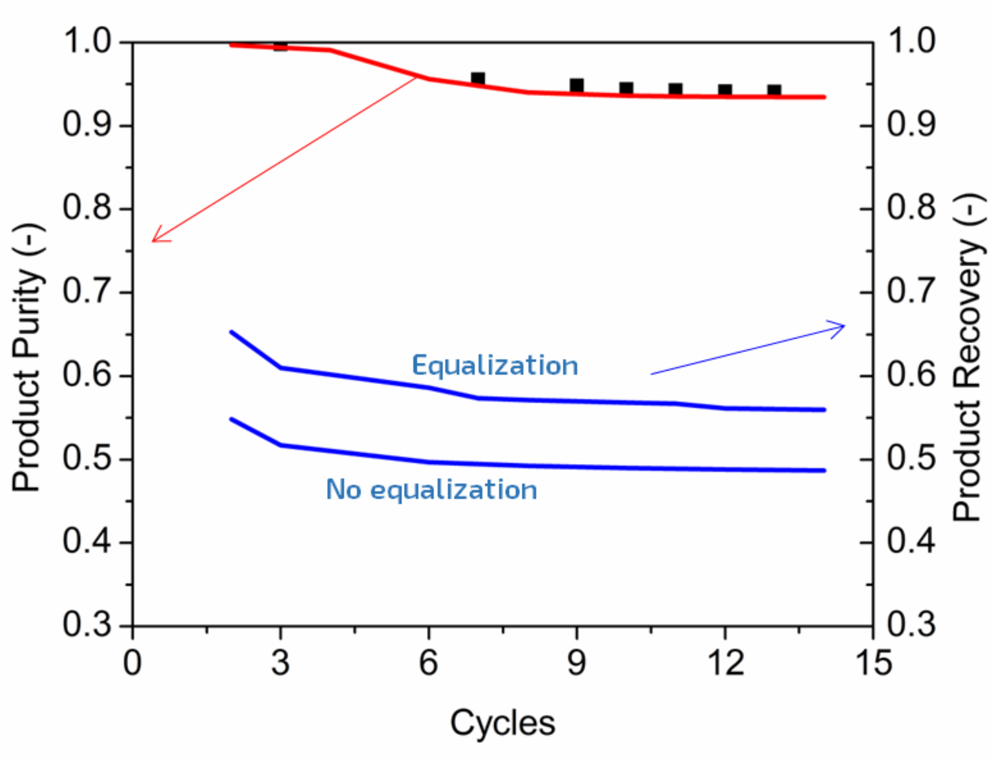

Source: Author

According to the N_2 recovery calculated by Equation (31) without equalization step, the PSA process responded a N_2 recovery value of 49% along the PSA cycles. Using the equalization step on simulation, it has shown that this step improves the product recovery as previously explained. By doing that, simulated results have shown the N_2 recovery using equalization (depressurization and pressurization equalization) between the two columns presented a higher recovery (above 55%) when compared to basic Skarstrom cycle. As the N_2 purity data showed; the explanation to the N_2 molar flow rate decreasing along the process can be explained by the increasing of CO_2 concentration leaving the column, which made the N_2 purity decreases. The results presented in Figure 36 can also be explained by the similar discussion. Decreasing the N_2 molar flow rate in the outlet of the column made the recovery decrease, since according to the Equation (31) reducing the numerator value of the equation and keeping constant its denominator, it tends to decrease the recovery value. The difference between the recovery values along the number of cycles is not so accentuate as the purity product. The N_2 recovery kept a constant value of 49% when the process reached the cyclic steady state. The low value of recovery can be explained by the low number of columns and consequently mainly due to the absent of equalization steps, which is a crucial step to improve the product recovery. According to Equation (32), the N_2 productivity was 330.4 g/h/kg$_{ads}$.

5.6.4. Dead volume influence

The PSA performance was also evaluated according to the dead volume that can be found in columns. As previously mentioned the dead volume of the fixed bed is approximated 50% of the total volume (column volume). Then, results of PSA performance were plotted in Figure 37 to demonstrate the dead volume influence on the performance when it is removed. In Figure 37 (a, b and c), the N_2 purity, recovery and productivity are presented according to the dead volume percentage in the column, respectively. It is noted then that dead volume does not significantly affect results of purity of a PSA process.

The N_2 purity along to dead volume percentage does not have significant variation. Since any gas purity determination is correlated only with adsorbent amount in the column, the dead volume cannot change gas purity value due to there is no adsorbent in such volume; the adsorption phenomenon occurs only in fixed bed. Then, regardless the volume of the column the performance of purity depends only on the adsorbent. The gas flows through the dead volume with the same concentration. Hence, when the mixture leaves the packed bed (bed filled with adsorbent), it flows through the column (dead volume z=L2 to L) without change its concentration. In other words, regardless the dead volume at the column end, $\partial C_{g,i} / \partial z = 0$.

Figure 37 ─ Influence of dead volume in a PSA process performance a) product purity, b) product recovery and c) productivity.

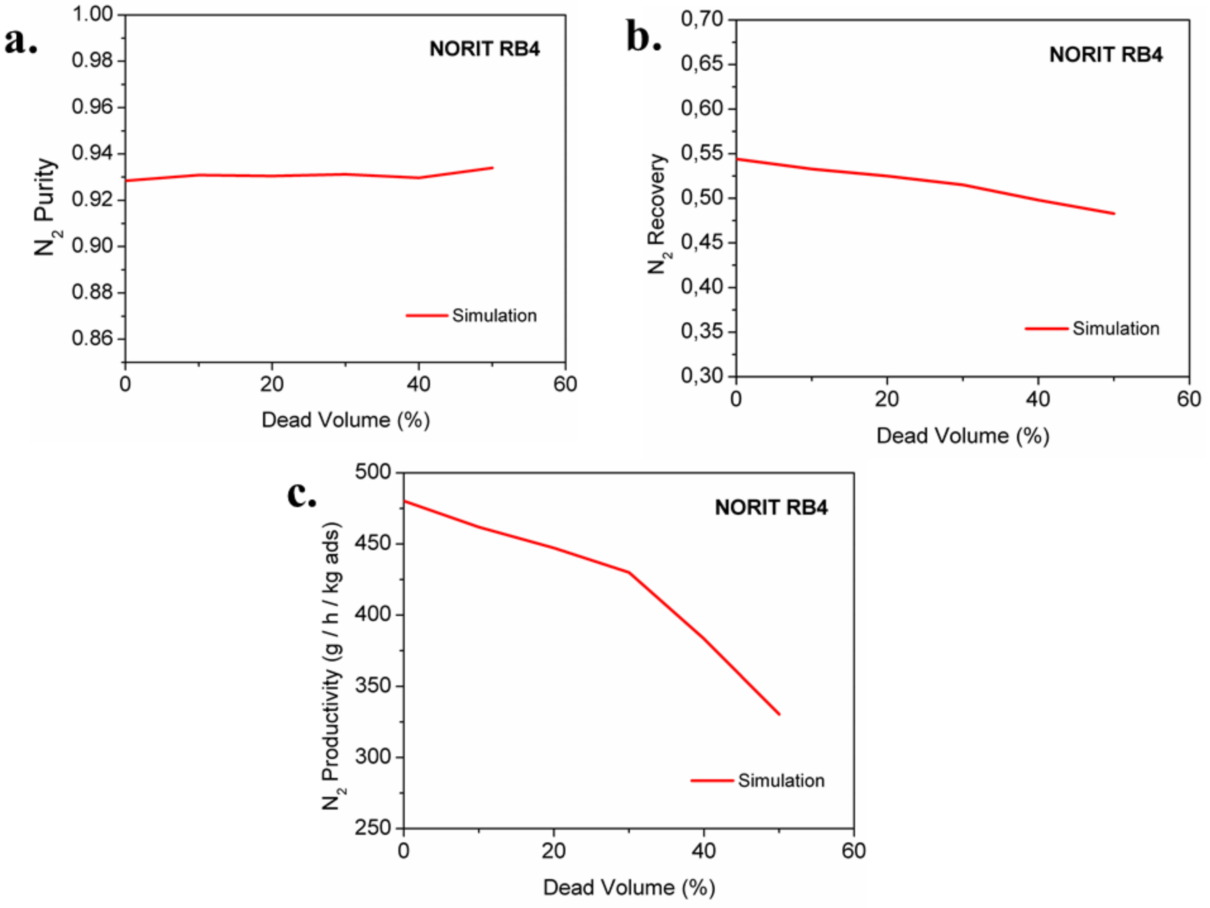

Source: Author

Conversely, N_2 recovery and specially its productivity performance are affected by the dead volume percentage in the fixed bed. Figure 37 (b and c) shows recovery and productivity from simulation results varying with dead volume percentage. When there is no dead volume at all, N_2 recovery and productivity reach their maximum value in this process. As long as the dead volume is increased in the column the gas both performance parameters are decreased. N_2 recovery decreases when dead volume is large due to the gas amount that enters in the column is also much larger during pressurization and adsorption steps. Then, this large amount of gas is removed during blowdown and purge steps. Furthermore, when there is no dead volume, the time of pressurization step is considerably decreased in this case. Thus, shorter time in pressurization step means less N_2 amount entering in the column and according to Equation (31); the equation denominator decreases its value increasing recovery product.

N_2 productivity decreasing can be explained by the pressurization and purge steps. Firstly, when pressurization is occurring, the gas mixture needs to fill the entire column so that it reaches the desired pressure. The dead volume makes that step take a longer time due to the largest volume of the column needed to be filled. Since productivity, according to Equation (32) is dependent on time, maintaining constant the other parameters of the equation, when pressurization step time is increased the entire cycle has its time also increased, the productivity then tends to decrease. So, as much as the cycle time the less the productivity, maintaining the same molar flow rate. Also, purge step can affect the productivity since the step needs more time to clean the column; before the N_2 of purge step reaches the fixed bed it is necessary to fulfill the dead volume of the top of the column. Those steps influence on the productivity due to the time needed to perform.

6. CONCLUSION

In this work, it was presented PSA process for separation of N_2/CO_2 from a gas stream with composition similar to dry flue gas (85% N_2, 15% CO_2, in molar basis). Firstly, studies of breakthrough curves maintaining the gas composition and varying the total pressure were essential to validate the model and to understand the behavior of the dynamic adsorption process of the gases. The design and model of a fixed bed or cyclic adsorption processes involve several differential equations solutions. The mathematical model and assumptions made in order to predict the behavior of the cyclic adsorption process for CO_2/N_2 separation was satisfactorily presented by results of pressure and temperature history as well product purity. A satisfactory value of N_2 purity was achieved by using the only the basic cyclic PSA process.

The time of adsorption step is an important parameter to reach a desirable purity value. Breakthrough curves experiments of gas mixture are recommended to give an idea of this step time and then to achieve the performance parameter requested, avoiding having unused part of the column. Then, since the adsorption procedure starts in the pressurization step it is recommended that this time of adsorption should be evaluated at low pressure, i.e. at the pressure in which the pressurization starts.

An alternative procedure to estimate the mass transfer coefficient for microporous materials has been presented and tested. The simple procedure of mass transfer coefficient estimative showed to be reliable and helped to confirm that the constant LDF parameter can be determined when an uptake experiment is performed sparing the need of experimental column dynamics data to evaluate or estimate the mass transfer properties. The determined k_{LDF} of the three activated carbons showed to be approximated values among them. It was indicated by the similarity of their textural properties.

The adsorption equilibrium isotherm models (adsorbed amount per mass unit) showed similar values between some different activated carbon in which only by fixed bed experiment was possible to see the different performance between them. Hence, it suggests that the different results of breakpoint time in the dynamic separation are due to the mass quantity inside the column volume. Charbon 500 can have a larger amount of adsorbent inside the same volume than Filtron N. Therefore, the bed density is one of the main parameter to be considered. Thus, in order to start comparing adsorbents performance in PSA processes it is then suggested that adsorption equilibrium isotherms should be performed according to their volume instead per mass unit. Another important point to be observed is the necessity of increasing the range of temperature for equilibrium isotherms in order to validate the model for a PSA process. It was seen by experimental data that PSA operates with pressure swing. Those changes in pressure levels tend to change the temperature inside the column due to the adsorption /desorption process. Then, equilibrium isotherms should be obtained also in lower temperature of that set in the PSA process to describe good agreement with the desorption step where the temperature decreases.

For a good representation of experimental data, empirical models of gas mixture are not recommended for separation process simulation in some conditions. This work showed that at high pressure levels, empirical equations such as Extended Sips model cannot well describe the separation of gas mixture. The large concentration of adsorbed gas and/or the characteristics of the material can cause difference in the competition adsorption phenomenon in which the empirical models cannot represent since they do not have physical meaning. IAST showed to be a representative model to be used for such conditions.

The model description considering the dead volumes inside the column made the simulation more representative. Dead volume has a large influence in the performance parameters of a PSA process. Moreover, the model description presented in this work also makes feasible to perform hybrid PSA process in which two ou more layer of different adsorbents can be put inside the same column.

The possibilities to design a PSA process can be numerous, which is difficult to define an optimum sequence and ideal steps for general separation processes. This particular separation process was easier to set up with the steps and sequence required and to evaluate their performance. However, higher number of columns can be advantageous taking into account the number of equalization steps available. In this context, others cycle sequence can be advantageous for others performance parameters such as product purity and productivity. The influence of a PSA cycle sequence and how to synchronize it should be considered to be studied detailed. Simulations of PSA processes linked with different cycle sequences are not easily found in literature. As a suggestion for future works it is essential to assess PSA configurations beside the adsorbent performance since different cycle sequences play an important key role on the results required for processes.

REFERENCES

AUROUX, A. **Calorimetry and Thermal Methods in Catalysis**. New York: Springer Series in Materials Science 154, 2013.

BASTOS-NETO, M. et al. Methane Adsorption Storage Using Microporous Carbons Obtained from Coconut Shells. **Adsorption,** v. 11, p. 911-915, 2005.

BEN-MANSOUR, R.; BASHA, M.; QASEM, N. A. A. Multicomponent and multi-dimensional modeling and simulation of adsorption-based carbon dioxide separation. **Computers & Chemical Engineering,** v. 99, p. 255-270, 2017. ISSN 00981354.

BEN-MANSOUR, R. et al. Carbon capture by physical adsorption: Materials, experimental investigations and numerical modeling and simulations – A review. **Applied Energy,** v. 161, p. 225-255, 2016. ISSN 03062619.

BIRD, R. B.; STEWART, W. E.; LIGHTFOOT, E. N. **Transport Phenomena**. 2nd. New York: W. International, 2006.

BOLIS, V. et al. Heterogeneous Nonclassical Carbonyls Stabilized in Cu(I)− and Ag(I)−ZSM-5 Zeolites: Thermodynamic and Spectroscopic Features. **The Journal of Physical Chemistry B,** v. 108, n. 28, p. 9970-9983, 2004/07/01 2004. ISSN 1520-6106. Disponível em: < https://doi.org/10.1021/jp049613e >.

BRANDANI, S.; MANGANO, E.; SARKISOV, L. Net, excess and absolute adsorption and adsorption of helium. **Adsorption,** v. 22, n. 2, p. 261-276, 2016. ISSN 0929-5607 1572-8757.

BUSS, E. Gravimetric measurements of binary gas adsorption equilibria of methane-carbon dioxide mixtures on activated carbon. **Gas Separation & Purification,** v. 9, n. 3, p. 189-197, 1995.

CAMPO, M. C. et al. Carbon dioxide removal for methane upgrade by a VSA process using an improved 13X zeolite. **Fuel Processing Technology,** v. 143, p. 185-194, 2016. ISSN 03783820.

CASAS, N. et al. Fixed bed adsorption of CO2/H2 mixtures on activated carbon: experiments and modeling. **Adsorption,** v. 18, n. 2, p. 143-161, 2012. ISSN 0929-5607 1572-8757.

CAVENATI, S.; GRANDE, C. A.; RODRIGUES, A. E. Separation of mixtures by layered pressure swing adsorption for upgrade of natural gas. **Chemical Engineering Science,** v. 61, n. 12, p. 3893-3906, 2006. ISSN 00092509.

CHATTERJEE, A.; SCHIEWER, S. Multi-resistance kinetic models for biosorption of Cd by raw and immobilized citrus peels in batch and packed-bed columns. **Chemical Engineering Journal,** v. 244, p. 105-116, 2014. ISSN 13858947.

CHIHARA, K.; SUZUKI, M. Simulation of nonisothermal pressure swing adsorption. **Journal of Chemical Engineering,** v. 16, n. 4, p. 293, 1983.

CLARKSON, C. R.; BUSTIN, R. M. Binary gas adsorption/desorption isotherms: Effect of moisture and coal composition upon carbon dioxide selectivity over methane. **International Journal of Coal Geology,** v. 42, n. 4, p. 241-271, 2000.

DANTAS, T. L. P. et al. Carbon dioxide–nitrogen separation through adsorption on activated carbon in a fixed bed. **Chemical Engineering Journal,** v. 169, n. 1-3, p. 11-19, 2011. ISSN 13858947.

DELGADO, J. A. et al. Adsorption and Diffusion of H2, CO, CH4, and CO2 in BPL Activated Carbon and 13X Zeolite: Evaluation of Performance in Pressure Swing Adsorption Hydrogen Purification by Simulation. **Industrial & Engineering Chemistry Research,** v. 53, n. 40, p. 15414-15426, 2014. ISSN 0888-5885 1520-5045.

DO, D. D. **Adsorption Analysis: Equilibra and Kinetics**. London: Imperial College Press, 1998.

DREISBACH, F.; STAUDT, R.; KELLER, J. U. High Pressure Adsorption Data of Methane, Nitrogen, Carbon Dioxide and their Binary and Ternary Mixtures on Activated Carbon. **Adsorption,** v. 5, p. 215-227, 1999.

FERREIRA, A. F. P. et al. Methane purification by adsorptive processes on MIL-53(Al). **Chemical Engineering Science,** v. 124, p. 79-95, 2015. ISSN 00092509.

GLUECKAUF, E.; COATES, J. I. Theory of chromatography. Part IV. The influence of incomplete equilibrium on the front boundary of chromatograms and on the effectiveness of separation. **Journal of Chemical Society**, 1947.

GOEL, C. et al. Carbon dioxide adsorption on nitrogen enriched carbon adsorbents: Experimental, kinetics, isothermal and thermodynamic studies. **Journal of CO2 Utilization,** v. 16, p. 50-63, 2016. ISSN 22129820.

GRANDE, C. A. et al. High-pressure separation of CH4/CO2 using activated carbon. **Chemical Engineering Science,** v. 89, p. 10-20, 2013. ISSN 00092509.

GRANDE, C. A. et al. CO 2 Capture in Natural Gas Production by Adsorption Processes. **Energy Procedia,** v. 114, p. 2259-2264, 2017. ISSN 18766102.

JOSS, L.; GAZZANI, M.; MAZZOTTI, M. Rational design of temperature swing adsorption cycles for post-combustion CO 2 capture. **Chemical Engineering Science,** v. 158, p. 381-394, 2017. ISSN 00092509.

KACEM, M.; PELLERANO, M.; DELEBARRE, A. Pressure swing adsorption for CO 2 /N 2 and CO 2 /CH 4 separation: Comparison between activated carbons and zeolites performances. **Fuel Processing Technology,** v. 138, p. 271-283, 2015. ISSN 03783820.

KAMARUDIN, K. S. N.; ZAINI, N.; KHAIRUDDIN, N. E. A. CO 2 removal using amine-functionalized kenaf in pressure swing adsorption system. **Journal of Environmental Chemical Engineering,** v. 6, n. 1, p. 549-559, 2018. ISSN 22133437.

KELLER, J.; STAUDT, R. **Gas Adsorption Equilibria: Experimental Methods and Adsorption Isotherms**. Boston: 2005.

KNOX, J. C. et al. Limitations of Breakthrough Curve Analysis in Fixed-Bed Adsorption. **Industrial & Engineering Chemistry Research,** v. 55, n. 16, p. 4734-4748, 2016. ISSN 0888-5885 1520-5045.

LANGMUIR, I. The Adsorption of Gases on Plane Surfaces of Glass, Mica and Platinum. **Journal of American Chemical Society**, p. 1361-1403, 1918.

LEE, S.-P. et al. High-pressure CO 2 -CH 4 selective adsorption on covalent organic polymer. **Journal of Natural Gas Science and Engineering,** v. 50, p. 139-146, 2018. ISSN 18755100.

LEUNG, D. Y. C.; CARAMANNA, G.; MAROTO-VALER, M. M. An overview of current status of carbon dioxide capture and storage technologies. **Renewable and Sustainable Energy Reviews,** v. 39, p. 426-443, 2014. ISSN 13640321.

LING, J. et al. Effects of feed gas concentration, temperature and process parameters on vacuum swing adsorption performance for CO2 capture. **Chemical Engineering Journal,** v. 265, p. 47-57, 2015. ISSN 13858947.

LIU, J. et al. Molecular Simulations and Theoretical Predictions for Adsorption and Diffusion of CH4/H2 and CO2/CH4 Mixtures in ZIFs. **The Journal of Physical Chemistry C,** v. 115, n. 25, p. 12560-12566, 2011. ISSN 1932-7447 1932-7455.

LOPES, F. V. S. et al. Adsorption of H2, CO2, CH4, CO, N2and H2O in Activated Carbon and Zeolite for Hydrogen Production. **Separation Science and Technology,** v. 44, n. 5, p. 1045-1073, 2009. ISSN 0149-6395 1520-5754.

LUBERTI, M. et al. New momentum and energy balance equations considering kinetic energy effect for mathematical modelling of a fixed bed adsorption column. **Adsorption,** v. 21, n. 5, p. 353-363, 2015. ISSN 0929-5607 1572-8757.

MARTÍN, C. F. et al. Wet impregnation of a commercial low cost silica using DETA for a fast post-combustion CO_2 capture process. **Applied Energy,** v. 183, p. 1705-1721, 2016.

MARX, D. et al. CO2 Capture from a Binary CO2/N2 and a Ternary CO2/N2/H2 Mixture by PSA: Experiments and Predictions. **Industrial & Engineering Chemistry Research,** v. 54, n. 22, p. 6035-6045, 2015. ISSN 0888-5885 1520-5045.

MENDES, P. A. P. et al. Separation of CO 2 /N 2 on binderless 5A zeolite. **Journal of CO2 Utilization,** v. 20, p. 224-233, 2017. ISSN 22129820.

MONDAL, M. K.; BALSORA, H. K.; VARSHNEY, P. Progress and trends in CO2 capture/separation technologies: A review. **Energy,** v. 46, n. 1, p. 431-441, 2012. ISSN 03605442.

MOREIRA, M. A. et al. Cryogenic pressure temperature swing adsorption process for natural gas upgrade. **Separation and Purification Technology,** v. 173, p. 339-356, 2017. ISSN 13835866.

MULGUNDMATH, V. P. et al. Fixed bed adsorption for the removal of carbon dioxide from nitrogen: Breakthrough behaviour and modelling for heat and mass transfer. **Separation and Purification Technology,** v. 85, p. 17-27, 2012. ISSN 13835866.

MURATA, K.; MIYAWAKI, J.; KANEKO, K. A simple determination method of the absolute adsorbed amount for high pressure gas adsorption. **Carbon,** v. 40, n. 3, p. 425-428, 2002/03/01/ 2002. ISSN 0008-6223. Disponível em: < http://www.sciencedirect.com/science/article/pii/S0008622301001269 >.

MYERS, A. L. Thermodynamics of adsorption in porous materials. **AIChE Journal,** v. 48, n. 1, p. 145-160, 2002/01/01 2002. ISSN 0001-1541. Disponível em: < https://doi.org/10.1002/aic.690480115 >. Acesso em: 2019/07/30.

MYERS, A. L.; PRAUSNITZ, J. M. Thermodynamics of Mixed-Gas adsorption. **AIChE Journal,** v. 11, n. 1, p. 121-127, 1965.

NIKOLAIDIS, G. N.; KIKKINIDES, E. S.; GEORGIADIS, M. C. Model-Based Approach for the Evaluation of Materials and Processes for Post-Combustion Carbon Dioxide Capture from Flue Gas by PSA/VSA Processes. **Industrial & Engineering Chemistry Research,** v. 55, n. 3, p. 635-646, 2016. ISSN 0888-5885 1520-5045.

NTIAMOAH, A. et al. CO2 capture by vacuum swing adsorption: role of multiple pressure equalization steps. **Adsorption,** v. 21, n. 6-7, p. 509-522, 2015. ISSN 0929-5607 1572-8757.

PILLAI, R. S.; PETER, S. A.; JASRA, R. V. Adsorption of carbon dioxide, methane, nitrogen, oxygen and argon in NaETS-4. **Microporous and Mesoporous Materials,** v. 113, n. 1-3, p. 268-276, 2008. ISSN 13871811.

PLAZA, M. G. et al. Experimental and Simulation Study of Adsorption in Postcombustion Conditions Using a Microporous Biochar. 1. CO2 and N2 Adsorption. **Industrial & Engineering Chemistry Research,** v. 55, n. 11, p. 3097-3112, 2016. ISSN 0888-5885 1520-5045.

PLAZA, M. G. et al. Post-combustion CO2 capture with a commercial activated carbon: Comparison of different regeneration strategies. **Chemical Engineering Journal,** v. 163, n. 1-2, p. 41-47, 2010. ISSN 13858947.

RIBEIRO, A. M. et al. A parametric study of layered bed PSA for hydrogen purification. **Chemical Engineering Science,** v. 63, n. 21, p. 5258-5273, 2008. ISSN 00092509.

RIOS, R. B. et al. Evaluation of carbon dioxide–nitrogen separation through fixed bed measurements and simulations. **Adsorption,** v. 20, n. 8, p. 945-957, 2014. ISSN 0929-5607 1572-8757.

ROCHA, L. A. M.; ANDREASSEN, K. A.; GRANDE, C. A. Separation of CO 2 /CH 4 using carbon molecular sieve (CMS) at low and high pressure. **Chemical Engineering Science,** v. 164, p. 148-157, 2017. ISSN 00092509.

ROTA, R.; GAMBA, G.; MORBIDELLI, M. On the use of the adsorbed solution theory for designing adsorption separation units. **Separations Technology,** v. 3, n. 4, p. 230-237, 1993/01/01/ 1993. ISSN 0956-9618. Disponível em: < http://www.sciencedirect.com/science/article/pii/095696189380022J >.

ROUQUEROL, F. et al. **Adsorption by Powder & Porous Solids - Principles Methodology and Applications**. 2nd. L. Academic Press, London, 2014.

RUDZIŃSKI, W. et al. On the theoretical origin and applicability of the potential theory approach to predict mixed-gas adsorption on solid surfaces from single-gas adsorption isotherms. **Chemical Engineering Science,** v. 50, n. 16, p. 2641-2660, 1995/08/01/ 1995. ISSN 0009-2509.

RUFFORD, T. E. et al. The removal of CO2 and N2 from natural gas: A review of conventional and emerging process technologies. **Journal of Petroleum Science and Engineering,** v. 94-95, p. 123-154, 2012. ISSN 09204105.

RUTHVEN, D. M. **Principles of Adsorption and Adsorption Processes**. Wiley, 1984.

RUTHVEN, D. M.; FAROOQ, S.; KNAEBEL, K. S. **Pressure Swing Adsorption**. New York: Wiley-VCH, 1994.

SCHELL, J. et al. Comparison of commercial and new adsorbent materials for pre-combustion CO2 capture by pressure swing adsorption. **Energy Procedia,** v. 37, p. 167-174, 2013. ISSN 18766102.

SERNA-GUERRERO, R.; BELMABKHOUT, Y.; SAYARI, A. Modeling CO_2 adsorption on amine-functionalized mesoporous silica: 1. A semi-empirical equilibrium model. **Chemical Engineering Journal,** v. 161, p. 173-181, 2010.

SHAFEEYAN, M. S.; WAN DAUD, W. M. A.; SHAMIRI, A. A review of mathematical modeling of fixed-bed columns for carbon dioxide adsorption. **Chemical Engineering Research and Design,** v. 92, n. 5, p. 961-988, 2014. ISSN 02638762.

SILVA, B. et al. H2 purification by pressure swing adsorption using CuBTC. **Separation and Purification Technology,** v. 118, p. 744-756, 2013. ISSN 13835866.

SIPS, R. On the Structure of a Catalyst Surface. **The Journal of Chemical Physics,** v. 16, n. 5, p. 490-495, 1948. ISSN 0021-9606

1089-7690.

SIQUEIRA, R. M. et al. Carbon Dioxide Capture by Pressure Swing Adsorption. **Energy Procedia,** v. 114, p. 2182-2192, 2017. ISSN 18766102.

SIQUEIRA, R. M. et al. Simulation of CO2/CH4 high pressure separation on microporous activated carbon. **Chemical Engineering Communications**, p. 1-12, 2018a. ISSN 0098-6445. Disponível em: < https://doi.org/10.1080/00986445.2018.1547713 >.

SIQUEIRA, R. M. et al. Simple Procedure to Estimate Mass Transfer Coefficients from Uptake Curves on Activated Carbons. **Chemical Engineering & Technology,** v. 41, n. 8, p. 1622-1630, 2018b. ISSN 0930-7516.

SKARSTROM, C. W. **Method and apparatus for fractionating gaseous mixtures by adsorption**. US: Esso Research and Engineering Company. Patent 2,944,627. 1960.

SRINIVASAN, R.; AUVIL, S. R.; SCHORK, J. M. Mass transfer in carbon molecular sieves — an interpretation of Langmuir kinetics. **Chemical Engineering Journal**, 1995.

SUNDARAM, N.; YANG, R. T. Isosteric Heats of Adsorption from Gas Mixtures. **Journal of Colloid and Interface Science,** v. 198, p. 378-388, 1998.

SUZUKI, M. **Adsorption Engineering**. Tokyo: Kodansha & Elsevier Science Publisher B.V., 1990.

THOMMES, M. et al. Physisorption of gases, with special reference to the evaluation of surface area and pore size distribution (IUPAC Technical Report). **Pure and Applied Chemistry,** v. 87, n. 9-10, 2015. ISSN 1365-3075

0033-4545.

TIEN, C. **Adsorption Calculations and Modelling**. London: 1994.

TOTH, J. Adsorption - Theory, Modeling, and Analysis. In: INC., M. D. (Ed.), v.107, 2001.

VICTOR, D. G. et al. **Introductory Chapter. In: Climate Change 2014: Mitigation of climate change. Contribution of working group III to the fifth assessment report of the intergovernamental panel on climate change. [Edenhofer O, Pichs-Madruga R, Sokona Y, Farahani E, Kadner S, Seyboth K, Adler A, Baum I, Brunner S, Eickemeier P, Kriemann B, Savolainen J, Schlömer S, von Stechow C, Zwickel T and Minx JC (eds)].** PRESS, C. U. 2014.

WON, W.; LEE, S.; LEE, K. S. Modeling and parameter estimation for a fixed-bed adsorption process for CO2 capture using zeolite 13X. **Separation and Purification Technology,** v. 85, p. 120-129, 2012. ISSN 13835866.

YANG, R. T. **Gas Separation by Adsorption Processes**. Imperial College Press, Boston, 1997.

YANG, R. T. **Adsorbents: Fundamentals and Applications**. New Jersey: John Wiley & Sons, Inc., 2003.

YAO, C.; CHEN, T. A new simplified method for estimating film mass transfer and surface diffusion coefficients from batch adsorption kinetic data. **Chemical Engineering Journal,** v. 265, p. 93-99, 2015. ISSN 13858947.

ZHANG, J. et al. Effect of flue gas impurities on CO2 capture performance from flue gas at coal-fired power stations by vacuum swing adsorption. **Energy Procedia,** v. 1, n. 1, p. 1115-1122, 2009. ISSN 18766102.

ZHAO, R. et al. A comparative study on CO 2 capture performance of vacuum-pressure swing adsorption and pressure-temperature swing adsorption based on carbon pump cycle. **Energy,** v. 137, p. 495-509, 2017. ISSN 03605442.

APPENDIX A ─ CORRELATIONS

1. Mass dispersion [$D_{ax}(Re, Sc)$] $$D_{ax} = \frac{u\ d_p}{Pe}$$

2. Peclet Number (Pe) $$\frac{1}{Pe} = \frac{0.45 + 0.55\varepsilon}{\mathrm{Re}\ Sc} + 0.5$$

3. Reynolds Number (Re) $$\mathrm{Re} = \frac{\rho\ u\ d_p}{\mu}$$

4. Schimdt Number (Sc) $$Sc = \frac{\mu}{\rho D}$$

5. Bed Porosity (ε) $$\varepsilon = 1 - (V_{sol} + V_p)\,\rho_b$$

6. Particle Porosity (ε_p) $$\varepsilon_p = 1 - \frac{V_{sol}}{V_{sol} + V_p}$$

APPENDIX B ─ SIMULATION PARAMETERS VALUES

λ	10 W m^{-1} K^{-1}
h_w	120 W m^{-2} K^{-1}
U_g	90 W m^{-2} K^{-1}
δ	100
$c_{p,w}$	470 J kg^{-1} K^{-1}
ρ_w	7860 kg m^{-3}
α_w	338 m^{-1}
α_{wl}	369 m^{-1}

Source: Author

APPENDIX C – HISTORY OF TEMPERATURE FROM BREAKTHROUGH CURVES OF PURE COMPONENT N_2 AT 6 BAR FOR CHARBON 500, FILTRON N AND NORIT RB4.

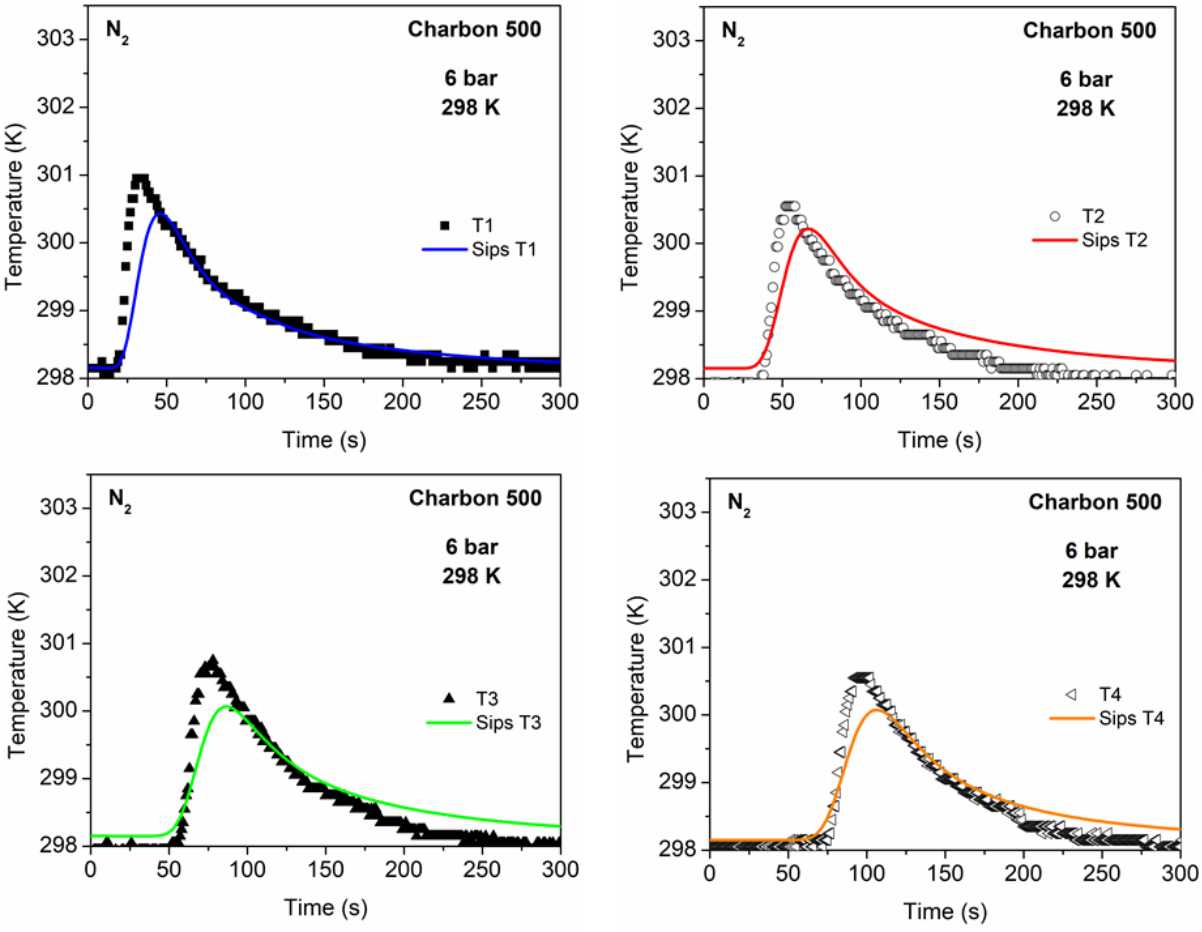

Source: Author

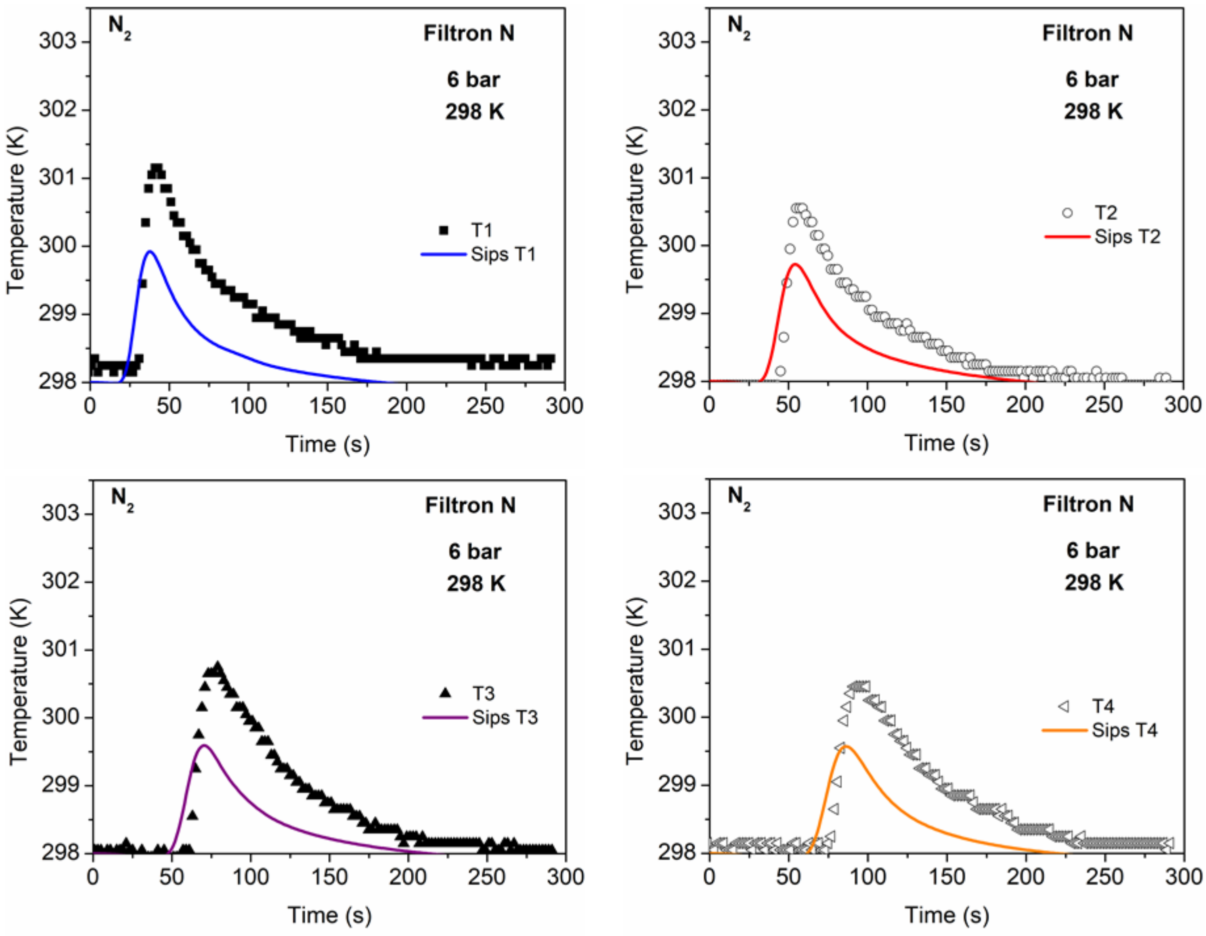

Source: Author

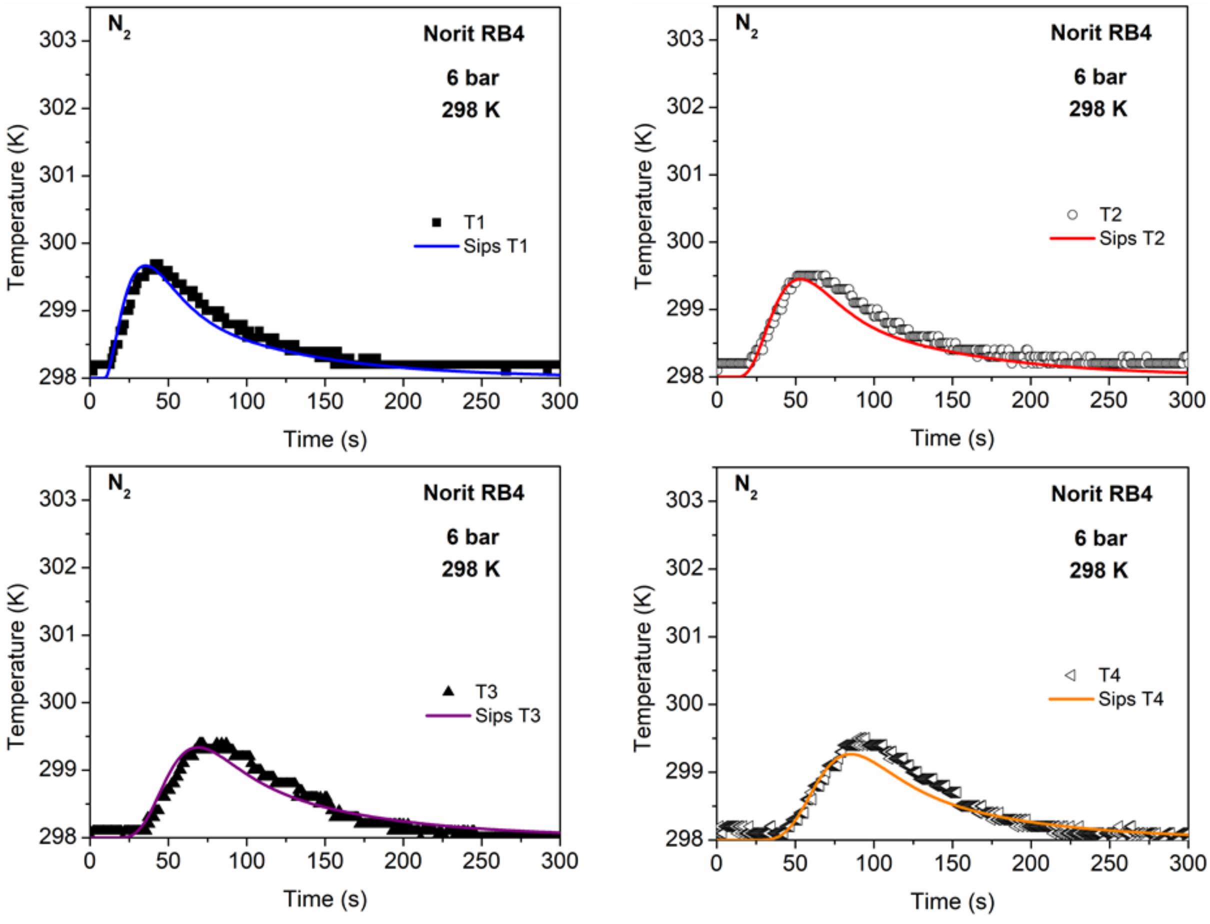

Source: Author

APPENDIX D – HISTORY OF TEMPERATURE FROM BREAKTHROUGH CURVES OF PURE COMPONENT CO_2 AT 6 BAR FOR CHARBON 500, FILTRON N AND NORIT RB4.

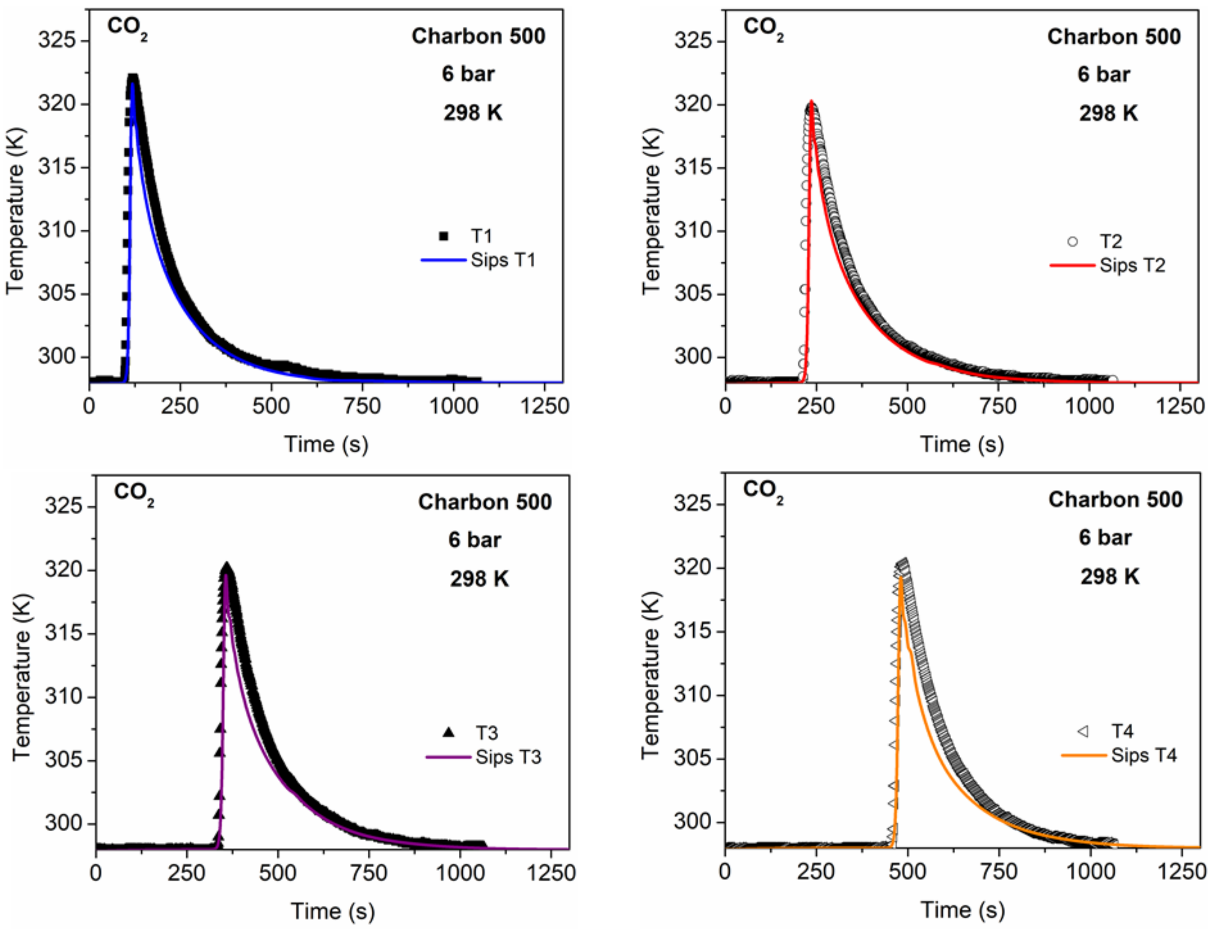

Source: Author

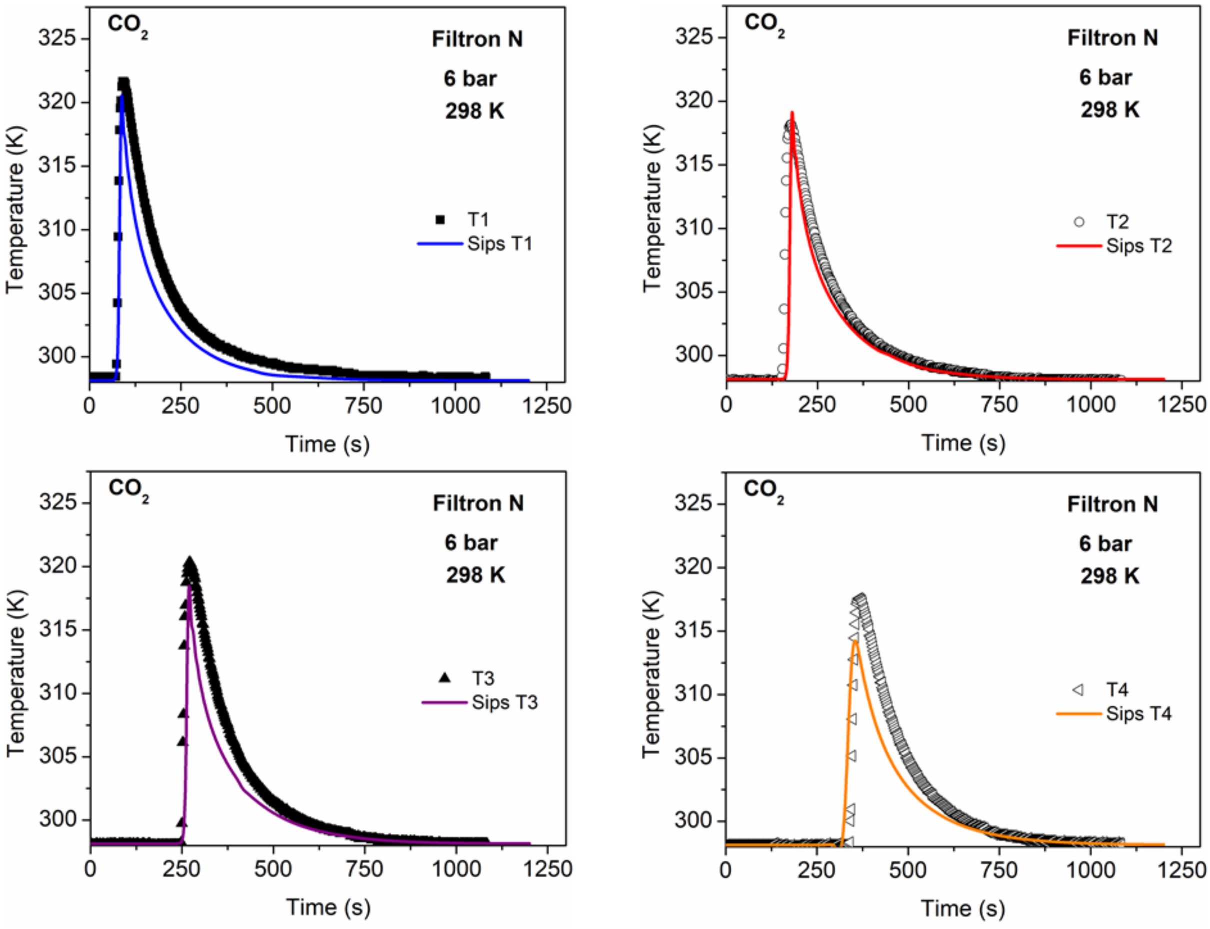

Source: Author

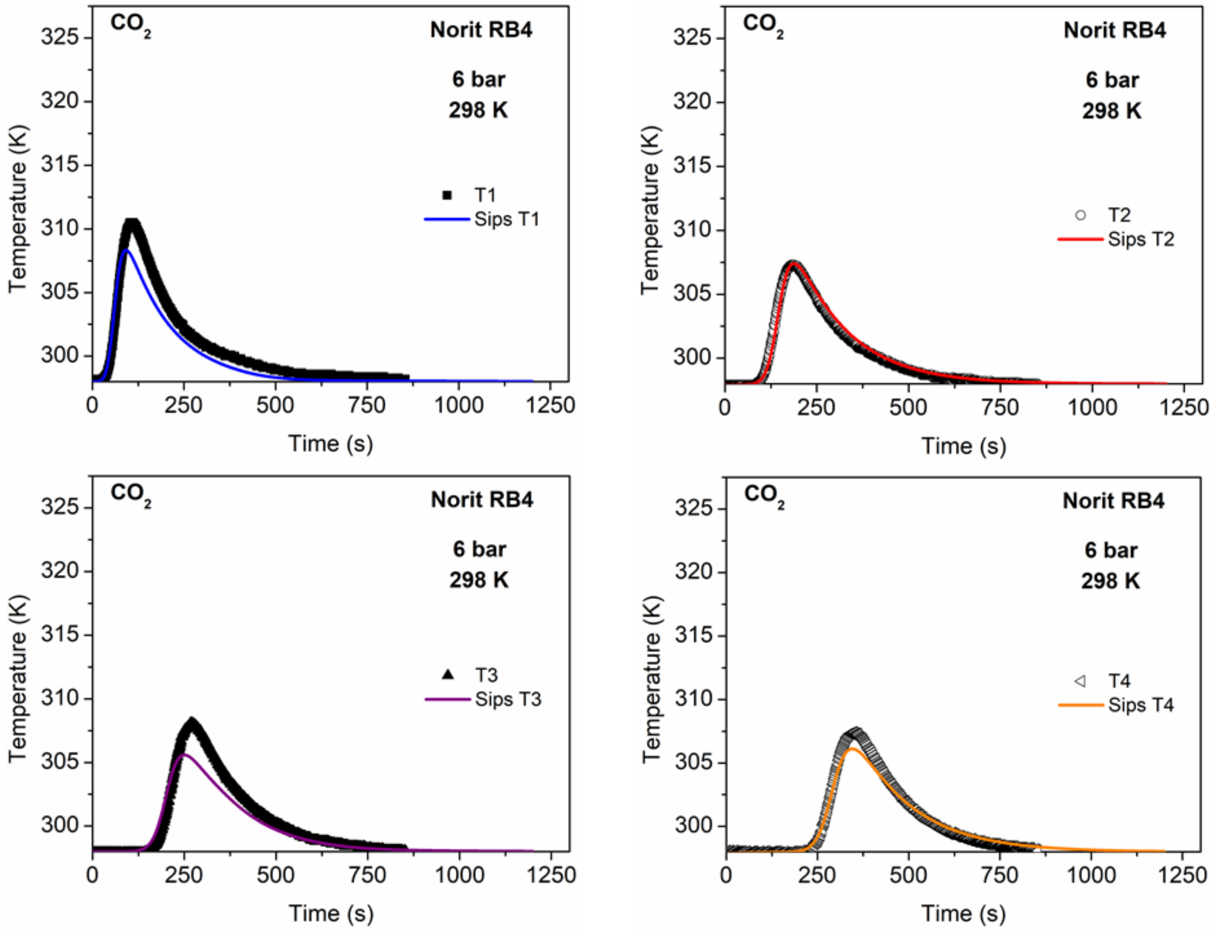

Source: Author

APPENDIX E ─ HISTORY OF TEMPERATURE FROM BREAKTHROUGH CURVES OF BINARY MIXTURE ($CO_2 + N_2$) AT 6 BAR, 12 BAR AND 18 BAR FOR NORIT RB4.

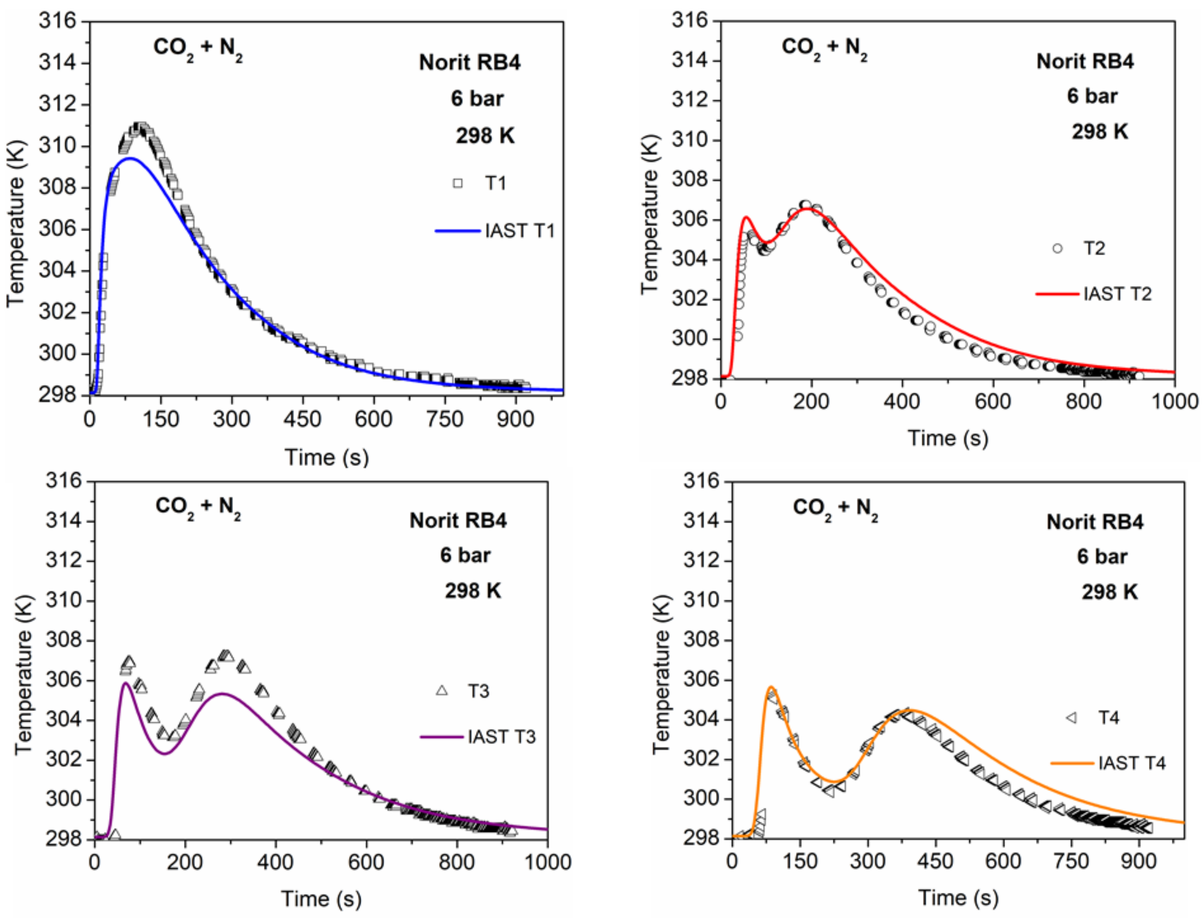

Source: Author

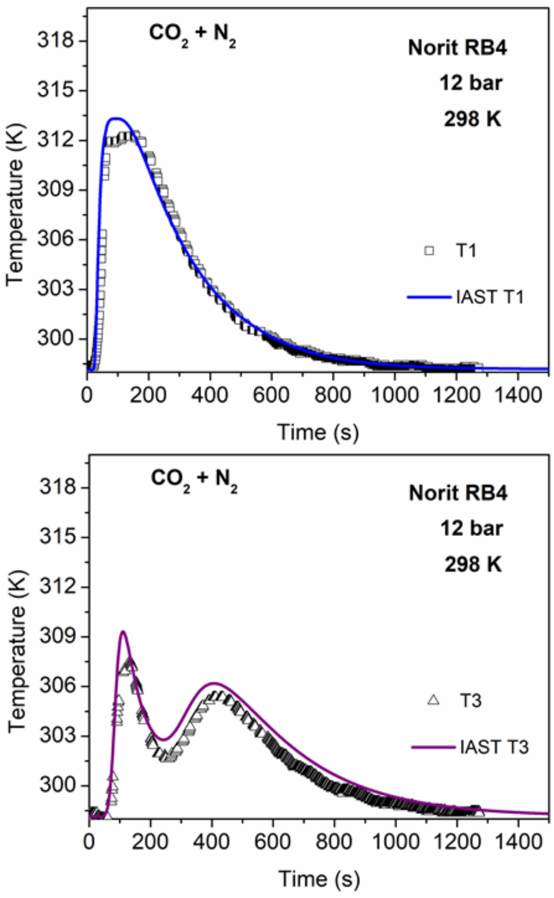

Source: Author

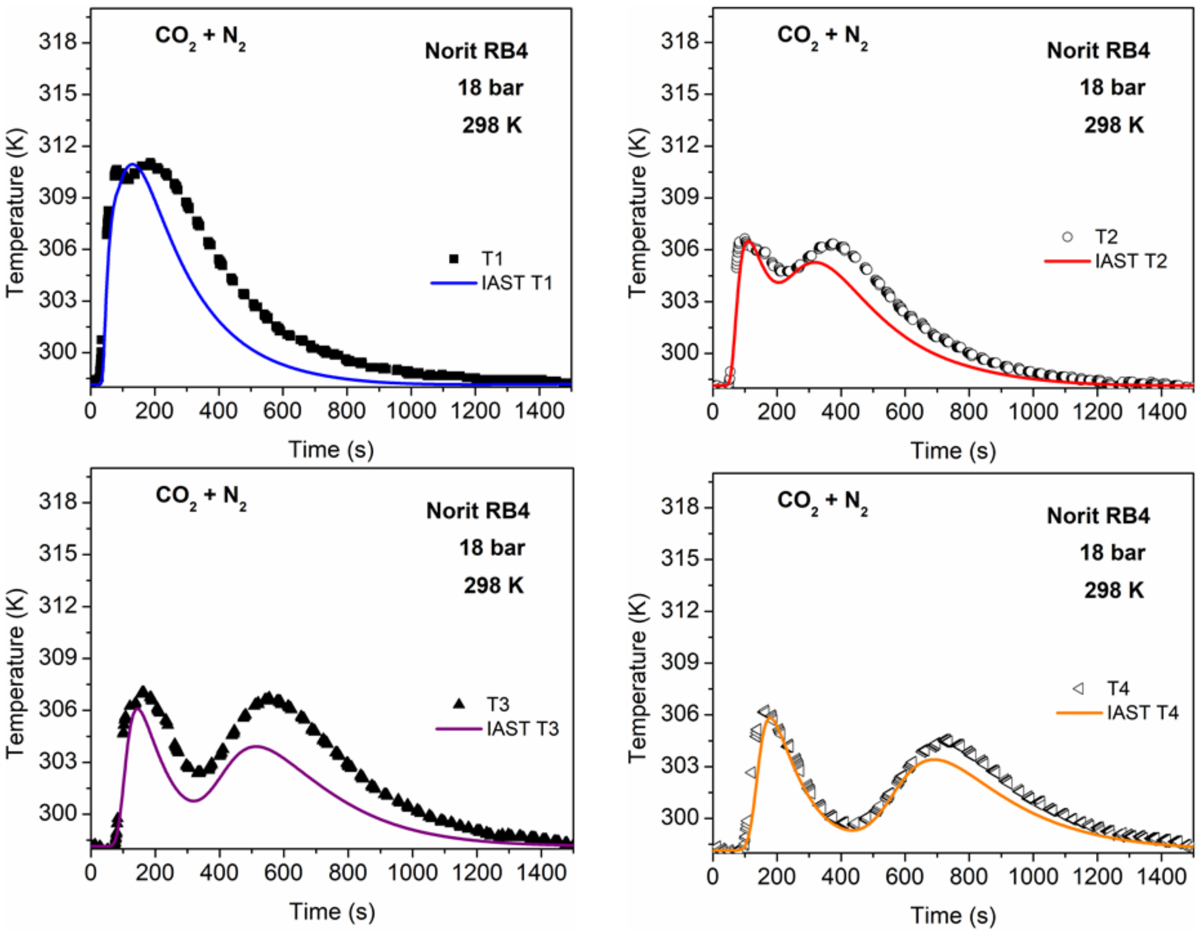

Source: Author